Advanced Technology Fuel Cell Program

EM-1328
Research Project 114

Annual Report, January 1980

Prepared by

UNITED TECHNOLOGIES CORPORATION
Power Systems Division
Post Office Box 109
Governor's Highway
South Windsor, Connecticut 06074

Principal Investigators
J. A. S. Bett
C. L. Bushnell
R. F. Buswell
G. A. Gruver
J. M. King
H. R. Kunz

Prepared for

Electric Power Research Institute
3412 Hillview Avenue
Palo Alto, California 94304

EPRI Project Manager
Arnold P. Fickett

Fuel Cells and Chemical Energy Conversion Program
Energy Management and Utilization Division

ORDERING INFORMATION

Requests for copies of this report should be directed to Research Reports Center (RRC), Box 50490, Palo Alto, CA 94303, (415) 965-4081. There is no charge for reports requested by EPRI member utilities and affiliates, contributing nonmembers, U.S. utility associations, U.S. government agencies (federal, state, and local), media, and foreign organizations with which EPRI has an information exchange agreement. On request, RRC will send a catalog of EPRI reports.

NOTICE

This report was prepared by the organization(s) named below as an account of work sponsored by the Electric Power Research Institute, Inc. (EPRI). Neither EPRI, members of EPRI, the organization(s) named below, nor any person acting on their behalf: (a) makes any warranty or representation, express or implied, with respect to the accuracy, completeness, or usefulness of the information contained in this report, or that the use of any information, apparatus, method, or process disclosed in this report may not infringe privately owned rights; or (b) assumes any liabilities with respect to the use of, or for damages resulting from the use of, any information, apparatus, method, or process disclosed in this report.

Prepared by
United Technologies Corporation
South Windsor, Connecticut

ABSTRACT

This report describes the results of activities carried out from April 1978 through March 1979 under Electric Power Research Institute Project RP114-2. The goals of the Project RP114-2 are to:

- demonstrate the basis for engineering development of fuel cell stack and fuel processing technologies consistent with dispersed fuel cell generators with reduced capital cost, 7500 Btu/kWh heat rate, and the ability to operate on heavier liquid fuels from coal or petroleum such as No. 2 fuel oil, and to
- define the best approaches for the use of coal and coal products in fuel cell power plants.

Molten carbonate fuel cells, advanced phosphoric acid fuel cells, advanced fuel processors, and the use of coal products in central stations or dispersed fuel cell power plants are under investigation. The RP114-2 effort is carried out in parallel with activities funded by United to define materials, configurations, processes, and power plant designs consistent with program goals, and pertinent results of that activity are also incorporated in this report.

During this period improvement in molten carbonate cell materials and design have resulted in subscale cells which have the demonstrated capability to withstand 12 thermal cycles in proof of principle tests and 9 thermal cycles with cost effective materials. These results have been successfully transferred to multicell 1 ft^2 stacks of 8 and 20 cells. Reactant leakage has been reduced at the same time. A four station test facility for subscale cells having the capability of testing at 10 atmospheres has been constructed and is in operation.

The formation of carbon and methane in molten carbonate cells has been studied and neither was found to be formed to a significant degree at pressures up to 5 atmospheres.

EPRI PERSPECTIVE

PROJECT DESCRIPTION

In 1973, the Edison Electric Institute (EEI) initiated the Advanced Technology Fuel Cell Program under EPRI Research Project (RP) 114 to advance fuel cell technology beyond the capabilities of the first generation (FCG-1) power plant. Specifically, RP114 was to investigate means of lowering cost and improving efficiency by 20% and to expand fuel capability to No. 2 fuel oil as well as coal liquids and gases. In early 1974, the project was transferred to EPRI's programs. Since its inception, RP114 has resulted in several successful developments that have been transferred to the FCG-1 Program, including:

- An advanced forced-commutated inverter
- A hydrosulfurizer capable of removing sulfur from naphtha feedstocks
- An improved phosphoric acid stack technology.

In 1977 the project was revised to focus on the molten carbonate fuel cell technology and concepts for fuel processing equipment capable of processing distillate fuels derived from both petroleum and coal.

This annual report describes the results of work conducted from April 1978 through March 1979.

PROJECT OBJECTIVES

The specific objectives of RP114-2 are to:

- Develop a molten carbonate fuel cell stack and a fuel processing technology consistent with use as a dispersed generator having a capital cost of $280/kW (1978 dollars), a heat rate of 7500 Btu/kWh, and the ability to operate on liquid fuels from coal or petroleum, such as No. 2 fuel oil.
- Define approaches for integrating fuel-cell power plants with coal products.

PROJECT RESULTS

During this reporting period two very significant results were achieved:

- Cell configurations were developed that successfully withstood a number of thermal cycles without increased anode-to-cathode gas leakage even at relatively high pressure differentials (10 psid) across the electrode-electrolyte interfaces.

- Subscale cells were tested at pressures up to 5 atmospheres with little, if any, carbon or methane formation in the fuel cell.

For three years, the inability of earlier molten carbonate cell configurations to thermally cycle without a loss of integrity has been a major impediment to molten carbonate fuel cell development. The availability of cell configurations capable of enduring thermal cycles is now allowing the project to move forward at an accelerated pace. The new cell configurations have since been successfully used in square-foot stacks of 8 and 20 cells.

The second result is important inasmuch as formation of carbon and/or methane at the fuel cell anode would have a deleterious effect on fuel cell operation: the former would tend to plug the system; the latter would represent a loss of electrochemically available hydrogen and thus an increase in power plant heat rate. The lack of significant methane formation is contrary to results reported by others. To clarify this situation, additional experiments will be conducted.

Besides the results noted above, three advanced fuel processing concepts were evaluated: an adiabatic reformer, a hybrid (high-temperature steam and adiabatic) reformer, and a cyclic reformer. At comparable power plant heat rates, the cyclic and hybrid approaches were projected to be less costly than the adiabatic reformer. At the present state of these concepts, this conclusion is preliminary and needs verification through additional development and testing.

Arnold P. Fickett, Program Manager
Fuel Cells and Chemical Energy Conversion Program
Energy Management and Utilization Division

ACKNOWLEDGMENTS

The effort reported herein was carried out by a number of personnel at United Technologies. Most of these personnel are located in the Technology and Research Group headed by Mr. William E. Houghtby. Molten carbonate fuel cell activities were managed by Calvin L. Bushnell and H. Russell Kunz. Phosphoric acid fuel cell activities were managed by Gary A. Gruver. Fuel processing activities were managed by John A. S. Bett. Joseph M. King served as United's Program Manager.

Authors contributing to this volume include Richard F. Buswell, Gary A. Gruver, Roger R. Lesieur, Joseph C. Pivar, Gregory F. Reynolds, Craig R. Schroll, Stanley W. Smith and Stephen J. Syzmanski.

Stanley W. Smith coordinated and edited the report.

CONTENTS

Section		Page
1	INTRODUCTION	1-1
2	TASK 1-ESTABLISH BASIS FOR ENGINEERING DEVELOPMENT OF MOLTEN CARBONATE FUEL CELL POWER PLANTS	2-1
	Introduction	2-1
	Stack Design Assessment	2-2
	Eight-Cell Stack Evaluation	2-2
	Twenty-Cell Stack Evaluation	2-4
	Cell Function	2-7
	Pressurized Subscale Cell Test	2-15
	Comparison of Pressurized Cell Performance and Model Predictions	2-18
	Methane Formation	2-22
	Carbon Formation	2-28
	iR Increase in Subscale Cells	2-29
	Long Term Cell Test History	2-32
	Conceptual Power Plant Design	2-33
3	TASK 2-ADVANCED PHOSPHORIC ACID CELLS	3-1
	Introduction	3-1
	Tolerance to H_2S	3-1
	Experimental Methods	3-3
	Experimental Results	3-4
	Performance on Adiabatic Reformer Gas	3-4
	Effect of CO	3-6
	Effect of H_2S Concentration	3-7
	Effect of Fuel Utilization	3-7
	Effect of Redox Couple	3-8
	Conclusions	3-9

CONTENTS (Continued)

Section		Page
4	TASK 3-ADVANCED FUEL PROCESSING	4-1
	Introduction	4-1
	Adiabatic Reforming	4-3
	Mixer Configuration Studies	4-3
	2-Inch Reactor Test Description	4-4
	Results of Configuration Tests in the 2-Inch Reactor	4-7
	Carbon Formation and Catalyst Evaluation	4-10
	Effect of Operating Parameters	4-19
	Six-Inch Diameter Adiabatic Reformer	4-21
	Summary of Adiabatic Reformer Testing	4-26
	Regenerable Metal Oxide Sulfur Scrubber (RMOSS)	4-27
	RMOSS Engineering Test Facility	4-28
	Laboratory Results	4-29
	Results from Engineering Test Rig	4-33
	Systems Analysis of Advanced Fuel Processors	4-38
5	TASK 4 - USE OF COAL AND COAL PRODUCTS IN FUEL CELL POWER PLANTS	5-1
6	REFERENCES	6-1

ILLUSTRATIONS

Figure		Page
S-1	Single Cell Thermal Cycling Experience	S-2
S-2	20-Cell Stack	S-3
S-3	Four Station Pressurized Test Facility	S-3
S-4	System Cost Comparision for 4.8-MW Power Plant	S-6
1-1	Advanced Technology Fuel Cell Program	1-2
2-1	8-Cell Stack Fuel Leakage History	2-3
2-2	8-Cell Stack Performance History	2-4
2-3	8-Cell Stack Performance Recovery	2-5
2-4	20-Cell Stack Assembly	2-5
2-5	20-Cell Stack Test Performance Comparison	2-6
2-6	20-Cell Stack Assembly Electrolyte Tile Thickness Variation	2-7
2-7	20-Cell Stack Test Cell Performance vs Tile Thickness Variation	2-8
2-8	20-Cell Stack Test	2-8
2-9	Cell Operating Time Until Loss of 10 psig Bubble Pressure (Type I Tile Approach)	2-12
2-10	Cell Operating Time Until Loss of 10 psig Bubble Pressure (Type H Tile Approach)	2-13
2-11	Cell 182 Bubble Pressure History vs Best Approach I & H History	2-13
2-12	Best Single Cell Thermal Cycling Experience	2-14
2-13	Pressurized Subscale Cell Test Stand Schematic	2-16
2-14	Pressurized Subscale Cell being mounted in Test Stand	2-16
2-15	Pressurized Subscale Cell Test Programs	2-17

ILLUSTRATIONS (Cont'd)

Figure		Page
2-16	Performance vs Pressure and Variable Fuel-Gas Composition at O/C, 100 ASF and 160 ASF for MCF-1	2-19
2-17	Changes in Performance vs Pressure and Variable Fuel Gas Composition at O/C, 100 ASF and 160 ASF for MCF-1	2-20
2-18	Cell Voltage vs Current Density at 15, 45 and 75 psia for ATR-13 at 59.1% H_2 and CO Utilization	2-20
2-19	Cell Voltage vs Current Density at 15, 45 and 75 psia for ATR-43 at 25% H_2 and CO Utilization	2-21
2-20	Cell Voltage vs Current Density at 15, 45 and 75 psia for ATR-43 at 85% H_2 and CO Utilization	2-21
2-21	Cell Performance as a Function of Temperature	2-22
2-22	Methanation at 10 ATM	2-24
2-23	Methanation Reaction Rate	2-25
2-24	Methane Concentration Profile	2-26
2-25	Shift Reaction Data	2-27
2-26	Estimated Carbon Limits	2-29
2-27	The Effects of Thermal Cycling on Internal Resistance	2-31
2-28	Cell No. 136 Life Data	2-31
2-29	Effect of Electrolyte Addition on Cell iR (Cell 136)	2-33
2-30	Power Plant Flow Diagram	2-35
2-31	Part Power Performance	2-37
2-32	Autothermal Reformer Design	2-38
2-33	Power Section Design	2-39
2-34	D. C. Module Arrangement	2-40

ILLUSTRATIONS (Cont'd)

Figure		Page
3-1	Cell Performance Stability Under Simulated Adiabatic Steam Reformer Conditions with and without 50 PPM H_2S Added to the Fuel	3-5
3-2A	Cell Performance with CO Containing Fuel (GM-3)	3-6
3-2B	Cell Performance with "Clean" Fuel (H_2/He) (GM-4)	3-7
3-3	Effect of H_2 Utilization on Time to Cell Decay, Phosphoric Acid Cell (with 100 PPM H_2S)	3-8
4-1	Example of Cold Flow Mixing Measurments Used to Design and Scale Reactant Mixing Nozzles	4-5
4-2	2-Inch Adiabatic Reformer	4-6
4-3	Schematic of 2-Inch Adiabatic Reformer and Reactor Preheater	4-7
4-4	Effect of Configuration on Carbon Boundary	4-8
4-5	Effect of Time on Carbon Boundary	4-9
4-6	Extrapolation of Carbon Free Point to Construct the System Carbon Boundary	4-9
4-7a	Carbon Formation in Adiabatic Reactor-Inter Pellet Space	4-10
4-7b	Carbon Formation in Adiabatic Reactor-Pellet Interior	4-11
4-8a	Carbon Formation in Adiabatic Reactor-Spherical Particles	4-11
4-8b	Carbon Formation in Adiabatic Reactor-Carbon Filaments	4-12
4-9	Carbon Formation Boundaries in the H-C-O System	4-13
4-10	Boudouard Reaction Ratios in 2-Inch and 6-Inch Reactors	4-13
4-11	Steady-State Rates of Carbon Formation and Removal in the Adiabatic Reactor	4-14
4-12	Effect of Catalyst on Carbon Boundary	4-15
4-13	Activity of Used Catalyst Samples from Configuration 9 Tests	4-16

ILLUSTRATIONS (Cont'd)

Figure		Page
4-14	Effect of Nickel Catalyst Activity on Carbon Boundary	4-16
4-15	Rates for Reforming Ethane - 2500 PPMWS	4-18
4-16	Effect of Catalyst Composition on Carbon Boundary	4-18
4-17	Effect of Inlet Catalyst on Reactor Temperature Profile	4-19
4-18	Effect of Pre-reaction Temperature and Residence Time on Methane Formation (Cracking) in Adiabatic Reforming	4-20
4-19	Effect of H_2 on Temperature Profile	4-20
4-20	O_2/C vs Run Time at Constant Prereaction Temperature	4-22
4-21	Fuel Conversion and Rig Exit Temperature vs Run Time	4-22
4-22	Activity of Catalyst Used in Adiabatic Reactor Build 3	4-23
4-23	Effect of Carbon on Carbon Boundary	4-24
4-24	Reactor Internals Showing Location, and Catalyst Shrinkage	4-25
4-25	Adiabatic Reformer Fuel Conversion vs. Bed Exit Temperature	4-26
4-26	Regenerable Metal Oxide Sulfur Scrubber Process	4-27
4-27	Simplified RMOSS Rig Schematic	4-29
4-28	Regenerable Sulfur Scrubber Results After Five Cycles	4-30
4-29	Effects of Temperature on Sulfur Capacity and Regenerability	4-31
4-30	Regeneration of Formulation D	4-32
4-31	Sulfur Removal on Formulation D - Effect of Particle Size	4-32
4-32	Effect of Steam Concentration on RMOSS Performance	4-33
4-33	Effect of Space Velocity and Water in Scrub Gas on Sulfur Breakthrough Time	4-34
4-34	Effect of Temperature on Sulfur Breakthough Time for Formulation E	4-35

ILLUSTRATIONS (Cont'd)

Figure		Page
4-35	Effect of Temperature on RMOSS Performance	4-36
4-36	Typical Sulfur Breakthrough Curve for Formulation E	4-37
4-37	Fuel Processing Systems Studied	4-39
4-38	Effect of Sulfur on Steam Reforming Activity of Supported Nickel Catalyst	4-40
4-39	System Cost Comparison for 4.8 MW Phosphoric Acid Power Plant at 9300 Btu/kWh	4-42

TABLES

Table		Page
S-1	Objectives of RP 114-2 and Parallel United Technologies Program	S-1
2-1	Summary of Various Tile Approaches Evaluated	2-10
2-2	Thermal Cycle Summary	2-10
2-3	Teardown Inspection Results	2-11
2-4	Cell Test Information	2-18
2-5	Test Gas Composition	2-23
2-6	Test Experience of Cells Using Electrolyte Tile Approach H	2-30
2-7	Dispersed Power Plant Requirement	2-34
2-8	Subsystem Efficiency	2-36
2-9	Computer Printout of Power Plant Design Conditions	2-36
3-1	Summary of Cell Tests	3-2
3-2	Fuel Mixes Used for Cell Testing	3-3
3-3	Cell Conditions Simulating Operation on Adiabatic Steam Reformer Effluent	3-4
4-1	No. 2 Fuel Oil Properties	4-2
4-2	Potential of Regenerable Sulfur Formulations Screened in the Laboratory	4-30
4-3	Influence of RMOSS Performance on Zinc Oxide Residual Sulfur Scrubber	4-38
4-4	Comparison of Fuel Processors	4-41

SUMMARY

Early fuel cell power plants are expected to find significant application as dispersed generators in replacing obsolete fossil generators in urban areas, in providing power to areas where transmission corridors are unavailable, in small municipal and rural systems and in spinning reserve duty. The application impact of fuel cell power plants would be extended by improving the heat rate, cost, and fuel flexibility of dispersed generators and by identifying the best approach to the use of coal and coal products in central station and dispersed fuel cell power plants. This report describes results of the Advanced Technology Fuel Cell Program carried out under EPRI RP114-2 and a complementary United Technologies effort from April 1978 through March 1979. The goal of this three-year effort is to demonstrate that new technology to provide these improvements is ready for engineering development. The complementary UTC funded effort is aimed at the identification of materials, configurations, processes, and designs consistent with improved fuel cell power plants.

Table S-1 shows the program objectives. Activities to achieve these objectives are carried out in four tasks, dealing with molten carbonate fuel cells, advanced phosphoric acid fuel cells, advanced reforming, and the use of coal and coal products. The highlights of program results are presented in this summary. Section 1 describes the program structure and context. Sections 2, 3, 4, and 5 describe the effort of each task in further detail.

Table S-1

OBJECTIVES OF RP114-2 AND PARALLEL UNITED TECHNOLOGIES PROGRAM

ESTABLISH READINESS FOR ENGINEERING DEVELOPMENT OF MOLTEN CARBONATE FUEL CELL TECHNOLOGY PERMITTING DESIGN OF DISPERSED GENERATORS WITH 7500 BTU/KWH HEAT RATE AND CAPITAL COST LESS THAN FIRST-GENERATION ACID ELECTROLYTE POWER PLANTS
ESTABLISH READINESS FOR ENGINEERING DEVELOPMENT OF LOW-COST, SULFUR-TOLERANT PHOSPHORIC ACID STACK
ESTABLISH READINESS FOR ENGINEERING DEVELOPMENT OF ADVANCED REFORMERS CAPABLE OF OPERATING ON NUMBER 2 FUEL OIL
DEFINE BEST APPROACHES TO USE OF COAL AND COAL PRODUCTS IN FUEL CELL POWER PLANTS

MOLTEN CARBONATE CELL RESULTS

The major effort during this report period has been to demonstrate in subscale cells and multi-cell stacks that the requirements for functionality and endurance can be met. During the previous period subscale cells had demonstrated that leakage could be eliminated for a few thousand hours with suitable seal design and that some tolerance to thermal cycling without loss of performance could be achieved. However these cells suffered an initial performance penalty, and they developed crossover on thermal cycling. At the end of this period subscale cells have demonstrated the ability to withstand up to 12 thermal cycles in a proof of principle test and 9 thermal cycles with cost effective materials without crossover, as shown in Figure S-1. These cells have the initial performance of earlier cells but performance loss may be experienced following thermal cycles. These results have been successfully transferred to multi-cell stacks having a nominal area of one square foot, with an 8-cell stack test completed and the 20-cell stack shown in Figure S-2 now in test.

A four station test facility for operation of subscale cells to 10 atmospheres has been constructed during this period. This test facility is shown in Figure S-3. Ten cells have been tested at pressures from 3 to 10 atmospheres, supplying information on performance as a function of operating parameters, carbon formation and methane reforming and providing inputs to the molten carbonate fuel cell model.

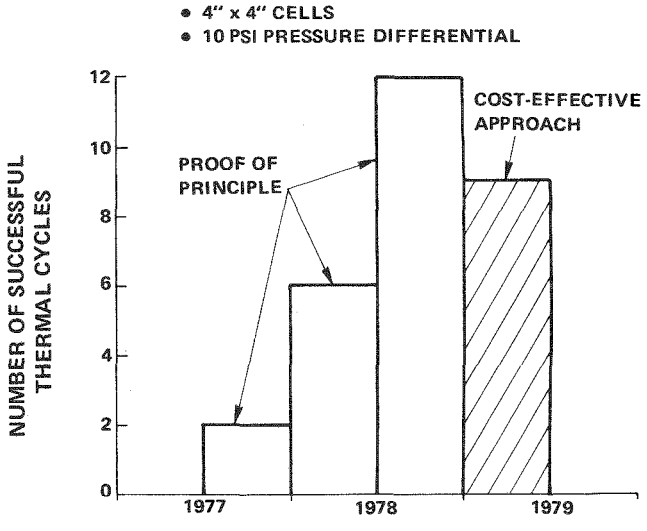

Figure S-1. Single Cell Thermal Cycling Experience

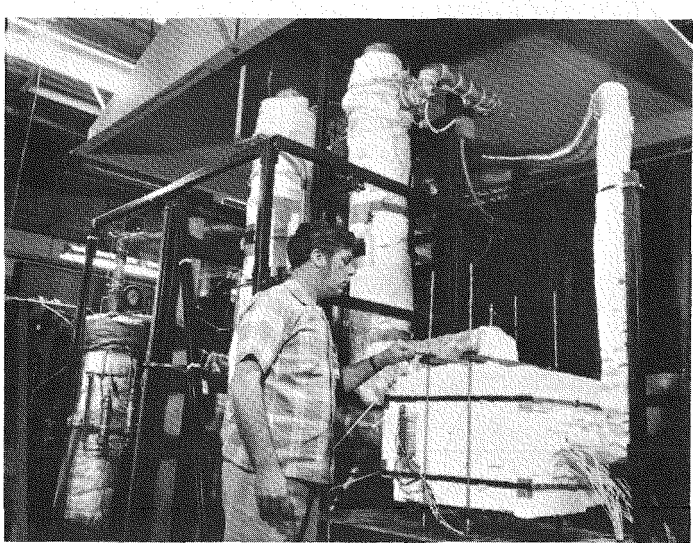

Figure S-2. 20-Cell Stack

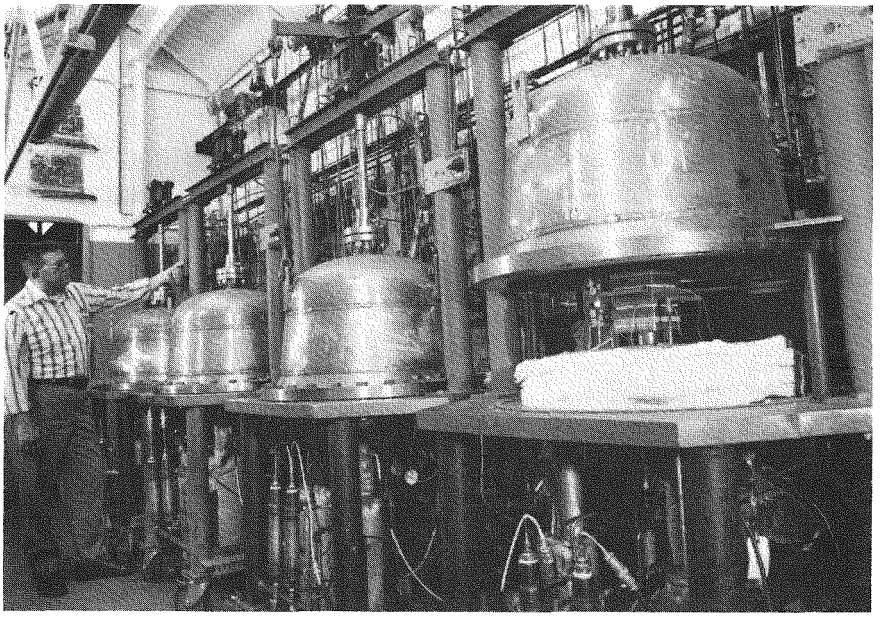

Figure S-3. Four Station Pressurized Test Facility

The kinetics of methanation and methane reforming were studied in cells. At pressures up to 3 atmospheres the reaction rates are so low that neither reaction occurs to a significant extent. Above 5 atmospheres a small amount of methanation occurs, corresponding to only a few percent of the equilibrium amount.

Under some conditions of fuel cell operation the cells are in a regime where, theoretically, carbon should be formed. Cell tests have demonstrated that the

carbon formation is kinetically controlled such that carbon does not form under any of the conditions tested, even though carbon was thermodynamically favored.

The effects of pressure on performance were found to agree with an analytical model.

PHOSPHORIC ACID CELL RESULTS

Efforts continued to determine the tolerance of phosphoric acid cells to hydrogen sulfide in the fuel gas. Cells operated on a fuel gas corresponding to that delivered by an adiabatic steam reformer show that the effect of H_2S is much more pronounced than that seen in previous testing with the H_2 rich fuel available from a thermal steam reformer. It was shown that CO is not required in the fuel for H_2S poisoning to be observed, apparently interacts with the H_2S to aid in the recovery process on H_2S removal from the fuel stream. The mechanism for anode decay is not well understood but the concentrations of and interactions between H_2, CO and H_2S are important to the process. Although the anode poisoning can be reversed, none of the known methods are viable for an operating power plant.

ADVANCED FUEL PROCESSING RESULTS

Adiabatic reforming was selected as the process most likely to be capable of efficient conversion of heavy petroleum fuels and synthetic liquid fuels from coal to hydrogen-containing gases. Adiabatic reforming experiments were performed to investigate the effects of reactor inlet configuration, catalyst formulation and operating parameters on the oxygen to fuel ratio required to prevent carbon formation. An alternative processing sequence was also investigated in a six inch reactor.

A wide throat reactant mixer/injector was developed in a two inch adiabatic reformer which completely mixes the reactants and eliminates fuel fouling in the mixing section of the reactor. Scaleup of this mixer from 2 inch reactor size to 6 inch reactor size was demonstrated. Similar reactant mixing resulted in a similar carbon boundary for each reactor. Even with this high intensity reactant mixer, however, the present adiabatic reforming process requires about 20% more air than the system study design goal. Test results indicate that improved catalyst formulations will decrease the air requirements. Studies during RP114-2 have improved the reforming process from one which was mixer limited to one which is catalyst limited.

Testing of regenerable metal oxide scrubber formulations for removing sulfur from gaseous processed fuel continued. One formulation was identified which has a low but significant sulfur capacity. Increased capacity is expected through formulation and process optimization. This should allow the operation of both molten carbonate and advanced phosphoric acid fuel cell power plants with sulfur bearing fuels.

EVALUATION OF ALTERNATIVE FUEL PROCESSORS

Advanced fuel processing systems are being developed to extend operation of dispersed fuel cell power plants to both petroleum and coal derived liquid distillate fuels. The sulfur and aromatic content of these fuels demand high process temperatures to achieve the required fuel conversion. Three possible candidate processes were evaluated: An adiabatic reformer, a hybrid reformer, and a cyclic reformer.

The processes were evaluated by system studies comparing the relative cost of 4.8 MW dispersed power plant with phosphoric acid fuel cells. For each power plant the fuel processing and fuel cell conditions were optimized to minimize cost at a heat rate of 9300 Btu/kWh. The fuel processing section, (FPS), reactor sizes were estimated using reactor models and measured activity of catalysts in the presence of sulfur. Fuel cell performance for the different gas compositions was estimated using a cell performance model.

Based on cost alone, the most promising fuel processor is the cyclic reformer, and then the hybrid reformer as shown in Figure S-4. These processes are in a very early stage of development. The study also identified the critical areas of concern in each candidate fuel processor. Confident selection between the candidates will required resulition of the critical issues for each of the systems.

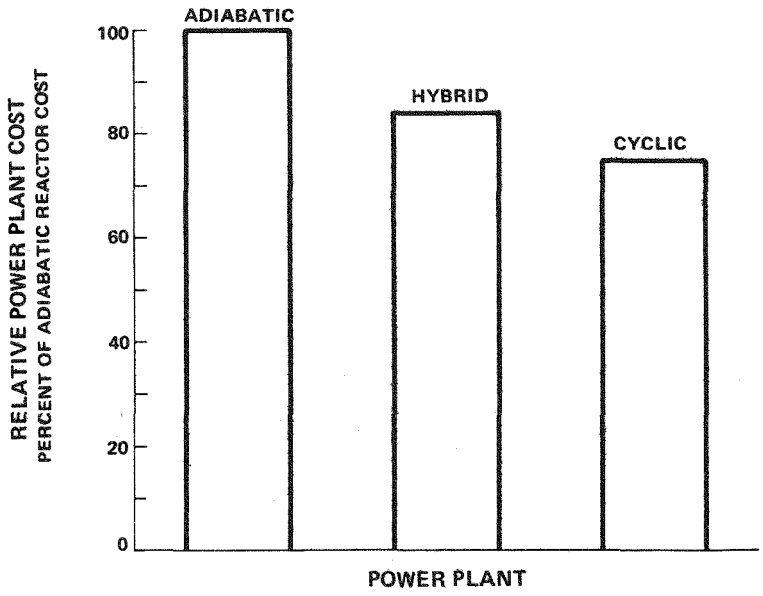

Figure S-4. System Cost Comparison for 4.8-MW Power Plant

Section 1

INTRODUCTION

Initial fuel cell power plants are expected to find significant application as dispersed generators in replacing obsolete fossil fueled generators in urban areas, in providing power to areas where transmission corridors are unavailable, in small rural and municipal utilities, and in "spinning reserve" duty. Demonstration of the initial fuel cell dispersed generator in a utility system will be carried out in New York City (1,2). Achieving maximum impact from the dispersed fuel cell generator requires improved heat rate, capital cost, and fuel flexibility. The impact of fuel cell power plants can be extended further through development of central station coal fuel cell power plants. The effort in Project RP114-2 has been directed toward development of technologies that broaden the impact of fuel cell power plants beyond that of the initial power plant.

In RP114-1, reported in Reference 3, a number of advanced fuel cell technology concepts were investigated. Figure 1-1 depicts the results of RP114-1 and shows its relationship to RP114-2. In two areas (hydrodesulfurizers and selfcommutated inverters), progress in RP114-1 was sufficient to permit incorporation in the 4.8-MW Fuel Cell Demonstrator. The technical feasibility of four concepts was demonstrated in RP114-1, and effort continued in RP114-2 to establish the basis for engineering development. Effort on other concepts was discontinued because the results showed that fundamental changes would be required to meet program goals.

Work performed under EPRI RP114-2 during the period April 1977 through March 1978 was reported in Reference 4. The results of activities in EPRI RP114-2 during the third year of the contract effort from April 1978 through March 1979 are described herein. The goals of RP114-2 are to:

- demonstrate readiness for engineering development of concepts permitting 7500 Btu heat rate, reduced capital cost below that of first-generation phosphoric acid power plants, and capability for the use of heavier liquids in dispersed generators, and
- define the best approaches to the use of coal and coal products in fuel cell power plants.

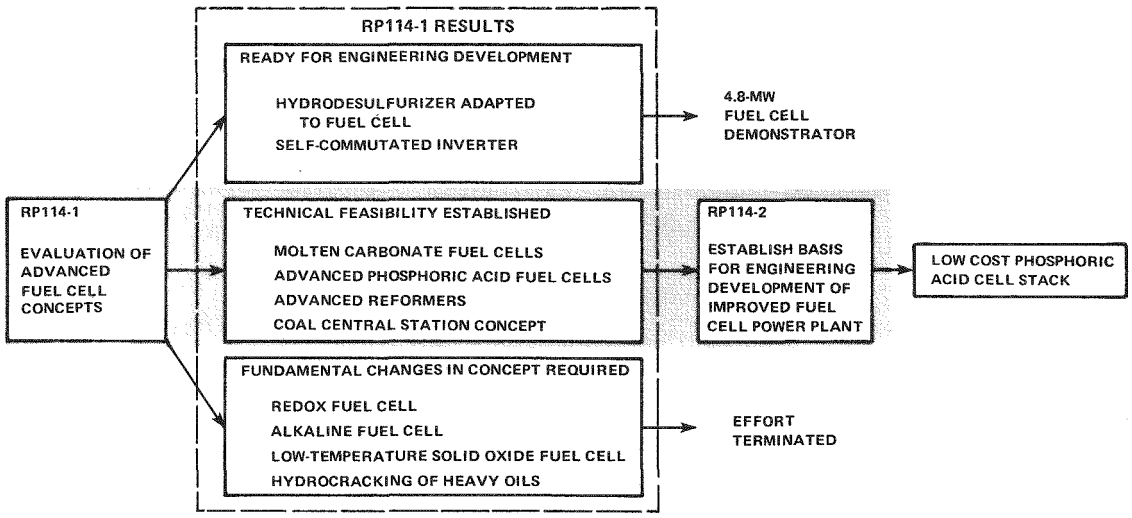

Figure 1-1. Advanced Technology Fuel Cell Program

These activities are carried out in parallel with an effort funded by United Technologies to identify materials, configurations, processes, and designs consistent with these goals. These parallel efforts are managed as an integrated program and are reported accordingly herein. The effort is organized in four tasks dealing with molten carbonate and phosphoric acid fuel cells, advanced reformers, and coal and coal products. Results of these tasks are described in Sections 2 through 5.

SECTION 2

TASK 1 - ESTABLISH BASIS FOR ENGINEERING DEVELOPMENT OF MOLTEN CARBONATE FUEL CELL POWER PLANTS

INTRODUCTION

The molten carbonate cell uses an electrolyte that is a mixture of alkali metal carbonates contained in a ceramic particulate matrix. At room temperature, the mixture is solid and resembles a ceramic tile. At the nominal operating temperature of 1200°F, the carbonates are liquid and are good ionic conductors. The electrodes are porous nickel structures. No noble metal catalysts are used since nickel is active enough at cell operating temperature to act as a catalyst for both the anode and cathode reactions. The cell structural materials are nickel and stainless steel.

The molten carbonate cell is capable of high operating efficiency at high power densities. Design studies conducted in prior programs showed that a 26 MW dispersed power plant based on the molten carbonate cell has the potential to meet the heat rate goal of 7500 BTU/kW. Subscale cells operating at ambient pressure met the performance required to achieve the heat rate goal during last year's reporting period. Studies also showed that the capital cost goals could be met by using pressurized reactant systems. Accordingly, a facility capable of operating to 10 atmospheres was constructed and a single cell test program at elevated pressures was initiated during this period.

Cell development activities focused on establishing cell tolerance to changing operating conditions and reactant gases.

As stated above, the cell operating temperature is nominally 1200°F and the power section must have a capability to withstand thermal cycling between operating temperature and ambient temperature without developing reactant mixing or seal leakage within the power section. Cell configuration studies conducted in a parallel UTC funded program resulted in a design that met this requirement. The validity of the configuration design was assessed in multicell stacks to test the functionality at more realistic conditions and sizes. A highlight of this year's activities was the construction and test of two short stacks with a nominal area

of one square foot. One 8-cell stack to verify thermal cycle capability and a 20-cell stack to verify performance, endurance, and thermal cycle capability were run. Testing was completed on the eight cell stack and the results indicated that the cell configuration was capable of being scaled to one square foot sizes while retaining its thermal cycle capability. The 20-cell stack test is continuing at the end of this report period.

There is concern that power plant operation on low BTU fuel will result in carbon formation and/or methanation, causing efficiency penalties. A test program was conducted in subscale single cells to determine the amount of methanation occurring in cells and carbon formation boundaries up to 10 atmospheres pressure. Only small quantities of either product have been found for the fuel compositions tested to date. We will continue to evaluate these reactions for future fuel compositions.

STACK DESIGN ASSESSMENT

Emphasis during the report period was on verifying the performance, endurance and restart characteristics of the present cell design using one square foot components. Two separate stacks have operated for this purpose:

- An 8-cell stack test which verified large-cell thermal cycle capability was completed during the period.
- A 20-cell stack test to verify performance, endurance, and thermal cycle capability was started late in the period; and this test is in progress.

Components for these stack tests were selected on the basis of successful demonstrations at the subscale cell level, and are discussed in more detail in subsequent sections of this report.

Eight-Cell Stack Evaluation

The 8-cell stack was assembled using one square foot size cell components. The tiles were of two configurations, designated Approaches H and I, and were fabricated by the closed-die molding process; four tiles of each approach were used. Approaches H and I are proprietary electrolyte configurations that offer improved thermal cyclability. Approach H is a proof of principle concept whereas approach I is thought to be cost effective. The electrodes were fabricated to a UTC developed specification by Gould Laboratories, Gould, Inc., who have been the principal supplier of UTC molten carbonate electrodes since 1969. Electrolyte inventory required to accommodate losses through evaporation during stack opera-

tion was provided by storage within the cells. Stack reactant gas separator plates were fabricated by UTC, and passive oxide protection of plate seal surfaces was applied by a local vendor using a UTC developed specification. Current collector components and nonrepeating stack hardware were vendor procured. Initial stack assembly was followed by disassembly and inspection, and showed that tile components remain free of cracks with the assembly procedures used. The 8-cell stack operated for 870 hours, and was subjected to five thermal cycles. The primary objective of this test was met. Figure 2-1 is an elapsed time plot of the test showing that reactant leakage and crossover were unaffected by temperature cycling. It shows that reactant gas crossover rate remained near zero, and that fuel leakage was reduced gradually to approximately 35 ccm independent of temperature cycling (measured at crosspressure differentials of 5" H_2O). This leakage corresponds to less than 1/3-of-one-percent of design fuel flow after the fifth cycle.

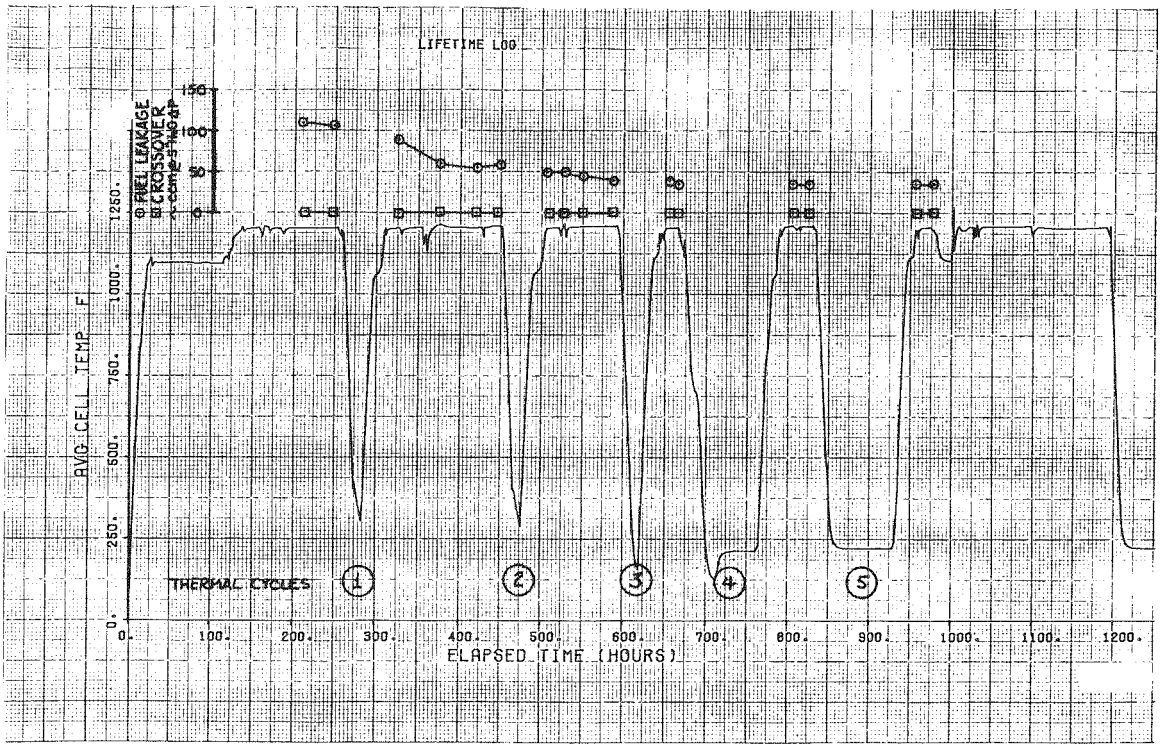

Figure 2-1. 8-Cell Stack Fuel Leakage History

Figure 2-2 is an elapased-time computer printout showing average cell voltage data for the various conditions of average stack temperature and current density at which the stack operated. It shows that the 8-cell stack started and operated with lower performance than subscale cells. The low stack performance was found

to be due to the use of a cathode startup gas which caused atypical cathode oxidation. At an elapsed-time of approximately 1000 hours, the stack cathodes were reduced, and again oxidized in-situ using a more typical cathode gas environment. This procedure produced the nearly 100 mV improvement in average cell performance as shown in Figure 2-2, for the last 200 hours of testing.

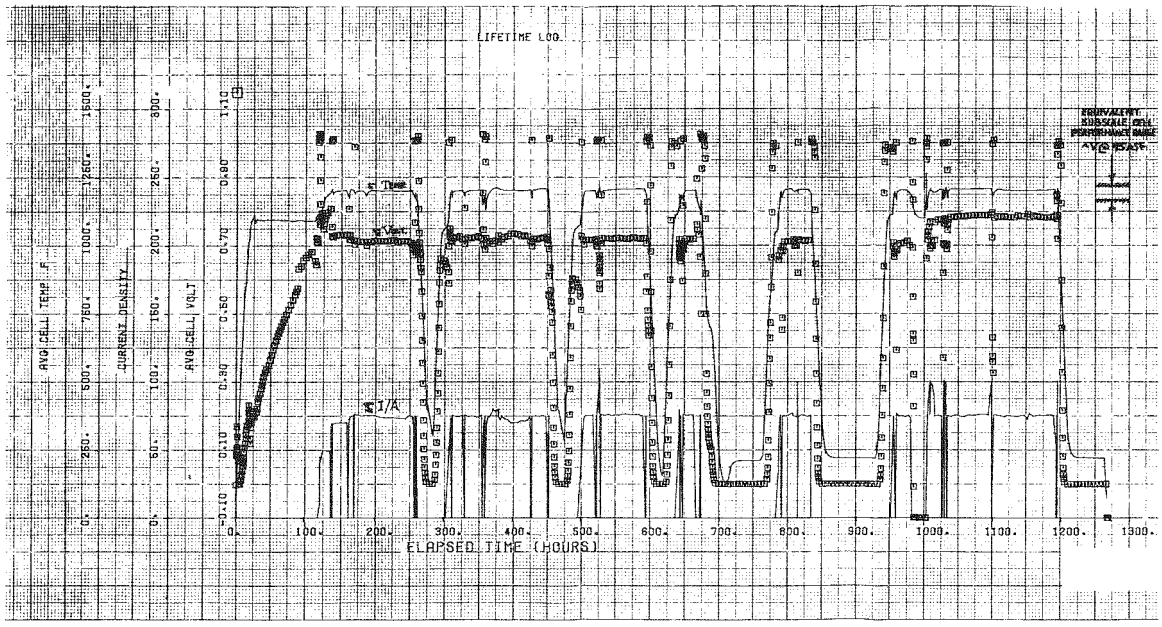

Figure 2-2. 8-Cell Stack Performance History

Figure 2-3 is a plot of individual cell voltage by position in the stack at a current density of 75 ASF. It shows that the reoxidation procedure improved the performance of two cells in the stack to subscale cell levels, and was responsible for the partial recovery of four others. The low initial performance and the differing responses of tile Approaches H and I to the recovery procedure were each reproduced in subscale cells using the same designs.

Diagnostics performed on these subscale cells explained the performance deficiencies of the 8-cell stack, and confirmed that a revised startup procedure was effective and could be used for the 20-cell stack test which followed.

Twenty Cell Stack Evaluation

The 20-cell stack test now in progress uses one square foot size cell components which, except for electrolyte tiles, are identical to the previous 8-cell stack. The 20-cell stack uses tile Approach H in the design arrangement which demon-

strated improved endurance capability in subscale cell testing (Cell 182 discussed in the following section). Figure 2-4 shows the 20-cell stack assembly with oxidant gas manifolds and insulation covering removed.

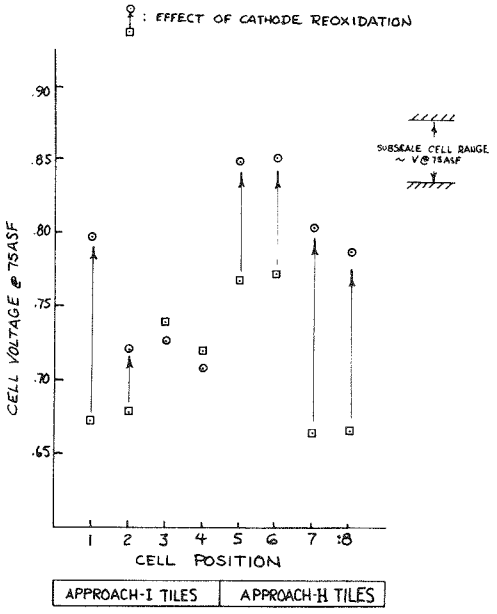

Figure 2-3. 8-Cell Stack Performance Recovery

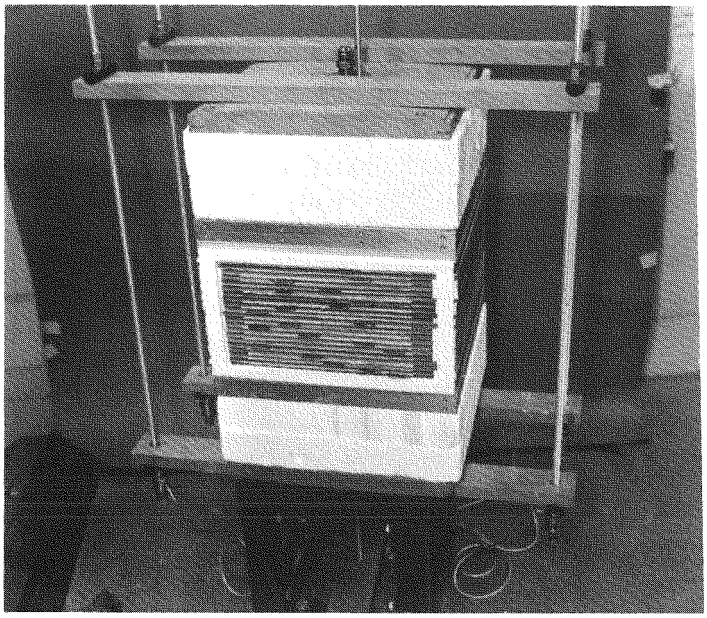

Figure 2-4. 20-Cell Stack Assembly

The 20-cell stack test has been in progress for 650 hours, and the stack is presently being thermal cycled for the first time. Fuel leakage was 120 ccm, or slightly less than 1/2-of-one-percent of design flow prior to the first cycle. On this basis, the low leak rate is comparable to that measured on the 8-cell stack for the same time period.

Figure 2-5 is a plot of individual cell voltages for operation at open circuit and 100 ASF, and of cell iR measured at 100 ASF. It shows that fourteen cells in the stack are demonstrating subscale cell performance levels and internal resistance values (iR) which compare favorably to subscale Cell 214 whose components were subsectioned from 20-cell stack spares. The plotted data also show that six cells in the stack have low performance and high iR values.

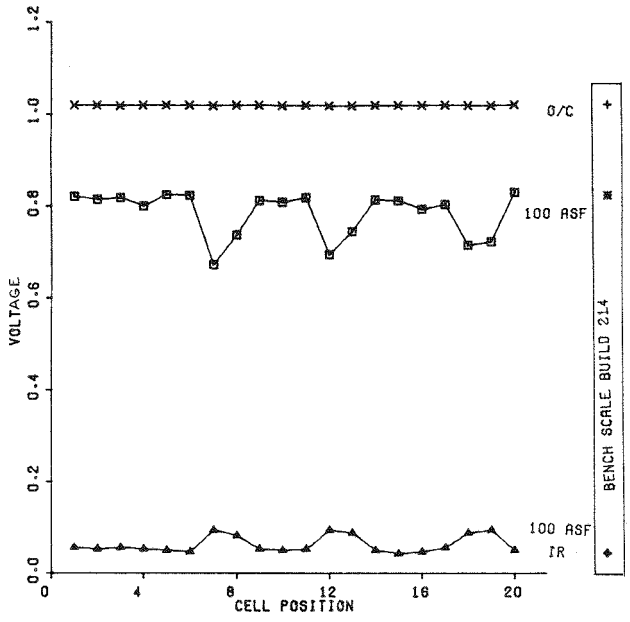

Figure 2-5. 20-Cell Stack Test Performance Comparison

Figure 2-6 is a plot of the minimum to maximum thickness differential for each tile by the cell position in which it was used. The cells with the lowest performance are shown as solid bars. The Figure shows that the low performing cells (7 and 8, 12 and 13, 18 and 19) contain electrolyte tiles with the greatest thickness variation. The tiles used by these cells were also found to be thicker in the center area as compared to the remaining tiles in the stack which were more generally wedge-shaped. These observations may explain the higher internal resistances and the lower performance of the six cells in question.

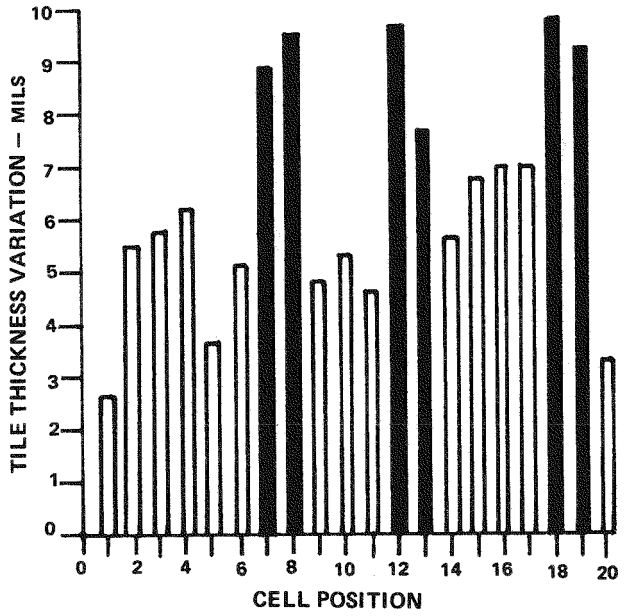

Figure 2-6. 20-Cell Stack Assembly Electrolyte Tile Thickness Variation

Figure 2-7 suggests that tile thickness variation may have a pronounced effect on cell performance. This figure shows the 100 ASF stack performance data given in Figure 2-5 plotted as a function of the tile thickness variation given in Figure 2-6. Cell position is indicated next to each data point. Not only do the deficient cells appear to be affected by the variation, the better cells also show this same trend. The figure serves to highlight the need for improved process control of tile thickness prior to future stack testing. The molding of full-size tiles with greater center-thickness has not been a common occurence, however, and possible reasons for this difference are still under investigation.

Testing of the 20-cell stack will be continued in an extension of the RP114-2 Program; five thermal cycles and 2000 hours of operation are planned. Figure 2-8 shows this 20-cell stack test in progress.

CELL FUNCTION

The acceptability of cell configurations and tile designs for fabrication development depends on their thermal cycle capability in stack size components. The configurations and tile designs now being tested in stacks are based on the demonstrated success of subscale cell tests, and have come about through the modified tile approach which continues to be the primary program effort.

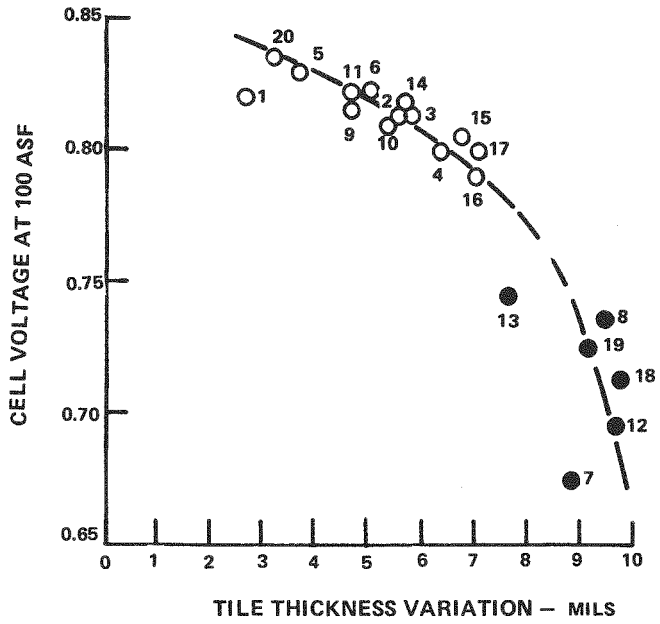

Figure 2-7. 20-Cell Stack Test Cell Performance vs. Tile Thickness Variation

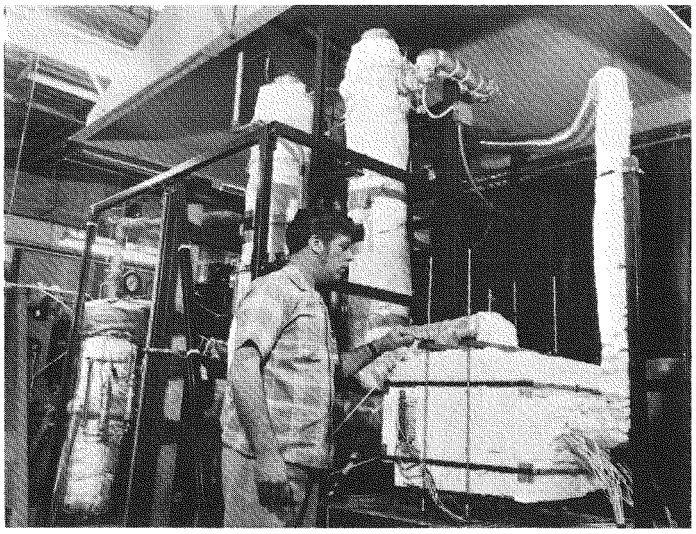

Figure 2-8. 20-Cell Stack Test

During this report period, subscale cell test activities were directed at evaluating cell components designed for improved thermal cycle capability. Prior program efforts resulted in an electrolyte tile that had adequate initial bubble pressure, provided electrolyte transfer from electrode to tile and retained its initial electrolyte inventory. Cells which met these requirements were described

in Reference 4. Since practical cells must also be capable of multiple thermal cycles associated with shutdown and restart, thermal cycle tests on cells with the improved tile were conducted. The principal criteria for a successful thermal cycle are that the cell maintain its ability to contain reactant gases and that cell performance is not affected. The initial test results from cells using the improved tiles were that the cells came close to satisfying the performance stability objective through a cycle, but adequate gas sealing and crossover protection (bubble pressure) were not maintained through multiple starts.

Mechanical property measurements and structural analysis of the prior electrolyte tile, conducted in the parallel UTC funded program, predicted that stresses due to differing thermal contraction rates among components during a thermal cycle would exceed the fracture strength of the tile. This study showed that the tile could be expected to crack in cooldown. The results of subscale cell tests and out-of-cell component tests confirmed these predictions. The tile and cell configuration modifications investigated during this report period were based on these findings.

A total of 75 subscale cells were evaluated during this report period. The average operating time for these cells was 1200 hours. The test procedure for these cells included periodic determination of the tile's bubble pressure using the method described in Reference 4. Upon loss of crossover protection, cells were "burned-in" prior to shutdown. Cells with no bubble pressure are "burned-in" by operating with 5 inches of H_2O oxidant-to-fuel overpressure for 24 hours before termination. This technique has provided a means of determining the location of crossover in cells. At teardown, the anodes are inspected for localized oxidation caused by the oxidant gas coming in contact with the nickel anode at the crossover point(s). In addition to this procedure, microscopic inspection of all electrolyte tiles is made to determine the incidence of cracks and their locations.

Teardown inspection of cells tested early in this report period confirmed the thermal stress analysis and proved that tile cracking was the failure mode. All twenty-six cells tested during the first 6 months of this report period contained cracks in the active-area or the wet seal area of the tile. Sixteen of these cells had observable "burn" marks on the anodes.

Eleven tile approaches were evaluated during this report period and the results are summarized in Table 2-1. Thermal cycling tests were conducted on all but two of the approaches. No cell was successfully thermal cycled more than two times until the successful demonstration of cells using Approach H. A successful thermal cycle is one in which a cell having 10 psi bubble pressure shows no change in bubble pressure after the thermal cycle. Significant improvement in thermal cycle capability was obtained with cells using Approach H and later Approach I tiles. A thermal cycle summary of cells using these modified tiles is shown in Table 2-2.

Table 2-1
SUMMARY OF VARIOUS TILE APPROACHES EVALUATED

Tile Approach	Number of Cells	Number Cells Cycled
A	21	15
C	4	2
D	7	0
E	4	2
F	5	4
G	2	1
H	14	9
I	12	5
J	3	2
K	2	0
Configuration Modification	1	1

Table 2-2
THERMAL CYCLE SUMMARY

Cell No.	No. of Successful Thermal Cycles	Tile Approach
167	10	H
169	4	H
171	1	H
175	6	H
176	8	H
182	12	H
187	5	H
207	2	H
208	11	H
152	0	I
189	8	I
192	2	I
193	3	I
194	2	I

Teardown inspection results for cells using Approach H or I tiles are shown in Table 2-3. Except for Cell No. 167, no Approach H tile cell contained wet seal edge or active area cracks, indicating that the loss of bubble pressure was due to some other mechanism. The six cells which were "burned-in" showed crossover in the wet seal area. The probable mechanism for electrolyte loss in this area is corrosion of the tile modifying material in the edge seal area.

Table 2-3
TEARDOWN INSPECTION RESULTS

Cell No	Tile Approach	No. T/C's	Burn-In	Burn-Marks	Tile Cracks
167	H	10	Yes	None	Edge
169	H	5	Yes	Yes	None
171	H	2	No	Not Inspected	Not Inspected
175	H	7	Yes	Yes	None
176	H	8	Yes	Yes	None
182	H	12	Yes	Yes	None
187	H	7	Yes	Yes	None
207	H	2	On Test		
208	H	11	On Test		
152	I	1	Yes	Yes	Body and Edge
189	I	9	Yes	None	None
192	I	3	Yes	Yes	Body and Edge
193	I	4	Yes	Yes	Body and Edge
194	I	3	Yes	None	None

Although cells using tile Approach I also demonstrated increased thermal cycle capability over earlier tile approaches, active area and/or wet seal tile cracks were observed in 3 out of the 5 cells following multiple thermal cycles. The failure mode for these cells is believed to be due to gradual corrosion of the tile reinforcing material which provided a crossover path through the tile. The time dependency of this mechanism was verified on two uncycled (196 and 201) cells using tile Approach I which lost bubble pressure in the same time period as cycled cells. This is shown in Figure 2-9, which summarizes the bubble pressure measurements made on cells evaluating Approach I tiles. The figure shows bubble pressure as a function of time with the number of thermal cycles on each cell also recorded. As shown by this figure, cells using Approach I tiles lost bubble pressure within a time period ranging from 200 to 1800 hours, independent of the number of thermal cycles. A number of cells using tile Approach I are not shown in Figure 2-9 because they included variations in the amount or type of tile reinforcing material used.

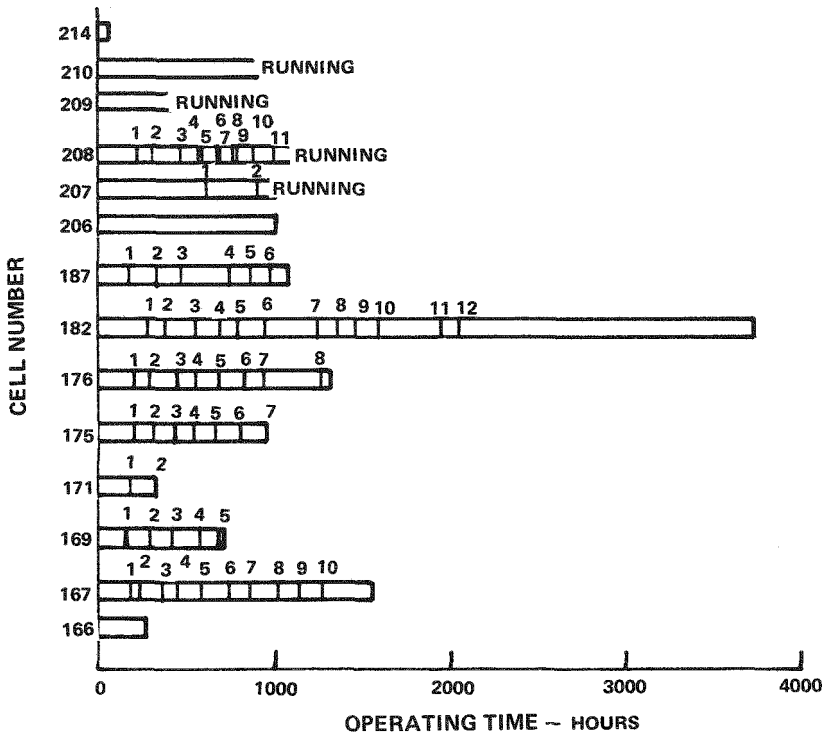

Figure 2-9. Cell Operating Time Until Loss of 10 psig Bubble Pressure (Type I Tile Approach)

Similarly, Figure 2-10 summarizes the bubble pressure measurements made on cells using Approach H tiles. It shows that the loss of bubble pressure in these cells was also time dependent, the time ranging from 250 hours to over 3000 hours. These cell tests and post-test findings continued to confirm that cells using either electrolyte tile Approach H or I have thermal cycle capability and that a common material deficiency has been responsible for their loss of bubble pressure.

Further evidence of the material deficiency is Cell No. 182 which uses Approach H but in a design which minimizes corrosion of the tile reinforcing material. Figure 2-11 shows the bubble pressure history of this cell compared to the best history of cells which use either Approach H or I alone. The figure shows that this design approach extended the useful life of the cell by an additional 2000 hours but did not eliminate the deficiency. This cell demonstrated that the cause of edge failure is understood and can be minimized. Because of the extended endurance capability offered by this tile and cell design, it was selected for evaluation in the 20-cell stack test now in progress.

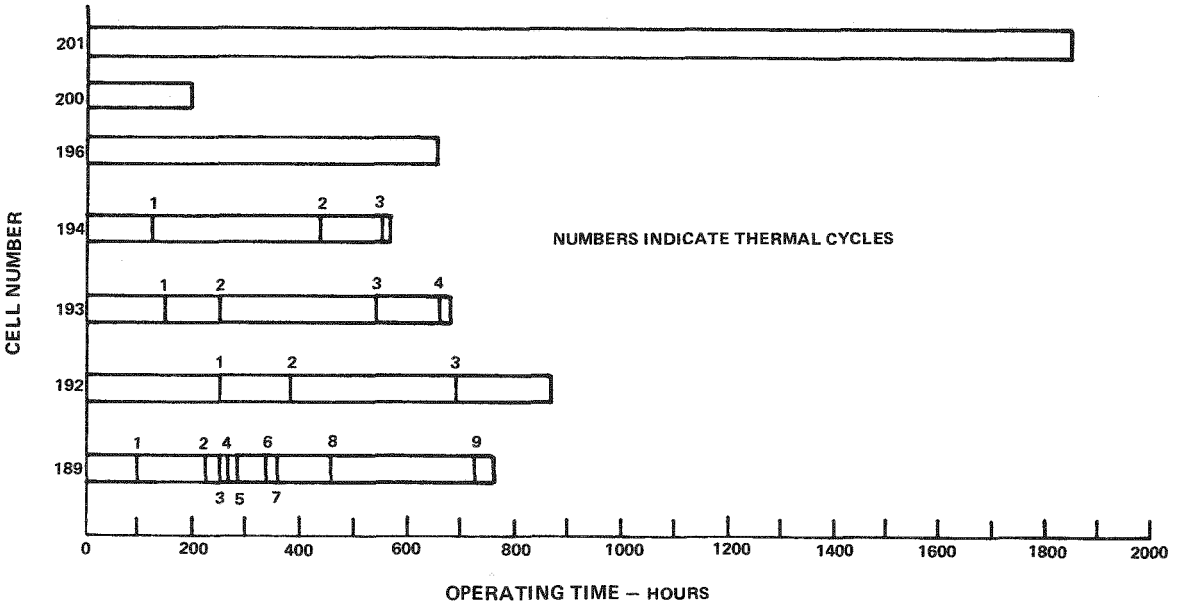

Figure 2-10. Cell Operating Time Until Loss of 10 psig Bubble Pressure (Type H Tile Approach)

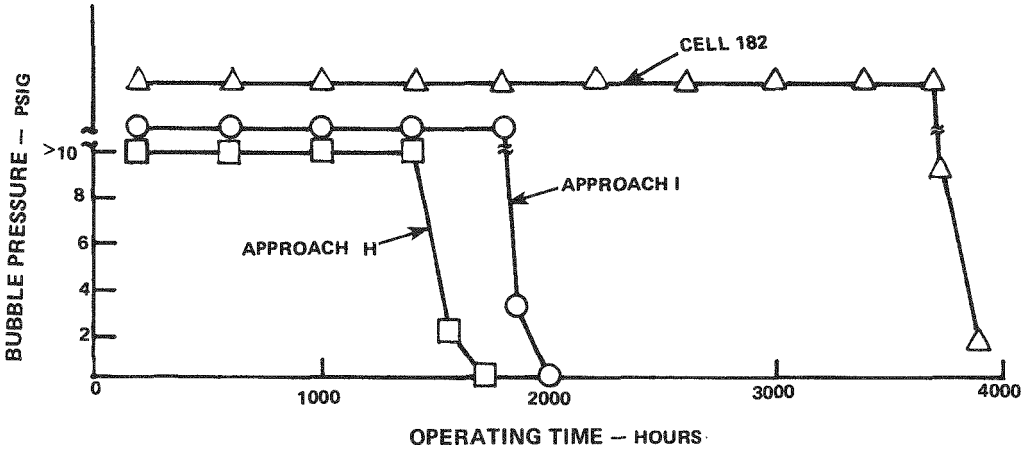

Figure 2-11. Cell 182 Bubble Pressure History vs. Best Approach I & H History

Also of interest is Cell No. 208 (Figure 2-10) which contains a half-thickness version of tile Approach H. After 1000 hours of operating time and 11 thermal cycles this cell retains >10 psig bubble pressure, indicating that reduced tile thickness needed for improved cell performance does not detract from thermal cycle capability.

A number of cells using tile Approach H, but evaluating alternate cell configurations, are not included in Figure 2-10. However, Cell Nos. 206 and 207 which were started to qualify the procedures used in heating and operating the 20-cell stack are included. The revised startup procedure qualified by these cells differed from that used in the eight-cell stack test after finding that the procedure was the primary cause of the low performance for that experimental configuration.

Five cells using more recent approaches than H and I have also been tested. Of the three cells using Approach J tiles, Cell No. 204 operated for over 800 hours and was successfully thermal cycled 9 times. This approach is of particular interest since it appears to offer the highest probability for simultaneously satisfying cost objectives and thermal cycle capability. Development of this approach is being continued in light of the favorable results obtained.

As shown in Figure 2-12, significant improvement was made in cell thermal cycling capability. The material deficiency which caused the loss in bubble pressure in the cells containing tiles of Approach H and I was identified. Two cost-effective alternative structures are presently under evaluation in cells using Approach I tiles.

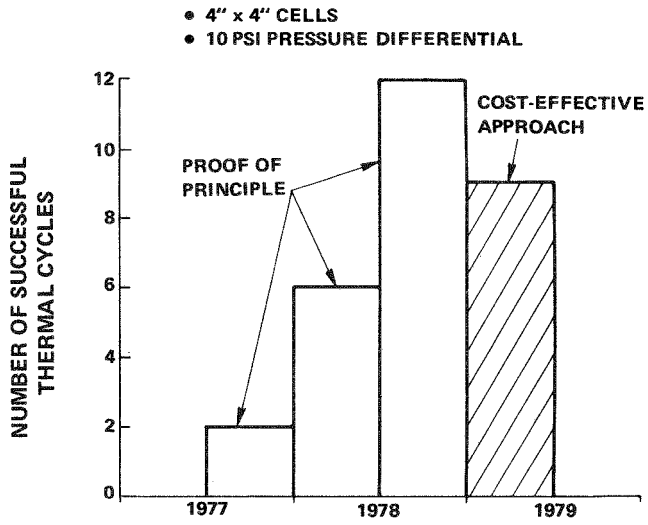

Figure 2-12. Best Single Cell Thermal Cycling Experience

In addition to the effort on modified tiles to improve the cell's thermal cycle capability, effort was continued on the fabrication and evaluation of cell configurations using alternative electrolyte retaining structures. This work has been carried out under a program funded by the Niagara Mohawk Power Corporation and the UTC funded parallel program.

PRESSURIZED SUBSCALE CELL TEST

A four-station pressurized test facility was constructed during this report period, and subscale cell testing to operating pressures of 10 atmospheres was begun.

Figure 2-13 shows the schematic flow diagram of a single test station. Each station is capable of operating up to 150 psia, with the blanket gas serving as the system reference pressure. Fuel and oxidant feed pressures to the cell are controlled against the blanket pressure reference and each pressure is maintained to within 0.5" H_2O of the absolute setting. The reactant gas pressure system is self-adjusting to allow unattended operation at any set point from ambient to 150 psia. Any operating parameter can be varied within the range shown in Figure 2-13. This flexibility permits diagnostic tests to be performed at various cell pressures, pressure differentials, temperatures, reactant flow rates, reactant compositions and cell current densities. Portable test equipment is used for vent gas analysis, internal resistance measurements and operation on special gas mixes. Each cell test is monitored by computer, automatically storing operational test data. Various software programs are available for data retrieval and correlation analysis.

Figure 2-14 shows a cell being mounted in the test station. Each cell is started at ambient pressure using the same schedule as ambient pressure subscale cells. Once operating, cell reactant gas and blanket gas pressures are raised to the desired level. The cell is then evaluated on different fuel gas compositions simulating the effluent of different fuel processor designs.

Figure 2-15 summarizes the test programs conducted on the 10 cells evaluated at pressure during this report period. Cell test objectives fell into one or more of the following test categories:

- Performance analysis
- Carbon formation studies
- Methane formation studies
- IR studies

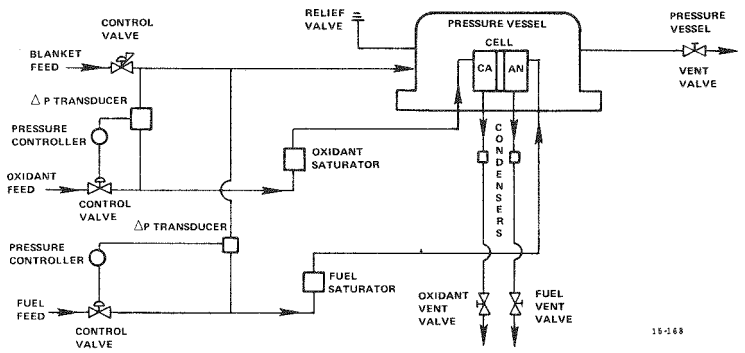

AUTOMATIC CONTROL FUNCTION	RANGE MINIMUM	RANGE MAXIMUM
PRESSURE LEVEL	AMBIENT	150 PSIG
PRESSURE DIFFERENTIAL	−10 IN. H_2O	+10 IN. H_2O
TEMPERATURE	AMBIENT	1350°F
CURRENT	0	30 AMPS
FUEL FLOW	PURGE RATE	< 10% AT 300 ASF
FUEL SATURATOR TEMPERATURE	AMBIENT	400°F
OXIDANT FLOW	PURGE RATE	< 10% AT 300 ASF
OXIDANT SATURATOR TEMPERATURE	AMBIENT	400°F
OPERATING MODE	MANUAL SETTING	AUTO. OUT OF LIMIT ACTIONS
DATA RETRIVAL	METER DISPLAY	COMPUTER PRINTOUT

Figure 2-13. Pressurized Subscale Cell Test Stand Schematic

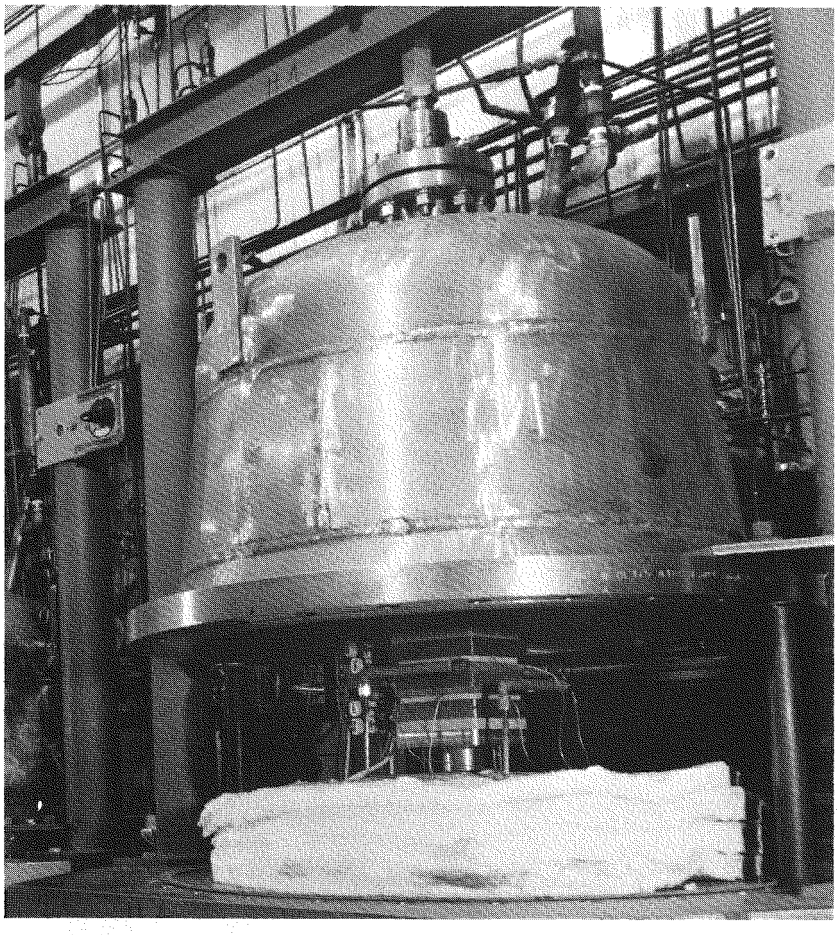

Figure 2-14. Pressurized Subscale Cell Being Mounted in Test Stand

Cell Number	Operating Time (Hours)	Pressure Level (PSIA)	Test Objective
165	680	45	Performance Analysis and Carbon Formation Studies
168	150	75	Performance Analysis
172	1500	75	Performance Analysis and Methane Formation Studies
173	1110	75	Performance Analysis
181	1500	75	Performance Model Studies
185	435	75	Carbon Formation Studies
186	600	75	Performance Model Studies
190	845	75	Performance Model Studies
205	1640	150	Performance Analysis and Methane Studies
213	930	75	IR Studies and Endurance Analysis

Figure 2-15. Pressurized Subscale Cell Test Programs

Performance data are obtained from cells operated over a range of current densities, gas compositions and reactant utilizations. Cell temperature and pressure may also be varied during the test. This performance program is designed to provide data for the mathematical models used in various UTC system studies.

The carbon formation studies involve setting fuel feed conditions over a composition range which will permit a comparison of actual and thermodynamic carbon boundaries.

Methane formation studies are conducted by analyzing the fuel vent gas with a gas chromatography over a range of operating temperature, pressure and current density for various fuel gas feed compositions.

IR studies are conducted on cells using isolated voltage probes to separate the contributions of individual components from overall cell iR.

The results of the above test programs are discussed in the sections which follow.

COMPARISON OF PRESSURIZED CELL PERFORMANCE AND MODEL PREDICTIONS

The operation of subscale cells at pressure provided the opportunity to test the suitability of the fuel cell model. This model had been developed in prior programs as a device for developing cell diagnostics and performance prediction and extrapolation.

Initial work was carried out with a synthetic reformed naphtha fuel (MCF-1) saturated sufficiently to be outside the thermodynamic carbon formation region. This method of operation, however, resulted in a different fuel gas composition with each pressure so that the sole effect of pressure on performance could not be determined.

This problem was subsequently resolved with the testing of two different types of autothermal reformer (ATR) fuel. In each of these cases it was possible to keep the water mole fraction (and hence gas composition) fixed at the design level and still be far removed from carbon formation.

Table 2-4 lists the various dry fuel gas compositions and other pertinent test information.

Table 2-4
CELL TEST INFORMATION

Test Test Gas Process Simulated Cooling Mode	MCF-1 Ambient Pressure CSR 3 Pass Cathode	ATR-43 Pressurized ATR 3 Pass Cathode	ATR-13 Pressurized ATR Anode Recycle
Composition			
H_2 Vol % dry)	71.5	43.3	13.8
CO "	13.8	10.5	3.2
CO_2 "	14.7	14.0	52.0
N_2 "	----	32.2	31.0
Water Content Vol. %	28.4 at 1 atm 37.2 at 3 atm 58.8 at 5 atm	41.4 at all pressures	48.3 at all pressures
Fuel Utilization, % $\frac{(H_2 + CO)cons}{(H_2 + CO)_{in}}$	49.2 at 100 ASF 78.7 at 169 ASF	25 & 85 at all ASF	59.1 at all ASF
Oxidant Composition	MCO-2	MCO-2	MCO-2
O_2 (vol % dry)	12.6	12.6	12.6
CO_2 "	18.4	18.4	18.4
N_2 "	69.0	69.0	69.0
Water Content, vol %	7.1	7.1	7.1
CO_2 Utilization, %	19.8 @ 100 ASF 31.7 @ 160 ASF	31.7 at all ASF	31.7 at all ASF
Cell Temperature 1200°F			

The mathematical model was utilized to predict absolute cell performance and performance changes for the systems tested. The model predictions are represented by the solid lines in Figure 2-16 through 2-20 with the data points giving the actual cell results.

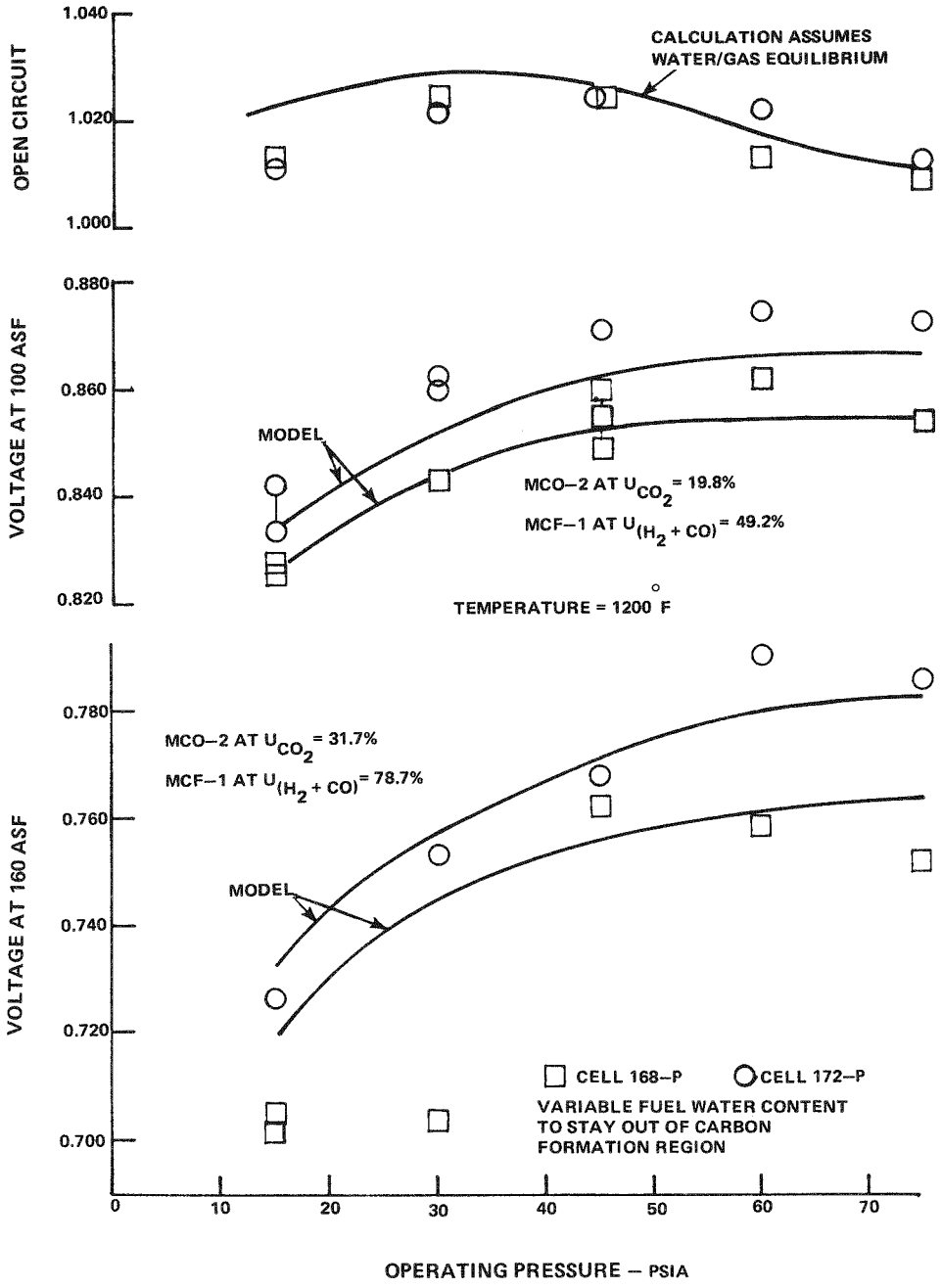

Figure 2-16. Performance vs. Pressure and Variable Fuel-Gas Composition at O/C, 100 ASF and 160 ASF for MCF-1

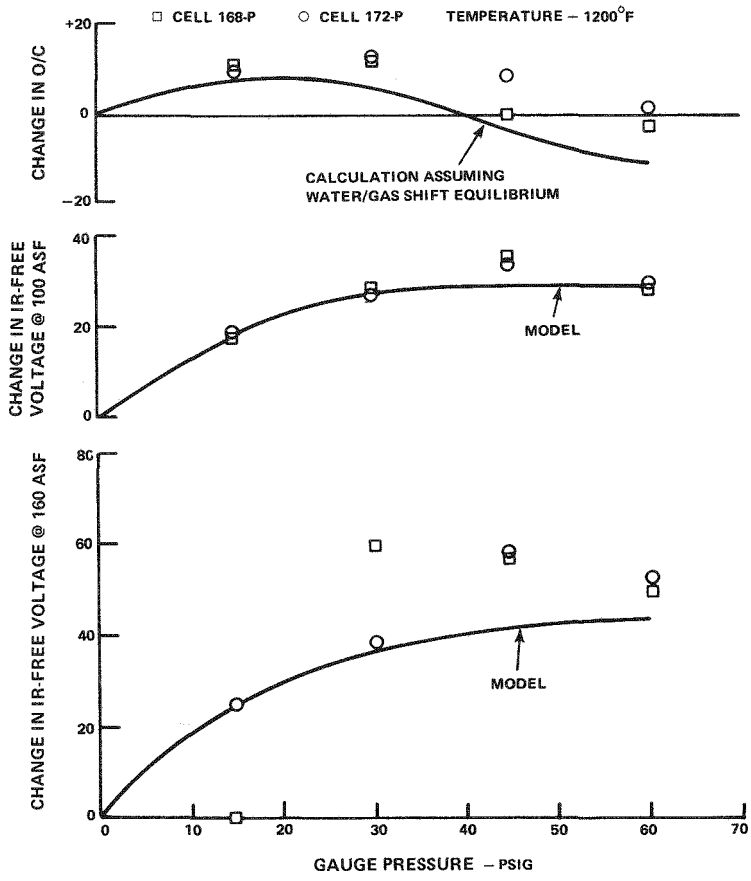

Figure 2-17. Changes in Performance vs. Pressure and Variable Fuel Gas Composition at O/C, 100 ASF and 160 ASF for MCF-1

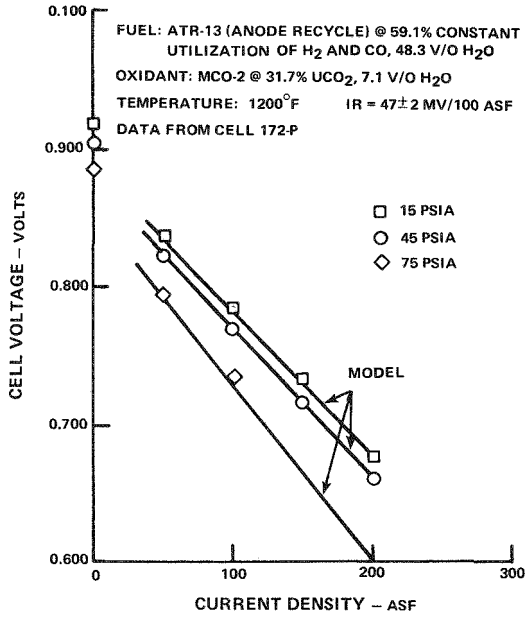

Figure 2-18. Cell Voltage vs. Current Density at 15, 45 and 75 psia for ATR-13 at 59.1% H_2 and CO Utilization

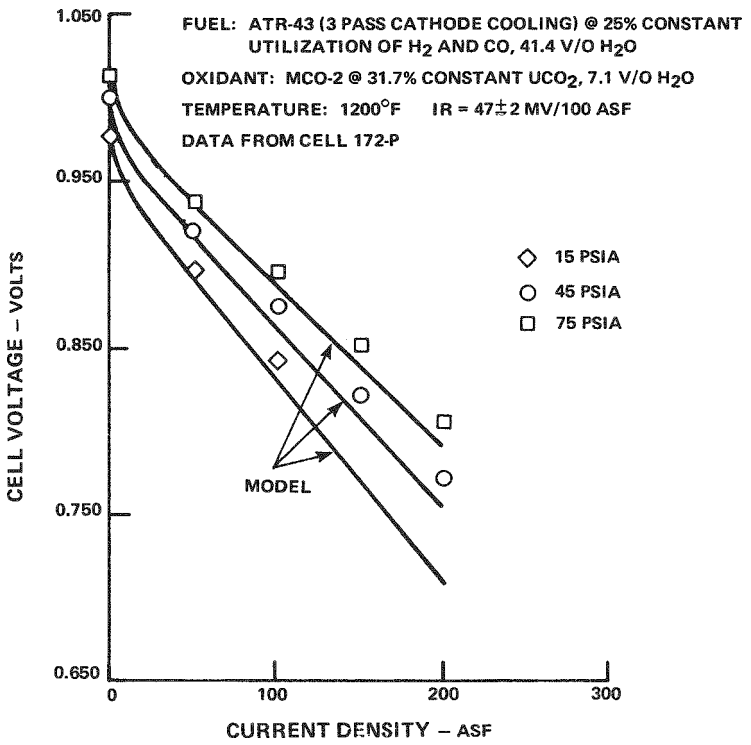

Figure 2-19. Cell Voltage vs. Current Density at 15, 45 and 75 psia for ATR-43 at 25% H_2 and CO Utilization

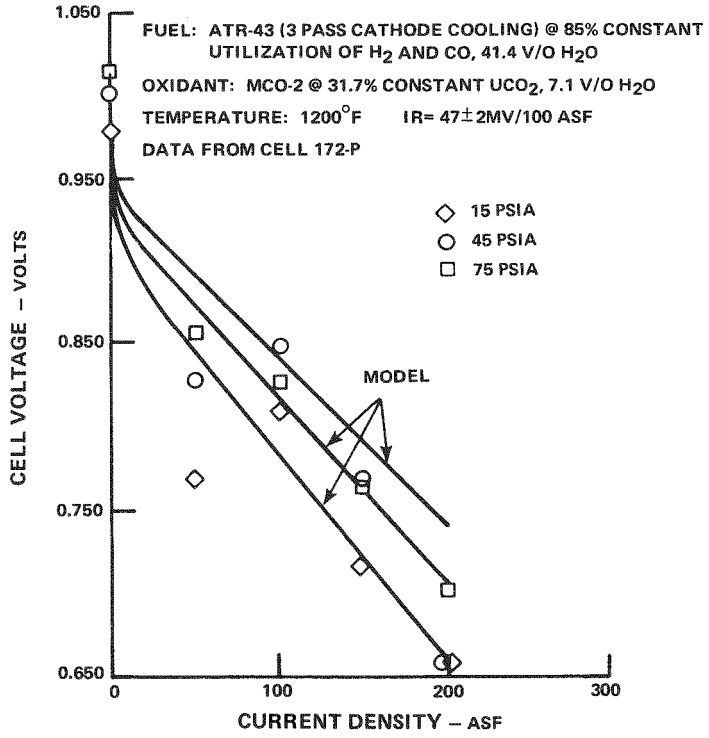

Figure 2-20. Cell Voltage vs. Current Density at 15, 45 and 75 psia for ATR-43 at 85% H_2 and CO Utilization

In addition to these tests, the performance as a function of temperature was compared to the model. These results are shown in Figure 2-21. The results of these tests demonstrate a good match between the predictions of the model and actual cell performance both at ambient and elevated pressure. This allows the model to be used to calculate cell performance over a wide range of operating parameters with confidence.

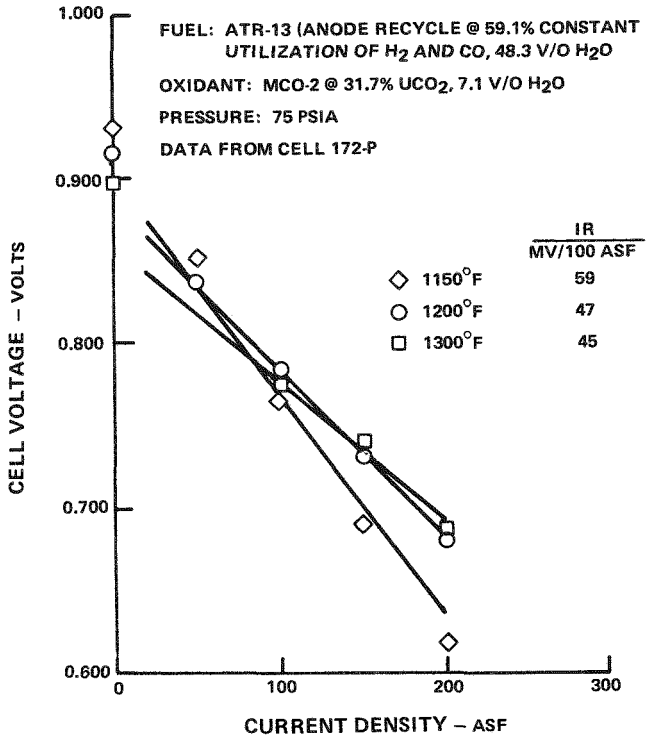

Figure 2-21. Cell Performance as a Function of Temperature

METHANE FORMATION

Several gas phase reactions are theoretically possible at the anode of a molten carbonate fuel cell. Equilibrium favors the formation of methane at the cell inlet conditions, shifting of CO to CO_2 throughout the cell, and reforming of methane to H_2 at the cell exit conditions. The methanation reaction was of primary concern since it can reduce the amount of H_2 available to generate power in the fuel cell, and thus directly increases the power plant heat rate.

Systems studies showed that methanation could be prevented by recycling a portion of the anode vent gases to the anode inlet. Sufficient H_2O and CO_2 can be added to the fuel gas by this means so that equilibrium no longer favors the formation of methane. However, the recycle gases dilute the fuel gas reducing the average

H_2 partial pressure, therby reducing the cell performance. With the lower performance, the total cell area must be increased to achieve the design heat rate. For typical power plant conditions, anode recycle to prevent menthanation increases the power plant cost about 10%. A program was undertaken to determine the amount of methanation that actually occurs in cells. This information was needed to determine the amount of recycle actually required and to optimize the system to minimize power plant costs.

The methanation reaction was studied by measuring the gas composition of the anode vent from a subscale molten carbonate fuel cell as a function of input fuel and operating conditions. The CH_4, CO, and CO_2 in the anode vent gases were measured by means of a gas chromatograph, a Fisher Gas Partitioner Model 25V. This gas analysis equipment is used routinely to measure the gas composition of fuel gas produced from catalytic steam reformer and autothermal reformer rigs operating at similar temperatures and pressures. Measurements taken were at cell temperatures of 1100°F to 1300°F, and at pressures from ambient to 10 atmospheres. The gas compositions were measured at open circuit, where methane formation is most favored, and on load at anode flow rates typical of power plant design conditions. Tests on load were run at fuel flows to provide 76% fuel utilization. Tests were run with fuel gas compositions representative of catalytic steam reforming of naphtha, (MCF-1), autothermal reforming of distillate fuels (ATR-43) and a methane rich synthetic mix. The gas compositions of these fuels are listed in Table 2-5.

Table 2-5
TEST GAS COMPOSITION

Gas	MCF-1	ATR-43 (Vol % Dry)	Methane Rich Gas
H_2	71.5	43.3	70.4
CO	13.8	10.5	0.9
CO_2	14.7	14.0	22.5
CH_4	----	----	6.2
N_2	----	32.2	----

Starting with MCF-1 or ATR43 the amount of methane in the anode vent was less that detection limit of the gas analyzer from ambient to three atmospheres pressure. With the methane rich gas, the methane content in the anode vent was the same as the feed gas even on load at 1300°F where reforming would be most likely. The conclusion from these results is that at 3 atmospheres pressure and below, the activity (reaction rate) is so low that neither methanation nor reforming reactions are significant.

At pressures from 5 to 10 atmospheres a small amount of methane was found in the anode vent gas. Typical results at 10 atmospheres, where the amount of methane was the highest, is shown in Figure 2-22. At open circuit the maximum methane measured was less than 0.5%. The methane concentration was essentially independent of temperature. The measured methane was only 6% of equilibrium at 1097°F and increased to 26% of equilibrium at 1285°F (the concentration is constant but the equilibrium concentration decreases with temperature). At 1285°F, decreasing the anode flow from 300 cc/min to 200 cc/min increased the methane concentration from 0.35% to 0.47%. At lower temperatures the measured increase was less. The most significant result was that on setting the load to consume 76% of the inlet H_2 plus CO, the methane concentration decreased to 0.1% or less at all temperatures.

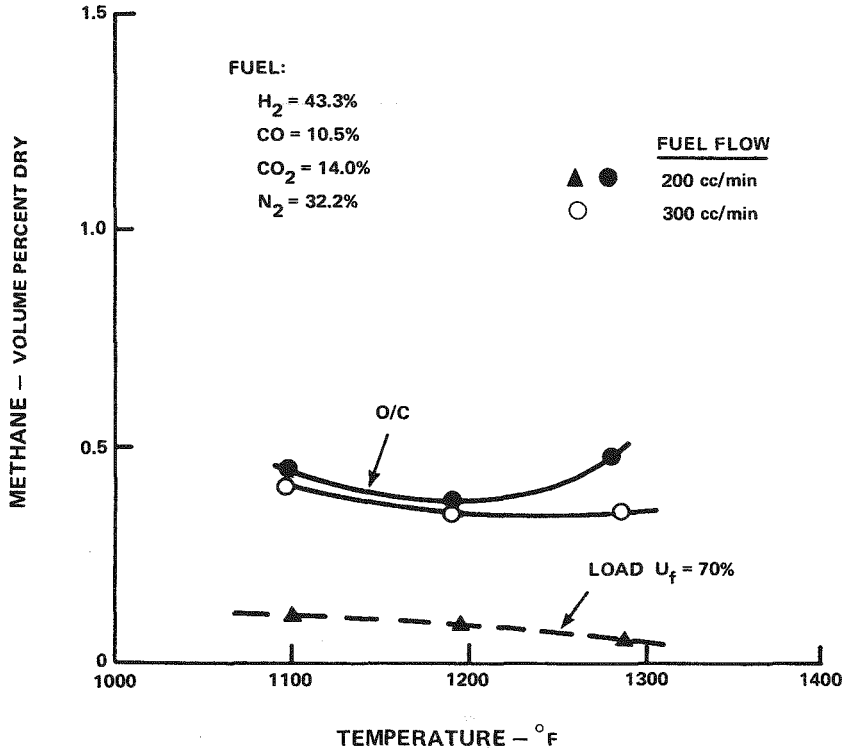

Figure 2-22. Methanation at 10 ATM

At open circuit conditions (zero load) there is no H_2 consumption or H_2O and CO_2 production in the fuel gas as it flows through the anode. Under these conditions the cell acts as a differential reactor and the methanation reaction rate can be calculated from the measured CH_4 in the anode vent gas. A first order reversible reaction rate equation was assumed. The methanation reaction rates were calculated from the experimental data at open circuit. The results follow a typical Arrhenius curve, as shown in Figure 2-23. Even though the measured CH_4 was essentially constant, the reaction rate increased with increasing temperature due to the decrease in the equilibrium concentration of CH_4 with increasing temperature. Within the limited range of the test data there was no effect of pressure, fuel flow rate, or fuel gas composition on the measured reaction rates.

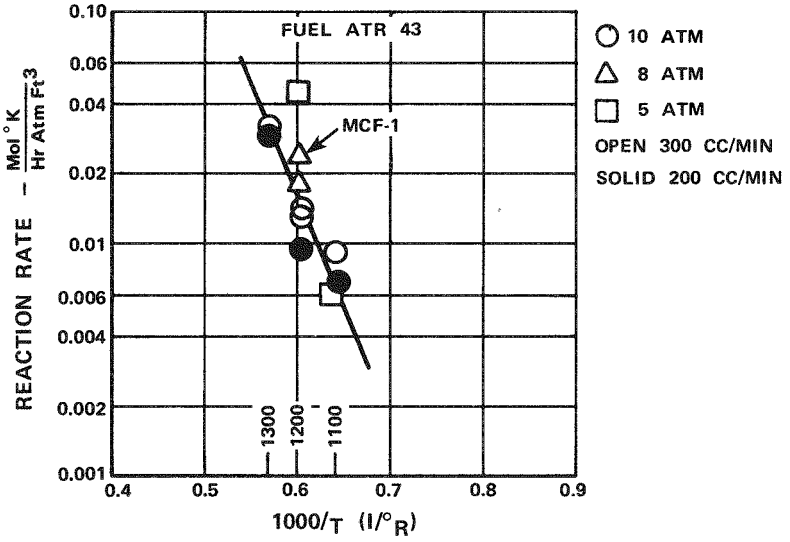

Figure 2-23. Methanation Reaction Rate

A cell on load consumes H_2 from the fuel gas. For each volume of H_2 consumed an equal volume each of H_2O and CO_2 are produced in the fuel gas. This change in fuel gas composition reduces the equilibrium CH_4 composition as H_2 is consumed. While this does not change the reaction rate, it does reduce the driving force. Thus, the CH_4 in the anode vent should be less on load than at open circuit. The effect of load was investigated analytically by calculating the CH_4 distribution in the anode compartment by an incremental method. The cell performance model was used to calculate the current distribution, thermodynamic equations to determine the equilibrium CH_4 distribution, and the methanation reaction equation and rates to calculate the actual CH_4 concentration based on kinetics.

The results of the calculations are shown in Figure 2-24. The estimated (kinetic) CH_4 content is compared to the equilibrium CH_4 content along the length of the anode passage at open circuit (dashed lines) and on load (solid lines). At open circuit the kinetic CH_4 content increases linearly from the inlet to the exit value of 0.36%. This matches the measured CH_4 in the anode vent since the reaction rate was calculated from this data. At the load condition of 100 ASF and a fuel flow for 76% utilization, the equilibrium is reduced from 3.97% at the inlet to 0.03% at the exit. At the cell inlet the rate of methane formed on load is almost the same as at open circuit. As shown, the rate of formation decreases with distance along the anode until it reaches zero at 90% of the way through the anode where the estimated CH_4 level equals the equilibrium value. Beyond this point the equilibrium CH_4 content is below the kinetic value and the model predicts that reforming will occur. The amount of reforming is very small since the difference from equilibrium is very slight. The significant fact is that the CH_4 content estimated by this incremental procedure is within 0.02% of the measured value of 0.09% Thus, the model confirms that the measured decrease in methanation with load is real and the amount of methanation at 10 atmospheres will have an insignificant effect on power plant operation. In summary, the methanation rate is very slow in molten carbon cells and the model can be used to estimate the effect of operating conditions on the amount of methane formed.

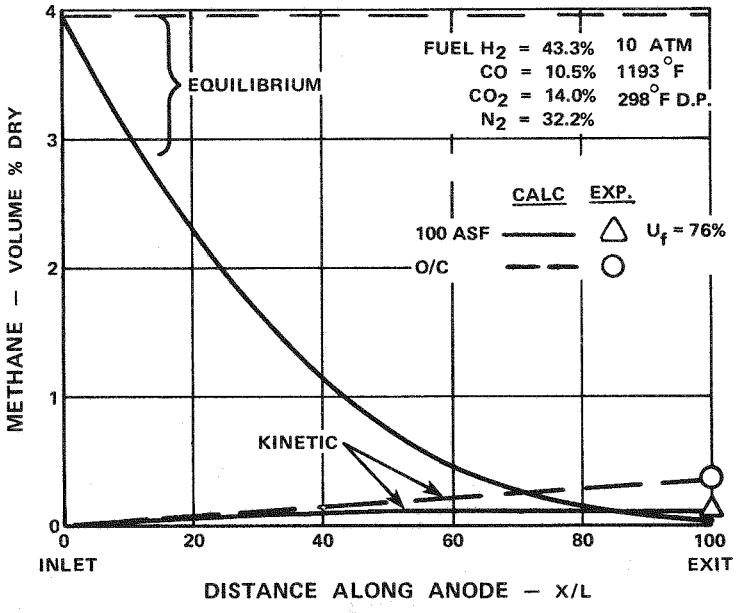

Figure 2-24. Methane Concentration Profile

Previous cell experience has shown that the shift reaction is very fast in the anode compartment. Measurements of the CO in the anode vent during the methanation tests confirm this fact. At all conditions tested the exit CO was close to the equilibrium value as shown in Figure 2-25. In general the measured values are slightly below the equilibrium values. This is not a kinetic effect but must be a slight measurement or test error since there is no consistent variation with any of the test conditions, even with the high CO fuel gas for which the CO should approach but always be slightly above the equilibrium value. The data also shows that the reaction is very fast whether in the forward or reverse direction. The tests discussed above were carried out with cells early in life. Futher effort is needed to confirm that these encouraging results prevail over the 40,000 hour required life and for all gas compositions.

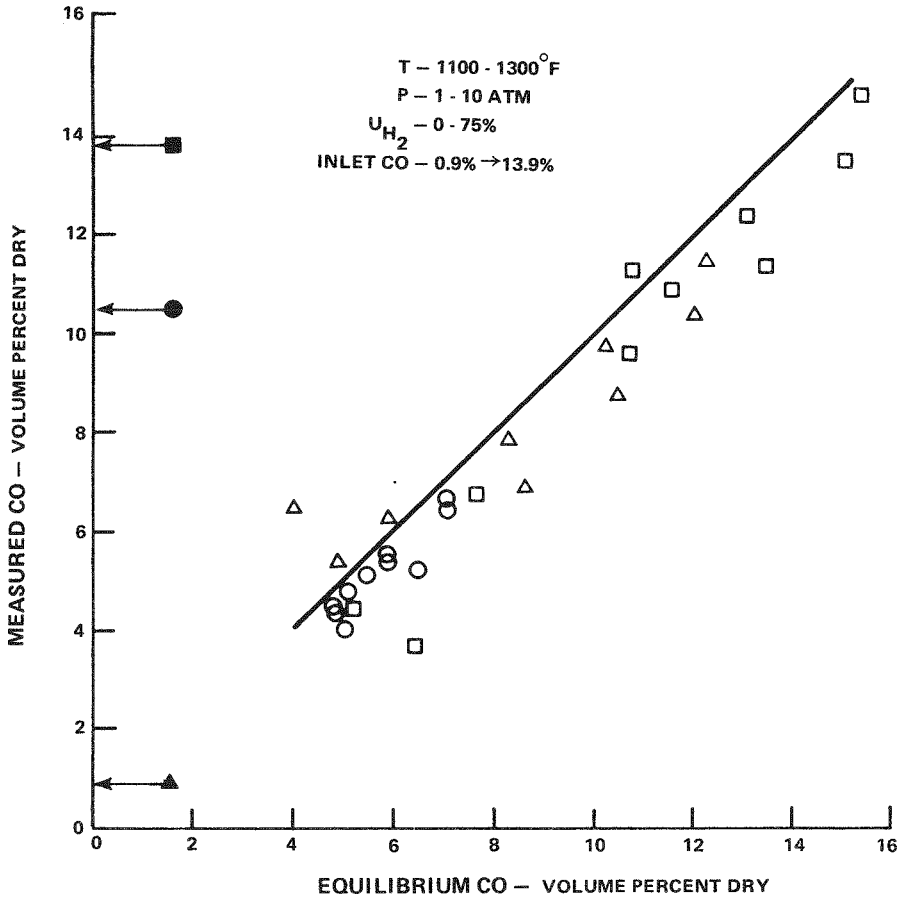

Figure 2-25. Shift Reaction Data

CARBON FORMATION

Carbon formation has occurred in molten carbonate fuel cells on several occasions, usually as a result of an accidental decrease in the moisture content of the inlet fuel gas. The conditions at which carbon formation started in these instances was not documented. While the system can be designed to operate outside the carbon limits, the actual boundary condition need to be determined since they can have a significant impact on the system configuration and cell performance.

The theoretical temperature below which carbon formation could occur is normally calculated assuming gas compositions at shift and methane equilibrium. However, since it was demonstrated that at ambient very little methanation occurs and the gas does shift to equilibrium, it is logical to calculate the carbon limits for the gas compositions assuming the shift reaction with no methanation. Since the shifting occurs in the cell, there was a concern that carbon formation might occur at the cell inlet before the gas reaches shift equilibrium.

The theoretical carbon limits as a function of dew point for the three reaction assumptions, 1) feed gas composition, 2) gas composition at CO shift equilibrium, and 3) gas composition at shift and methane equilibrium are shown in Figure 2-26. Carbon formation is thermodynamically possible when the dew point and cell temperature are below the theoretical curves. To be safe, the initial pressurized cell tests were run with sufficient water added to the fuel gas to be outside the worst carbon limit (test condition No. 1). As a quick screening test to determine actual carbon limits, the cell temperature was first decreased to 1100°F which is within the carbon limit assuming no reaction. With no sign of plugging after 72 hours at point 2, the saturator temperature was decreased to points 3, 4, and 5. Each point was held for 24 hours. There was no sign of plugging even at point 5 which is within the carbon formation limit assuming shift equilibrium. The cell was then removed from the stand and disassembled; there was no visual sign of carbon formation.

A second cell was put on test and operated at point 6 which is within the carbon limit assuming shift reaction only. The cell ran 265 hours with no sign of plugging and was removed and inspected. Teardown showed no carbon in the cell. A slight amount of carbon was found in the fuel preheater line to the cell. While these tests have not determined the carbon limit they do show that the practical limit is below the theoretical limit assuming only shift equilibrium.

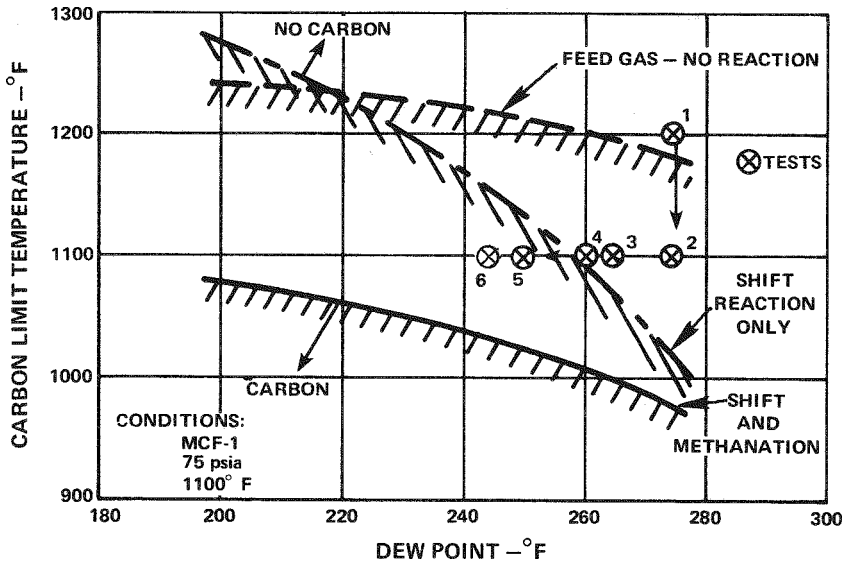

Figure 2-26. Estimated Carbon Limits

This results for molten carbonate fuel cells is consistent with experience in other equipment. Methanators are used to convert gasified coal or oil to methane using nickel catalysts where similar carbon formation problems have been reported. Numerous articles (Ref. 5,6,7) in the literature on the operation of methanators were examined. Most significant is the article on the RM process (Ref.5) which describes operation of a methanator at 900°F and 400 psi on a feed gas containing 53% CO. While the actual carbon formation limits are not defined, carbon free operation for thousands of hours are reported provided sufficient steam is added to the gas so that the gas composition with shift and methane equilibrium is outside the theoretical carbon limits.

Further tests are required to define the exact carbon formation limits in molten carbonate cells. Based on the cell tests and the literature information, it was assumed for the conceptual power plant design that the carbon formation limit was the theoretical value for shift and methane equilibrium.

iR INCREASE IN SUBSCALE CELLS

The resistive losses in subscale cells are customarily measured over the life of all cells. Some cells have been instrumented with a reference electrode which permit a division of iR losses into anode side and cathode side, where the dividing line is at some poorly defined position within the tile. The results of these measurements lead to the conclusion that there are multiple causes for the

observed iR increased not a single mechanism. This is illustrated by the data given in Table 2-6, Figure 2-27 and Figure 2-28. The most rapid iR increase (with respect to time) is found for Cell #166 which had not been thermal cycled and the least for Cell #171 which had 2 thermal cycles. The largest total loss was experienced by Cell #167 which had 10 thermal cycles. This data clearly indicates that thermal cycles cause an immediate loss, however, the iR loss decreases with time between cycles and it is not possible to judge what portion of the overall increase was caused by the thermal cycles. Data from cells with reference, as represented by Cell #136 discussed below, generally indicates that increases in iR are associated with the cathode side of the cell, occur at a moderate rate for a period of 1000 to 4000 hours, then accelerate rapidly, and seem to be a leading indication of end of cell life. Cells have recently been fabricated that have three voltage probes to cathode side components in addition to a reference electrode so that the locale(s) contributing to the resistance can be determined. This test will involve both thermal cycled and constant temperature cells. In addition to these tests a program of component and half cell testing is being carried on in the laboratory under the parallel UTC funded program. The combination of these programs will permit the location of the sources of the resistance and the mechanisms so that corrective action can be taken.

Table 2-6.
TEST EXPERIENCE OF CELLS USING ELECTROLYTE TILE APPROACH H

Cell Number	Anode* Type	Initial Cell Data IR MV/100 ASF	Number of Thermal Cycles	Total Operating Time Hours	Present or Final Cell Data IR MV/100 ASF
166	Unmod.	44	0	300 (T)	72
167	"A"	54	9	1,200	138
169	"B"	95	5	1,000 (T)	100
171	Unmod.	44	2	450 (T)	45
175	"B"	83	4	600	103

*The "A" and "B" modifications were designed to increase crossover protection and do not appear to affect the rate of iR increase, although "B" increases the initial iR value.

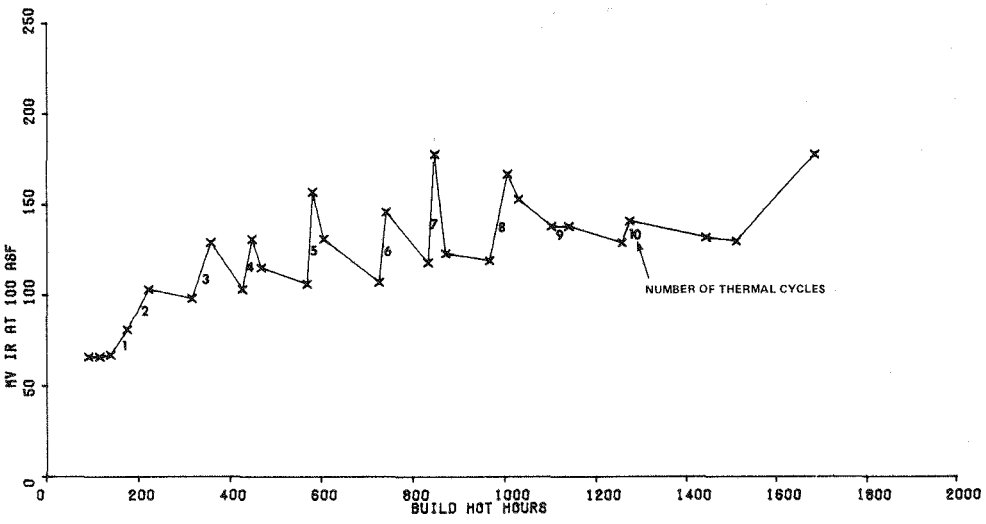

Figure 2-27. The Effects of Thermal Cycling on Internal Resistance

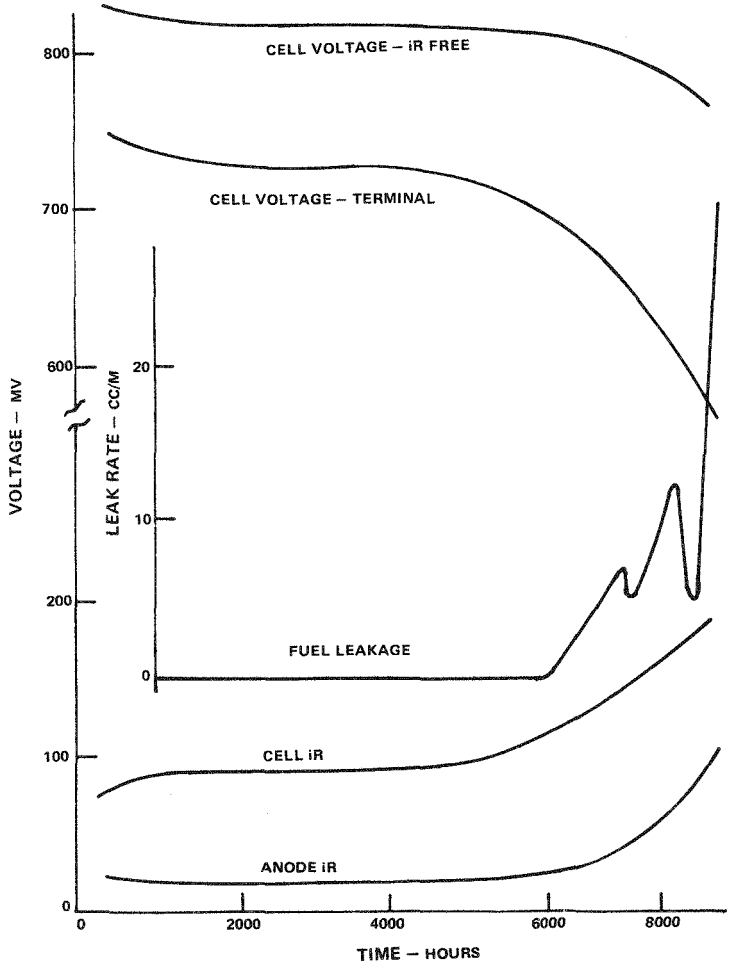

Figure 2-28. Cell No. 136 Life Data

LONG TERM CELL TEST HISTORY

Cell 136 was recently terminated after 8792 hours of testing - our longest operating cell to date without periodic electrolyte addition. Its unique feature was the use of a dual porosity, unsupported cathode run in conjunction with a standard, stabilized nickel anode and a 66 v/o binary electrolyte/34 v/o $LiAlO_2$ tile with screen F reinforcement. Since its primary purpose was to evaluate the performance characteristics of the dual porosity electrode, this cell was fitted with a cathode reference probe. Terminal and iR-free voltages, component iR, open circuit, crossover and leakage measurements were continuously taken to assess the performance chacteristics with time. These data are presented in the accompanying figures.

Figure 2-28 shows the terminal voltage and iR measurements at 160 ASF vs. operating time. The cell performance remained high until about 5500 hours at which point the iR started to increase rapidly. The initial increase in iR was attributed to greater cathode side tile resistance. This trend is consistent with previous reference probe data. However, after this time, the iR increase accelerated as a result of higher anode side resistance. This resistance increase coincides with a significant increase in fuel leakage as shown in Figure 2-28. The probable causes are loss of electrolyte in the wet seal area and/or a build up of corrosion products on the non-aluminized anode housing.

On an iR-free basis, the voltage remained relatively stable for the first 7000 hours, except for a temporary drop at 3000 hours due to anode fluctuations. At the 7000 hour point, cell iR-free voltage was only 14 mV below the peak performance recorded at 400 hours. Beyond this time cathode polarization increased substantially. At this time an attempt was made to obtain a more conductive NiO cathode. This electrode was first reduced in a H_2 environment and then reoxidized. This procedure was not successful and resulted in greater cathode polarization. At this point, 30 grams of electrolyte was added to the cell in six 5 gram increments. This amount was calculated to be that needed to completely flood the tile and electrodes. The effect of the added electrolyte on the cell iR is shown in Figure 2-29. The iR decreased with each addition until it had reached the initial value. The overall performance of the cell decreased to very low levels as the additions flooded the electrode structures. Upon termination and cooldown, the electrolyte will act as a glue holding all components together, and

allow for the cross-sectioning of the cell package for metallographic and instrumental analysis. The purpose of these studies (the location of the large resistance elements in the cell) is to determine whether gaps existed between the electrodes and tile as indicated by the electrolyte addition result and to examine very closely the many interfaces present with respect to resistance and changes in composition.

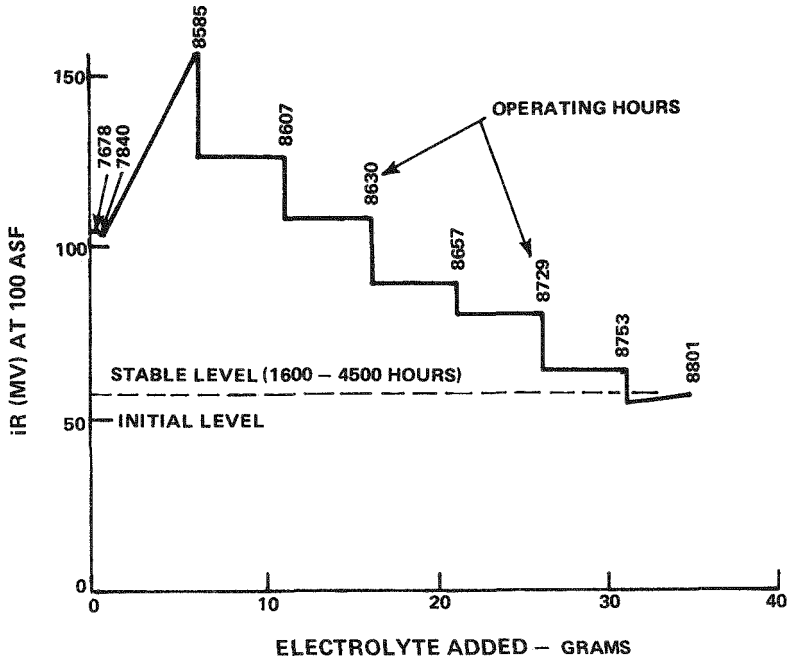

Figure 2-29. Effect of Electrolyte Addition on Cell iR (Cell 136)

Conceptual Power Plant Design

A study was conducted to define a conceptual design of a dispersed molten carbonate power plant. The results of the study are summarized in the following discussion.

The basic design requirement, was to produce 10 MW (net AC) power at a heat rate of 7500 Btu/kWh. A summary of the important powerplant characteristics is given in Table 2-7. The unit was designed to operate on #2 fuel oil or an equivalent coal derived liquid fuel. The assumed fuel sulfur level was one that would satisfy the environmental limits without sulfur recovery equipment at the dispersed sites. The unit was required to operate down to 25 percent of rated power with a 15 second response time. An additional requirement was that the power

plant should be air cooled, with water recovery to supply the process water required. To minimize power plant cost all components were designed for shop fabrication and arranged in truck-transportable pallets with minimum field connections. This requirement limited the module size to 10 MW output.

Table 2-7
DISPERSED POWER PLANT REQUIREMENTS

Heat Rate	7500 Btu/kWh
Fuel	No. 2 Fuel Oil
	Light Coal Derived Liquids
Module Size	10 MW (Net A.C.)
Turndown	To 1/4 Power
Response	15 Seconds

The power plant design was based on the use of an autothermal reformer (ATR) and a molten carbonate power section. The detailed process flow arrangement is shown in Figure 2-30. The primary features of the power plant are:

1) sulfur removal from the process gas by means of a regenerable metal oxide sulfur scrubber (RMOSS), regenerated by the cathode vent gas

2) residual sulfur from the RMOSS absorbed by a ZnO polisher

3) pressurized operation (127 psia) to minimize power plant cost and size

4) air supplied by a 2-stage turbocompressor of 8.7:1 compression ratio and 20.9 pps air flow

5) anode vent burned in a catalytic burner to provide the energy to drive the turbocompressor and add the required CO_2 to the cathode air

6) stack cooling by recycle of the cathode vent with fuel processing steam generated by sensible heat in the cathode and anode vent gases

7) process water recovered by an anode vent condenser, and

8) cell cross pressure controlled by means of a blower after the anode condenser

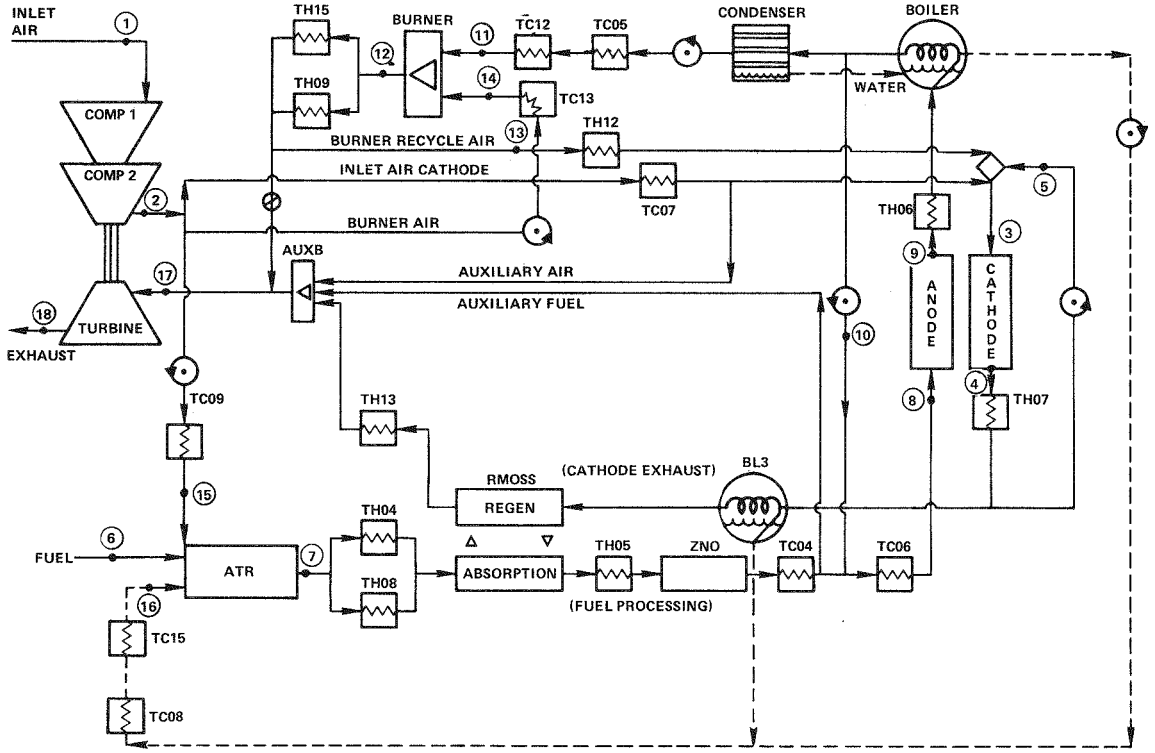

Figure 2-30. Power Plant Flow Diagram

A computer program that establishes material and energy balances consistent with component performance was used to select the component arrangement and operating conditions. Numerous computer runs resulted in the selection of the process flow arrangement shown in Figure 2-30. The subsystem efficiencies required to achieve a heat rate of 7500 Btu/kWh are shown in Table 2-8. The effective thermal efficiency of the ATR is 79%, even through the process heat required is generated within the reactor. The amount of fuel that reacts with air in the reactor reduces the amount of H_2 produced, reducing the thermal efficiency. The computer printout of the process flow, compositions, pressures, and temperatures, at all primary stations within the power plant for the design point selected is shown in Table 2-9.

Table 2-8

SUBSYSTEM EFFICIENCY

(Heat Rate = 7500 Btu/kWh)

System	Efficiency, % (LHV)
Fuel Processing	79.3
Power Section	66.4
Power Conditioner	96.0
Mechanical	96.0
Power Distribution	99.6
Overall	48.3%

Table 2-9

COMPUTER PRINTOUT OF POWER PLANT DESIGN CONDITIONS

STRM	1 TF (Temp °F)	PT Pressure (PSI)	MH_2 lb mole/hr	MH_2O lb mole/hr	MCH_4 lb mole/hr	MCO lb mole/hr	MCO_2 lb mole/hr	MO_2 lb mole/hr	MN_2 lb mole/hr	MA lb mole/hr	$CH_{1.82}$ lb mole/hr
1) AIR	94.999	14.696	.0	.0	.0	.0	.0	544.83	2025.4	25.437	.0
2) AST3	657.19	127.34	.0	.0	.0	.0	.0	544.83	2025.4	25.437	.0
3) ASP5	1100.0	127.16	.0	829.34	.0	.0	1444.0	726.36	6640.1	83.396	.0
4) TH07	1300.0	126.12	.0	829.34	.0	.0	909.04	458.89	6640.1	83.396	.0
5) CREC	1267.2	127.16	.0	576.39	.0	.0	631.78	318.93	4614.9	57.960	.0
6) FUEL	70.000	200.00	.0	.0	.0	.0	.0	.0	.0	.0	278.3
7) FST2	1600.0	135.00	486.85	804.47	2.7832	117.06	158.46	.0	362.11	4.5478	.0
8) ANOD	1100.0	127.16	495.42	1023.8	3.2743	120.67	297.87	.0	426.00	5.3503	.0
9) FST4	1300.0	126.51	57.131	1462.1	3.2745	24.019	929.45	.0	426.00	5.3503	.0
10) AREC	440.00	127.34	8.5695	219.31	.49115	3.6030	139.42	.0	63.900	.80254	.0
11) TC12	591.56	128.52	48.027	196.92	2.7526	20.192	781.35	.0	358.12	4.4978	.0
12) ESP2	1717.9	127.34	.0	253.04	.0	.0	812.48	8.0035	540.59	6.7894	.0
13) TH12	1403.5	127.16	.0	252.95	.0	.0	812.20	8.0007	540.40	6.7871	.0
14) AMX4	852.31	128.34	.0	.57654E-01	.0	.0	.63195E-01	48.018	178.85	2.2462	.0
15) AMX2	1501.6	140.00	.0	.0	.0	.0	.0	97.406	362.11	4.5478	.0
16) SMX1	1656.9	140.00	.0	1033.2	.0	.0	.0	.0	.0	.0	.0
17) TURB	879.60	123.96	.0	252.93	.0	.0	277.28	139.93	2024.9	25.431	.0
18) EXIT	390.05	14.902	.0	252.93	.0	.0	277.28	139.93	2024.9	25.431	.0

The performance of the power plant at part power is shown in Figure 2-31. With a single turbocompressor, the heat rate is essentially constant at 7500 Btu/kWh down to 60 percent of rated power and then increases to slightly over 9300 Btu/kWh at 25 percent of rated power. The power section pressure is held constant at all power levels to satisfy the requirement of fast response to load changes. This requires that the turbocompressor speed be held constant, and thus the process airflow. By using a low flow turbocompressor at low power, the amount of energy required by the turbocompressor can be reduced. By this means a heat rate of 7800 Btu/kWh can be achieved at 25 percent of rated power.

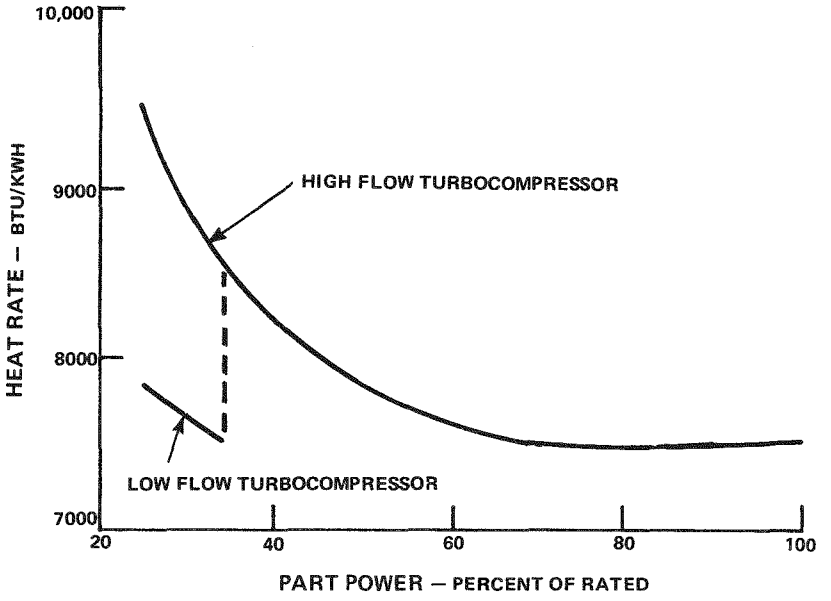

Figure 2-31. Part Power Performance

The design of the autothermal reformer is shown in Figure 2-32. It consists of a single internally insulated reactor with a single mixer at the top of the reactor. The reactor is 96" in diameter, 127" high, and the estimated weight is 25,300 pounds. The assumed fuel conversion is 99% when operating at a oxygen-carbon ratio of 0.35 and a catalyst exit temperature of 1600F.

Each of the RMOSS reactors will be 51.1" in diameter, 128" high, and weigh 7650 pounds. The absorption cycle time will be about 1 1/2 hours based on the experimental results previously reported. The beds are purged with steam before and after each absorption cycle. The beds can be purged adequately in 1 minute with a steam flow of 3% of the process steam flow for rated conditions. A volume dynamic computer program was utilized to study bed switchover. The study showed that the switchover is possible with conventional on/off ball valves, valve response time is not critical, no accumulator volume is necessary, pressure perturbations are negligble, and H_2 utilization peaks at just under 93 percent, exceeding 90 percent for only 4 seconds. The ZnO polisher was sized for replacement once a year. It was sized conservatively to remove 30 ppm sulfur over 8000 hours at an average power level of 50 percent. The polisher is 128" in diameter, 141" high, and weighs an estimated 41,000 pounds.

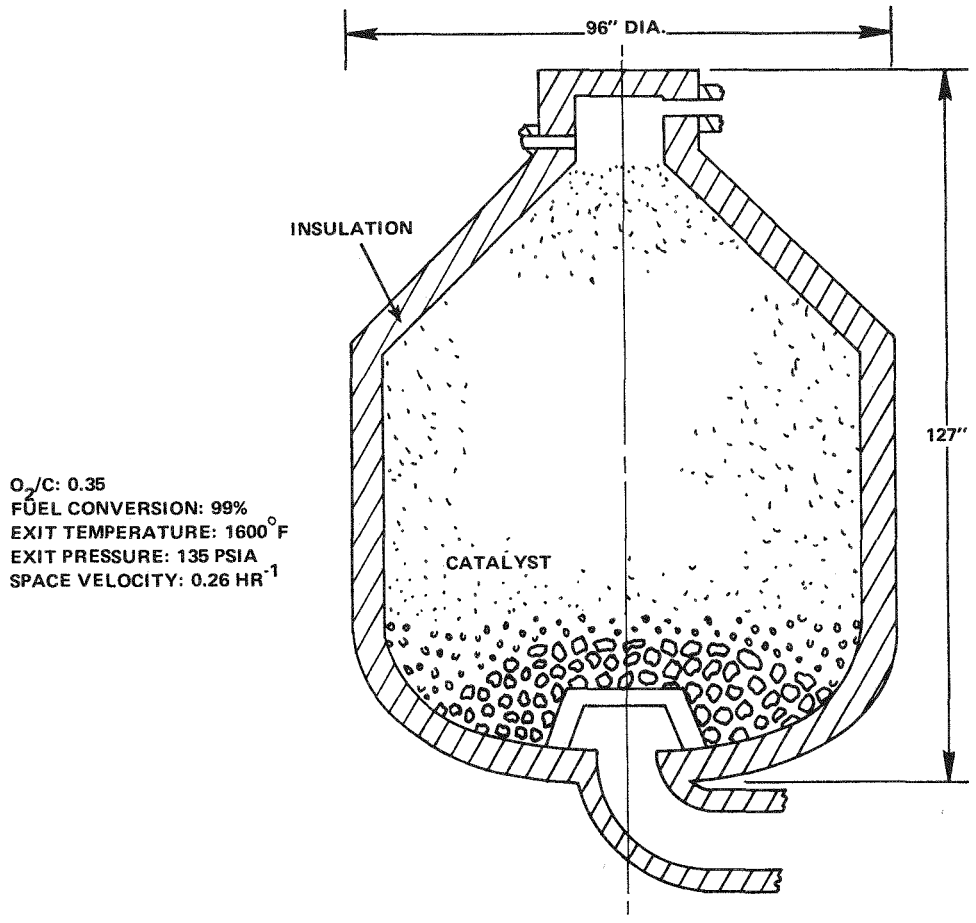

Figure 2-32. Autothermal Reformer Design

The criteria to prevent carbon formation and methanation in the cell have a significant impact on the selection of the stack cooling system. Based on the cell tests discussed in the previous section, the methanation reaction rate was so slow that the estimated methane content was insignificant at power plant condition. Carbon-free operation is possible provided the gas composition after shift and reaching methane equilibrium is outside the carbon limit. Based on these results anode recycle is not required to prevent carbon formation or methanation. A study was conducted comparing stack cooling by recycle of anode and cathode vent gases. Cathode recycle was selected since increased cell performance due to the higher H_2 pressure reduces the stack area required by 40 percent.

The repeating elements of the power section have been described in the stack development program. The power section design is shown in Figure 2-33. Cell

costs decrease as cell size increases. A cell active area of 8.2 ft^2 was selected as being the largest size that matches the voltage and current limits of our present inverter design. Each stack contains 442 cells that are contained within an internally insulated pressure vessel. The vessels are 68.5" in diameter and 96" high and are pressurized with a self-generated inert gas containing CO_2 and N_2. The total stack and container weight is 17,100 pounds. Six stacks are connected in series to have the DC input to the inverter required to produce 10 MW ac power. At rated power, the individual cell voltage is 0.836 vdc at 150 ASF.

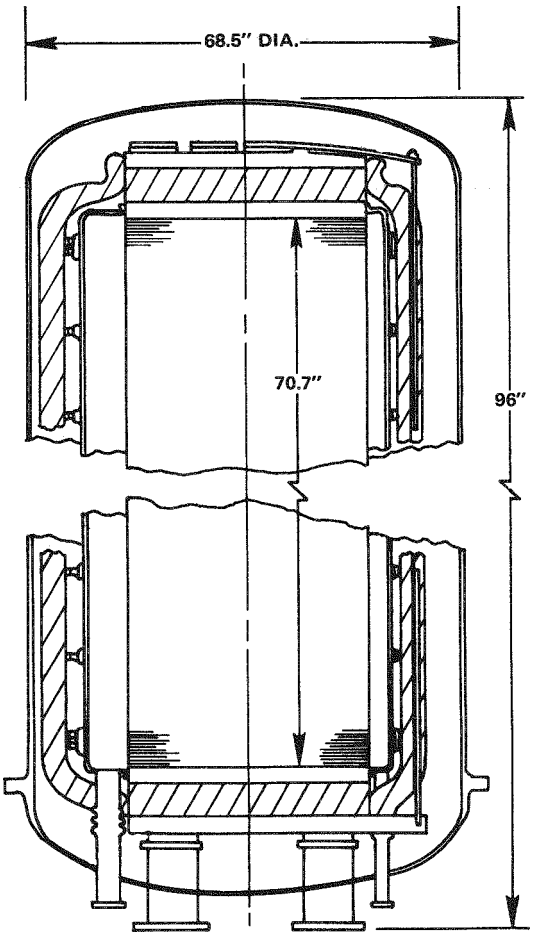

CELL AREA (FT^2): 8.2*
No. CELLS/CAN: 442
No. OF CANS/STRING: 6
No. OF STRINGS: 4
CELL VOLTAGE: 0.836
CURRENT DENSITY: 150 ASF
PRESSURE: 127 PSIA
AVERAGE TEMPERATURE: 1200°F

*TO MATCH INVERTER VOLTAGE-CURRENT LIMITS

Figure 2-33. Power Section Design

The power section arrangement is shown in Figure 2-34. Three stacks are connected to manifolds and shipped as a pallet. Each pallet butts against a pipe rack containing the piping to connect the eight power section pallets. The fuel processing, thermal management, and air supply systems are arranged on four

pallets that parallel the pipe rack as shown. The component arrangement was selected to minimize the amount of piping and connections between pallets.

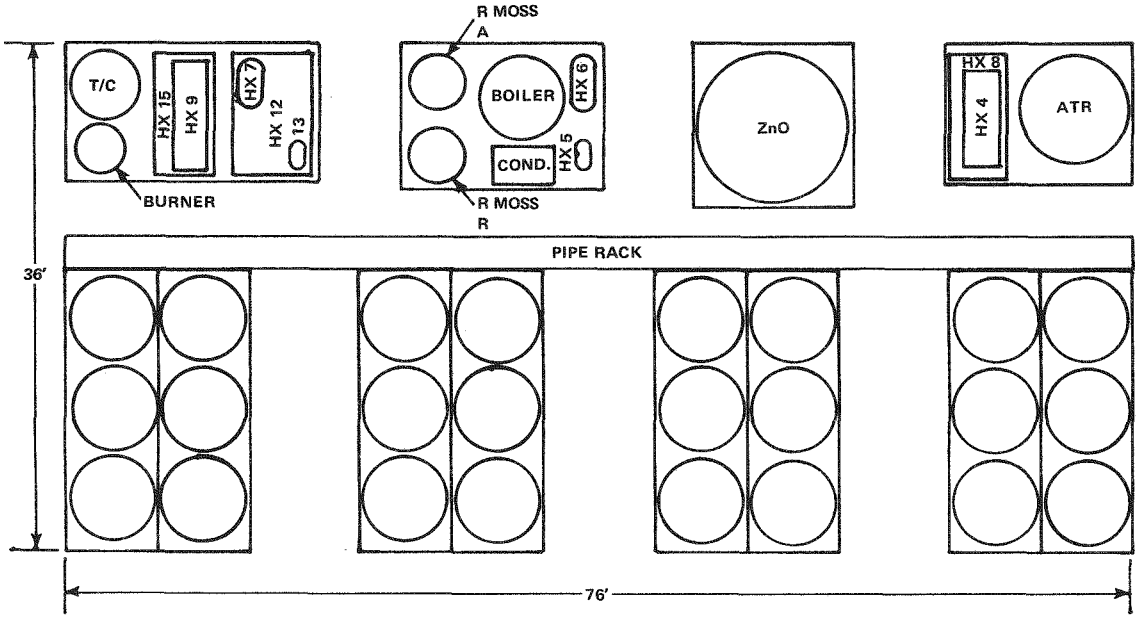

Figure 2-34. D. C. Module Arrangement

Section 3

TASK 2 - ADVANCED PHOSPHORIC ACID CELLS

INTRODUCTION

The versatility of advanced acid cell systems can be increased if increased tolerance to fuel impurities can be demonstrated. For instance, if fuel processors capable of direct operation on No. 2 fuel oil supply hydrogen sulfide (H_2S)-containing fuel gas to the cell stack, cell tolerance to H_2S could avoid the need for sulfur-removal systems.

TOLERANCE TO H_2S

Previous tests performed on subscale phosphoric acid fuel cells showed that initial cell performance losses due to H_2S present in simulated reformed naphtha (70-80 dry volume percent H_2) were small and reversible at 375°F cell operating conditions (Ref.3). Subscale cell endurance testing showed that anodes are tolerant for long times to H_2S at levels of about 200 ppm in simulated reformed naphtha, but that they eventually suffer from abrupt performance decay (Ref.4). Decayed cells could be easily regenerated in a variety of ways, but the mechanism of the actual decay process was not understood. It was suspected, however, that this decay resulted from some complex interaction of H_2S and carbon monoxide (CO) at the catalyst surface. Several other hypotheses for the decay mechanism were eliminated as a result of laboratory and subscale cell testing (Ref.4).

Experimental work during this report period focused on the effect of H_2S on the performance characteristics of subscale phosphoric acid cells operating under conditions intended to simulate those which will be encountered in a power plant which utilizes an adiabatic steam reformer. This type of reformer would not require removal of sulfur from fuel prior to reforming it. Other tests were done to help understand the anode decay mechanism. Table 3-1 summarizes the subscale cell testing accomplished during this period.

Table 3-1

SUMMARY OF CELL TESTS

Cell No.	Anode Pt Loading (mg/cm^2)	Total Load Time (Hours)	Fuel*	Purpose of Test
149	0.4 (nom.)	427	GM-3	Performance at adiabatic reformer conditions (no H_2S)
			GM-3 + H_2S	Effect of H_2S on performance at adiabatic reformer conditions
150	0.4 (nom.)	445	GM-3 + H_2S	Effect of H_2S at ambient pressure (with CO)
			GM-4 + H_2S	Effect of H_2S at ambient pressure (no CO)
			GM-3 + H_2S	Effect of H_2S concentration
			GM-3 + H_2S	Effect of cell current density (lower fuel utilization)
151	0.4 (nom.)	192	GM-3 + H_2S	Test not completed; anode failed unknown cause
153	0.4 (nom.)	238	GM-3	Effect of fuel utilization on anode decay
156	0.4 (nom.)	73	GM-3 + H_2S	Effect of Fe^{+2}/Fe^{+3} redox couple

*-Fuel compositions are given in Table 3.2.

EXPERIMENTAL METHODS

The cell tests described below were conducted in 2" x 2" fuel cells. The fuel electrodes were backed by porous, uncatalyzed electrolyte reservoir plates (ERP). Standard Teflon-bonded electrodes were used for both fuel and air electrodes. The electrocatalysts used consisted of nominally 10 weight-percent platinum (Pt) dispersed on a high surface area, conducting carbon black. Anode Pt loadings were nominally 0.4 mg/cm^2. Several fuel gas mixes were used, including one intended to simulate adiabatic reformer effluent (see Table 3-2). Pure hydrogen and GM-4 were used as diagnostic gases, and GM-2 was used to provide initial performance calibrations on the cells. It should be noted that GM-2 was one of the simulated reformer mixes used previously (Ref. 4) on which phosphoric acid cells operated stably for periods up to 1000 hours with 200 ppm H_2S added.

Table 3-2
FUEL MIXES USED FOR CELL TESTING

Gas Mix	Volume %, Dry Basis
GM-2	H_2, 70.0; CO, 1.0; CO_2, 29.0
GM-3 (sim. adiabatic reformer)	H_2, 19.9; CO, 1.72; CO_2, 31.3; N_2, 47.08
GM-4	H_2, 20; He, 80%

H_2S was introduced into the fuel gas stream by using permeation tubes obtained from Metronics (Santa Clara, Calif.; Part No. 1101000345, standard emission rate, 10 cm length). H_2S concentrations were varied by changing the number of tubes used and/or varying tube temperatures. A separately-heated, dead-ended chamber "teed" into the normal wet fuel (cell) inlet line housed the permeation tubes (see reference 4, Figure 3-2, Scheme 2). H_2S concentrations at the cell's fuel inlet were calculated based on periodic weight-loss measurements on the permeation tubes, averaged over the total fuel flow into the cell: the presence of water in the fuel cell exit gas precluded the use of Kitagawa Tube detectors for H_2S analysis.

The test conditions for cell 150 used to simulate operation on adiabatic steam reformer effluent are shown in Table 3-3. The other cells tests were done,

unless otherwise noted, with 14.7 psia reactant pressures (fuel and air), 375°F cell temperature, 200 ASF (amps/ft^2), 90/50 percent utilizations of H_2/O_2, and fuel saturated with water to a dew point of 141°F.

Table 3-3
CELL CONDITIONS SIMULATING OPERATION ON
ADIABATIC STEAM REFORMER EFFLUENT

Reactant Pressure	58 psia
Cell Temperature	375°F
Current Density	243 ASF
H_2 Utilization	90%
O_2 Utilization	60%
Fuel Dew Point	180°F
Fuel	GM-3

EXPERIMENTAL RESULTS

Performance on Adiabatic Reformer Gas

Cell 149 was tested to determine the performance characteristics of a 2" x 2" phosphoric acid cell operating under conditions intended to simulate those which will be encountered when operating in a power plant which utilizes an adiabatic steam reformer. This advanced fuel processing system would obviate the need to remove sulfur from fuel before the reforming operation. Systems studies done previously in conjunction with adiabatic steam reforming tests were used to specify optimum power plant operating conditions. Table 3-3 details the operating conditions and Table 3-2 the fuel gas composition used in the 2" x 2" cell tests. The small amount of methane present in the actual reformer effluent was ignored for these tests since previously reported testing (Ref.3) showed methane to be inert in 375°F phosphoric acid cells.

The initial cell test was done at the conditions specified in Table 3-3 without any hydrogen sulfide (H_2S) added to the fuel. Systems studies project the concentration of H_2S in the reformer effluent to be about 320 ppm. The initial cell performance level projected for these conditions in the absence of H_2S and the cell operated stably at these conditions for 200 hours. It was then shut down so it could be moved to another test stand for H_2S tests.

The cell was restarted and stabilized on H_2S-free fuel at the conditions listed in Table 3-3. The gas delivery system used was capable of delivering only 50 ppm H_2S in the fuel rather than the 320 ppm projected by system studies. The effect of the H_2S in this H_2-poor fuel was more pronounced than that reported previously for the H_2-rich fuel expected from a thermal steam reformer. The cell voltage decayed overnight, slowly at first, then rapidly, until the cell automatically shut down. It was determined that the fuel flow rate had decreased during this period (faulty flow valve), and the cell might have decayed due to fuel starvation. The cell was restarted with H_2S added to the fuel. The fuel flow was set purposely high overnight, and both fuel flow and cell voltage were monitored continuoulsy. Once again, cell voltage decayed, slowly at first, then more rapidly, until the cell automatically shut down (see Figure 3-1). It was concluded that the H_2S was responsible for the rapid cell voltage decay.

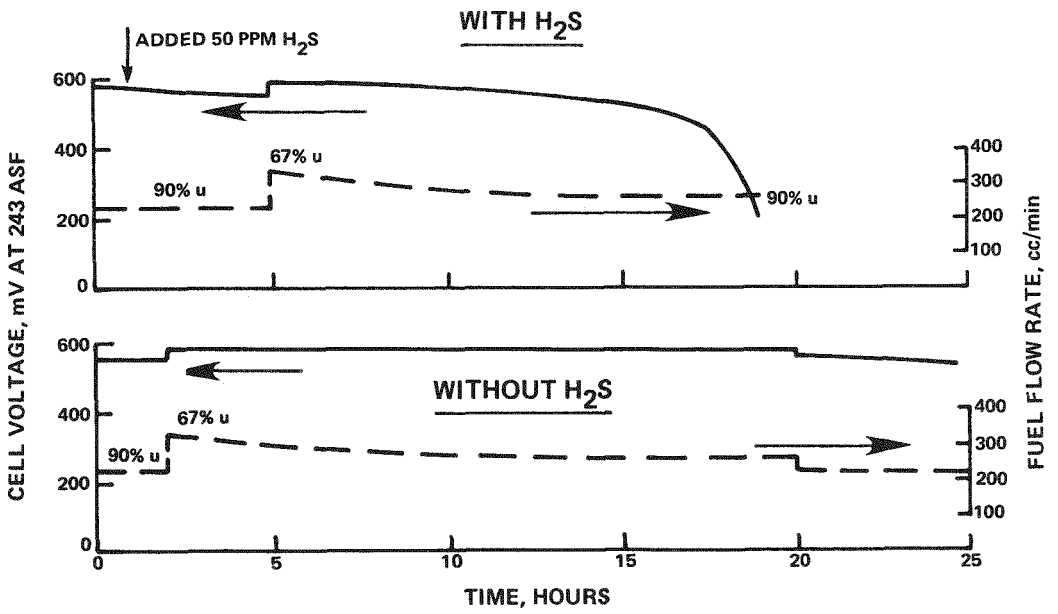

Figure 3-1. Cell Performance Stability Under Simulated Adiabatic Steam Reformer Conditions with and without 50 PPM H_2S Added to the Fuel

The impact of H_2S on anode performance with the low H_2-content fuel (19.9%) was dramatic; 50 ppm H_2S caused anode failure in only 17 hours, whereas anodes operating on a H_2-rich fuel such as GM-2 (70% H_2), operated stably for hundreds of hours (Ref.4). In order to simplify further testing, another cell (150) was started at ambient pressure conditions but with the same fuel gas composition used for cell 149 (GM-3) to see if the cell behaved in a similar manner.

Cell 150 was started and stabilized at 375°F, 200 ASF, 90% H_2 utilization operating on GM-3 at atmospheric pressure. After adding 100 ppm H_2S to the fuel gas, the cell voltage decayed rapidly after only 4-5 hours of operation. This rapid decay is shown in Figure 3-2A. Removal of the H_2S from the fuel stream resulted in a performance recovery symmetric with the performance decay, which would be expected in light of previous H_2S testing. Switching a failed anode under these conditions to a H_2-rich fuel, such as GM-2 or pure H_2 also restored performance, as expected from previous H_2S testing. Since this combination of test conditions led to the reproducible failure of anodes due to H_2S in a relatively short and manageable time period, it was decided that additional cell testing to understand the decay mechanism could be easily accomplished at these same test conditions.

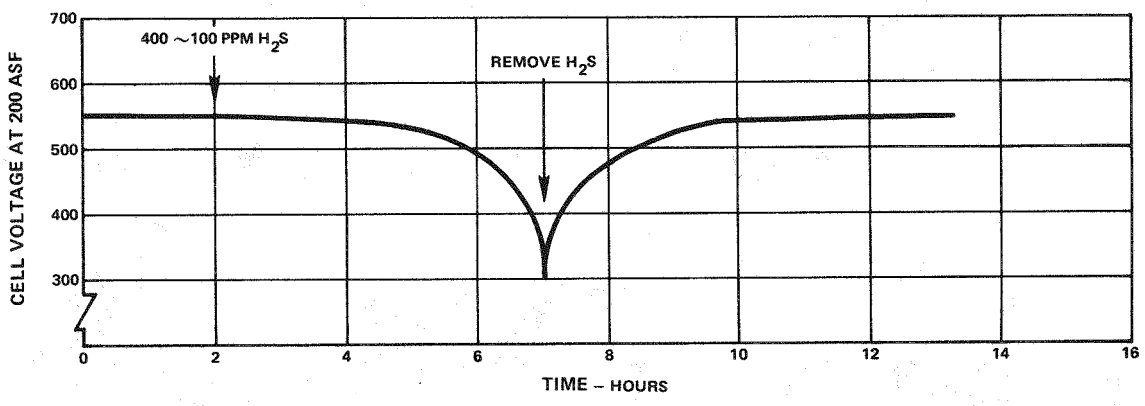

Figure 3-2A. Cell Performance with CO Containing Fuel (GM-3)

Effect of CO

Previous speculation regarding the anode decay mechanism centered about some complex interaction between CO and H_2S at the catalyst surface. Another test was done on cell 150 to investigate this possibility. A test identical to that discussed above was performed using a "clean" fuel mix of 20% H_2 in helium with 100 ppm H_2S added. This also resulted in rapid cell voltage decay about 5 hours after the introduction of H_2S. In this case, however, the removal of the H_2S did not result in any noticeable performance recovery over a one hour period (see Figure 3-2B). When the cell was returned to CO-containing fuel (GM-3 with no H_2S), the voltage recovered very rapidly to its initial level (Figure 3-2B). This cell behavior was quite reproducible.

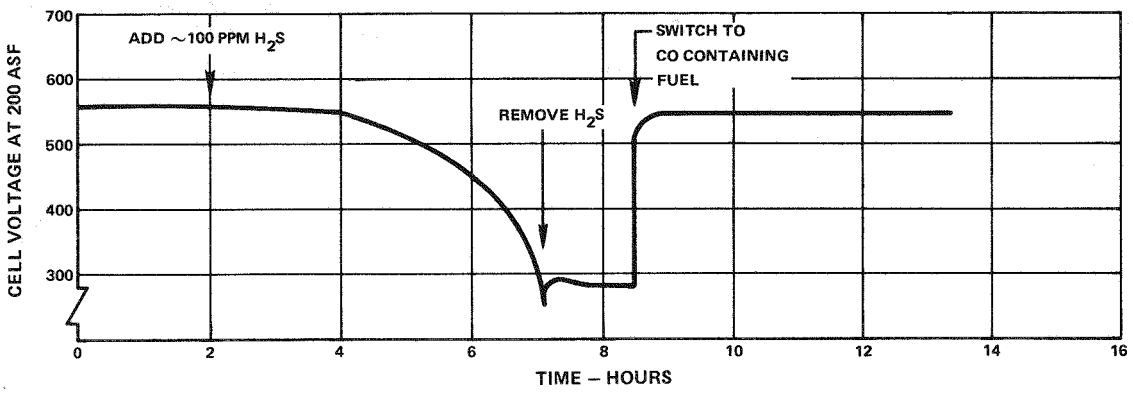

Figure 3-2B. Cell Performance with "Clean" Fuel (H_2/H_e) (GM-4)

It can be concluded from these experiments that (at least in low H_2-content fuels) CO is not required in the fuel gas in order to cause H_2S poisoning and that the CO apparently interacts with H_2S in the presence of H_2 to aid in the recovery process when H_2S is removed from the fuel gas. These results were not expected in light of previous sulfur testing with high H_2-content fuels.

Effect of H_2S Concentration

One test was conducted to determine the effect of H_2S concentration on the time until cell failure. Cell 150 was operated under the same conditions as previous tests but with 50 ppm H_2S in the H_2/He fuel gas. This cell operated for 10 hours before exhibiting rapid cell voltage decay indicating that H_2S concentration has a direct inverse effect on the time to cell failure.

Effect of Fuel Utilization

In another test, the current density of cell 150 was reduced to 100 ASF (i.e., 45% H_2 utilization) with all other parameters being held constant. This cell ran for 20 hours on GM-4 with 100 ppm H_2S added with no adverse effects on cell voltage. Subsequent attempts to return this cell to 200 ASF conditions were unsuccessful. Only after exposure to CO containing fuel (GM-3) without H_2S would the cell run at 200 ASF conditions. These results indicate that normal load cycling at power plant conditions will not alleviate the H_2S decay problem at high current densities. Cell 151 was started to determine the effect of fuel utilization on anode decay. This cell was terminated because, for some unknown reason, the anode operated very poorly on GM-3.

A new cell (153) was started to determine the effect of fuel utilization on time-until-performance-decay. Hydrogen utilization was varied by changing cell current density so that fuel flow and H_2S concentration would remain constant for all tests. This cell was even more sensitive to H_2S than previous cells. Figure 3-3 shows how time-until-decay increased as H_2 utilization decreased. However, even at 65% utilization the cell decayed in four hours, indicating that if a fuel utilization could be determined whereby the cell operated stably, it would be too low to be of practical value.

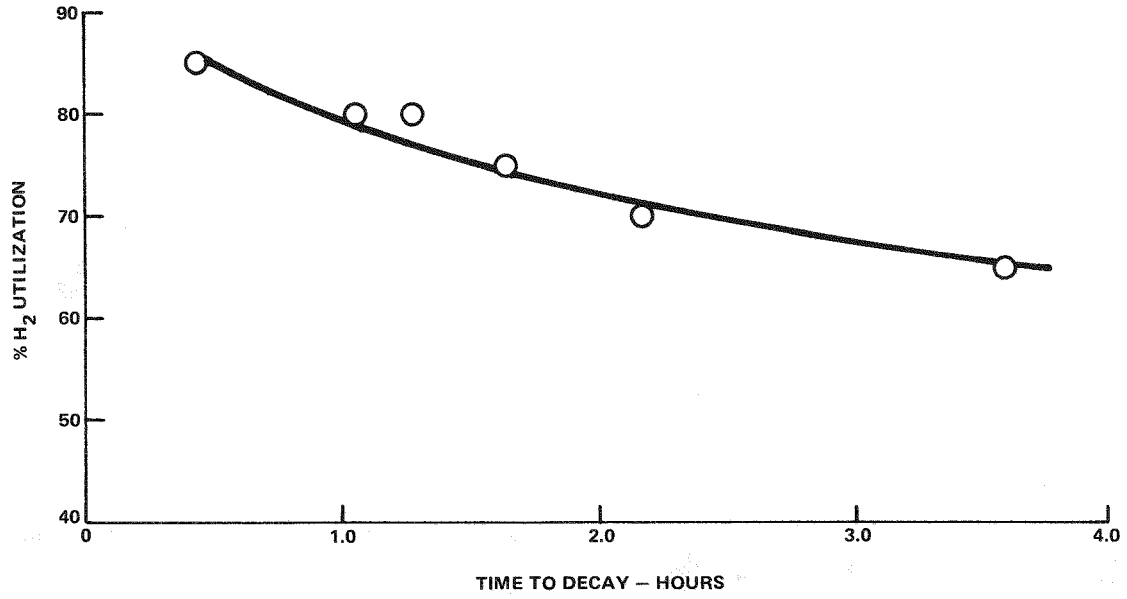

Figure 3-3. Effect of H_2 Utilization on Time to Cell Decay, Phosphoric Acid Cell (With 100 PPM H_2S)

Effect of Redox Couple

Experiments were done to determine whether a redox couple added to the H_3PO_4 electrolyte would alleviate the H_2S poisoning problem by oxidizing the adsorbed species off the anode catalyst. The Fe^{+2}/Fe^{+3} couple was chosen since previous testing had shown it was compatible with H_3PO_4 cells. Laboratory tests were done first to determine if the iron and H_2S would form insoluble sulfides in hot, concentrated H_3PO_4; no significant sulfide formation was observed. H_3PO_4 was then saturated with ferric phosphate and used as the electrolyte in a new cell (156); this cell showed no increase in H_2S tolerance compared to previous cells.

CONCLUSIONS

A review of these data and data from previous testing indicates that present day, phosphoric acid cell Pt-anode catalysts are poisoned by quantities of H_2S projected to be present in advanced reformer effluents. This catalyst poisoning is extremely rapid with low (~20%) H_2-content fuels. The mechanism for anode decay is not well understood, but the concentrations of and interactions between H_2, CO, and H_2S are clearly important to the process. Although the anode poisoning effect can be reversed, none of the known methods are viable for an operating power plant. The concentration of H_2S to which an anode would be tolerant for 40,000 hours is not known.

Section 4

TASK 3 - ADVANCED FUEL PROCESSING

INTRODUCTION

Advanced fuel cell powerplants require a fuel processor capable of efficiently producing hydrogen from heavy sulfur bearing petroleum fuels and synthetic liquid fuels. Because of impurities such as sulfur found in these fuels, and the refractory nature of these fuels caused by their high aromatic content, either high temperatures or very active catalysts are required to reform them to hydrogen. A conventional low temperature reformer would require a very active sulfur and carbon tolerant catalyst to operate efficiently and the high temperatures required to process the fuel with conventional catalysts are inconsistent with the efficiency requirements of the power plant. Therefore, adiabatic reforming was selected as the best approach to efficient conversion of these heavy fuels to hydrogen.

In the adiabatic reforming process the heat required to reform the fuel is obtained through preheated reactants and internal combustion from added air or oxygen. This internal heat generation allows the process to run at high temperatures without the need for heat transfer surfaces capable of withstanding the high temperatures. Since there are no heat transfer surfaces, the reactor can be internally insulated, and fabricated from inexpensive alloys rather than the expensive high temperature alloys of conventional reformers.

System studies of the adiabatic reformer/fuel processor, incorporated in a power plant, show that the fuel processor must satisfy the following requirements:

- Operation at or near the system performance goals of:
  - -- O_2/fuel ratio = .36
  - -- Steam/carbon ratio $\leq$ 5.0
  - -- Fuel conversion = 99.8%
  - -- Exit temperature = 1600°F

Engineering development for powerplant use also requires:

- Scalability of pilot hardware to megawatt size.
- Hardware durability shown by an endurance demonstration.

In order to be compatible with a fuel cell, sulfur from the fuel must also be removed before the hydrogen stream enters the cell.

No. 2 fuel oil is being used in these reformer studies as representative of distillate fuels from coal or petroleum. The properties of the No. 2 fuel oil are shown in Table 4-1.

Table 4-1
NO. 2 FUEL OIL PROPERTIES

Aromatics, Vol %	=	27.3
Paraffins, Vol %	=	31.2
Olefins, Vol %	=	0.77
Naphthenes, Vol %	=	40.8
Sulfur, wppm	=	3220.0
Hydrogen-Carbon Ratio	=	1.78
Distillation Temperature, °F		
Initial	=	135.0
10% Point	=	370.0
50% Point	=	510.0
90% Point	=	590.0

During the previous reporting period, the two inch adiabatic reformer was used to develop a fuel vaporizer and a scalable nozzle which eliminated fouling by fuel decomposition products and produced a well mixed reactant feed. The six inch adiabatic reformer test facility and reactor started operation. This reactor demonstrated scale-up of the mixer nozzle to the 10 PPH level, with performance similar to that of the two inch reactor. In the UTC funded effort, investigations were carried out in the laboratory to study high temperature sulfur adsorption on nickel reforming catalysts. Various catalyst formulations were also tested in the high temperature reforming region up to 1900°F. The effect of sulfur on reforming rates was studied, as was the reactivity of various pure

compounds. Present technology fuel cells are poisoned by sulfur, and hence require a hydrogen stream which is free of sulfur. A regenerable metal oxide sulfur scrubber formulation was identified with the potential for high capacity multi-cycle sulfur removal.

During this reporting period, work was done in the following areas:

- Adiabatic reforming:
  - -- Mixer configuration studies.
  - -- Catalyst studies in a laboratory reactor.
  - -- Catalyst evaluations in the two inch reactor.
  - -- Parametric studies.
  - -- Alternate processing sequence (Scheme B) in the six inch reactor.
- Regenerable sulfur scubbing of adiabatic reformer exhaust.

In addition, a system study was conducted in the parallel UTC effort to compare a drabatic reforming to other advanced full processing concepts.

ADIABATIC REFORMING

Mixer Configuration Studies

Tests were continued to investigate reactant mixer configurations which would allow operation of the system at conditions defined in the system study. Tests have shown that the O_2/C ratio requirement of an adiabatic reformer is a strong function of the reactor inlet configuration. In order to minimize carbon formation:

- Rapid mixing of the fuel must occur to minimize the fuel partial pressure since high fuel partial pressures increase the concentration of cracking products which lead to carbon formation.

- The residence time of the reactants in the catalyst section must be short to minimize the time during which the fuel is subjected to high cracking temperatures.

- Reactants must be completely mixed prior to entering the catalyst bed so that catalytic carbon is not formed.

Since the mixing and reaction processes in the adiabatic reformer are not unlike combustion, generalized mixing criteria normally used in the design of combustion nozzles were used to design and scale up the mixer nozzle of the adiabatic reformer. Cold flow tests were run with carbon dioxide to simulate the vaporized fuel stream, and air to simulate the air plus steam stream. Flow rates were chosen which simulated momentum fluxes and Reynolds' numbers of the hot gas streams at appropriate locations in the mixing nozzle. Gas samples were continuously removed through a probe to be analyzed by a gas chromatograph. Two mutually perpendicular traverses were made with the probe across the exit plane of each mixer to obtain the carbon dioxide concentration variation. From these analyses, the different mixing nozzles could be compared. Comparison was made by calculating the coefficient of variation in the carbon dioxide concentration for each mixer. This coefficient is defined as the standard deviation divided by the mean, so a low coefficient of variation indicates a relatively uniform reactant profile.

These cold flow mixing tests demonstrated that all of the new nozzle designs (configurations 8, 9 and 10 from the two inch rig, and build 4 of the six inch rig) produce relatively uniform mixing. The results of these tests are shown in Figure 4-1. This figure shows the distribution of fuel species (simulated by carbon dioxide) across the mixer diameter and the coefficient of variation for each of the configurations tested. Configurations 9, 10 and build 4 all showed low coefficients of variation, and relatively uniform carbon dioxide distribution. Each of these mixers was built using similar mixer design criteria. They showed that efficient mixing was obtained with the design used and that the design could be scaled up, as indicated by the similar results obtained with the 2 inch and 6 inch mixers. The cold flow evaluation was completed by checking for catalyst fluidization which did not occur in any of these mixers. After cold flow tests the mixers were used for hot reactor testing.

2-Inch Reactor Test Description

The 2 inch adiabatic reformer hardware which was used to develop scalable mixer nozzle configurations and to study the effects of reactant mixing and reform catalysts on reactor performance is shown in Figure 4-2. The reactant preheater is the large vessel on the left, and the reactor which is constructed of 2 inch schedule 40 pipe, is on the right. This configuration, 1, did not have a fuel vaporizer.

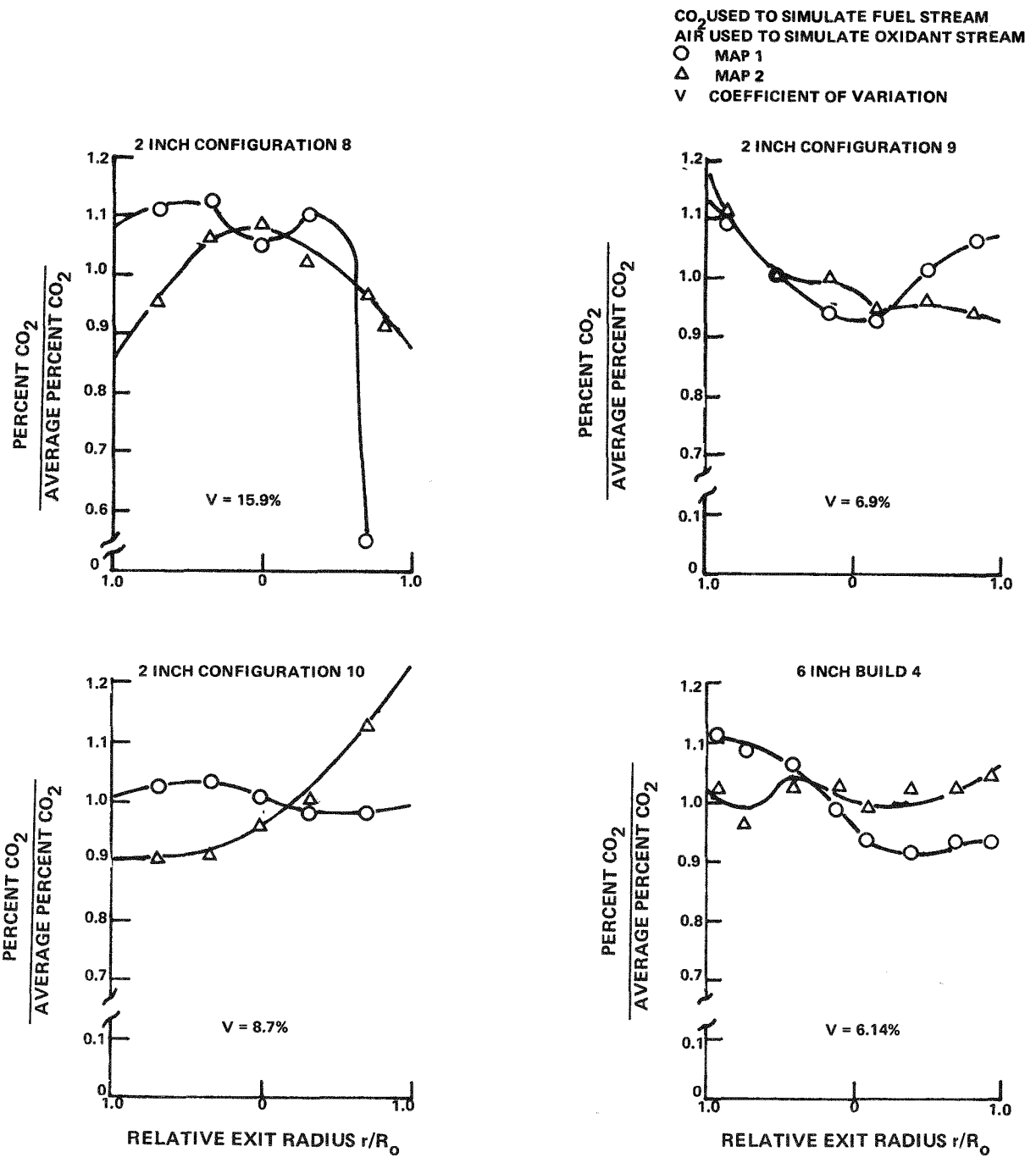

Figure 4-1. Example of Cold Flow Mixing Measurements Used to Design and Scale Reactant Mixing Nozzles

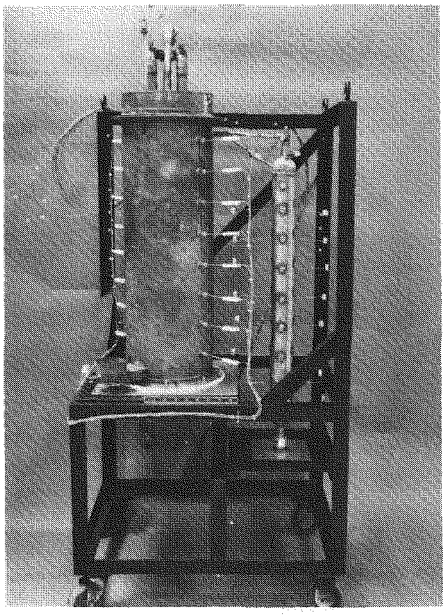

Figure 4-2. 2-Inch Adiabatic Reformer

A diagram of the present system, showing the fuel vaporizer as well as control and monitoring probes is shown in Figure 4-3 with the reactor assembly on the left, and the reactant preheater on the right. The preheater simulates powerplant heat exchangers and is used to heat the steam and air prior to their entering the reactor. The reactor assembly consists of a fuel vaporizer which utilizes steam (steam-1) to vaporize the fuel, followed by the reactant mixer, where the vaporized fuel is mixed with air plus the rest of the steam (steam-2) just prior to entering the catalyst section. The upper part of the reactor has electrical heaters which are used only to decrease start-up time. The vaporizer heater is used during start-up, and to increase reactant preheat temperatures when required. Bed and wall temperatures are monitored with the thermocouples (T/C's) shown, and gas concentrations are monitored along the length of the reactor by periodically extracting samples from taps 1 through 8. The reactor holds 1.4 - 2.0 lbs. of catalyst between taps 1 and 7, and the charge can be almost doubled by removing the support screen at tap 7 and filling from tap 8. All of the reactor materials are high alloy steels which can withstand temperatures in excess of 2000°F for reasonable lengths of time. A full scale reactor for a powerplant would be internally insulated and would not need these expensive alloys. Most of the test runs in the 2 inch reactor during RP-114-2 were at 30 psig.

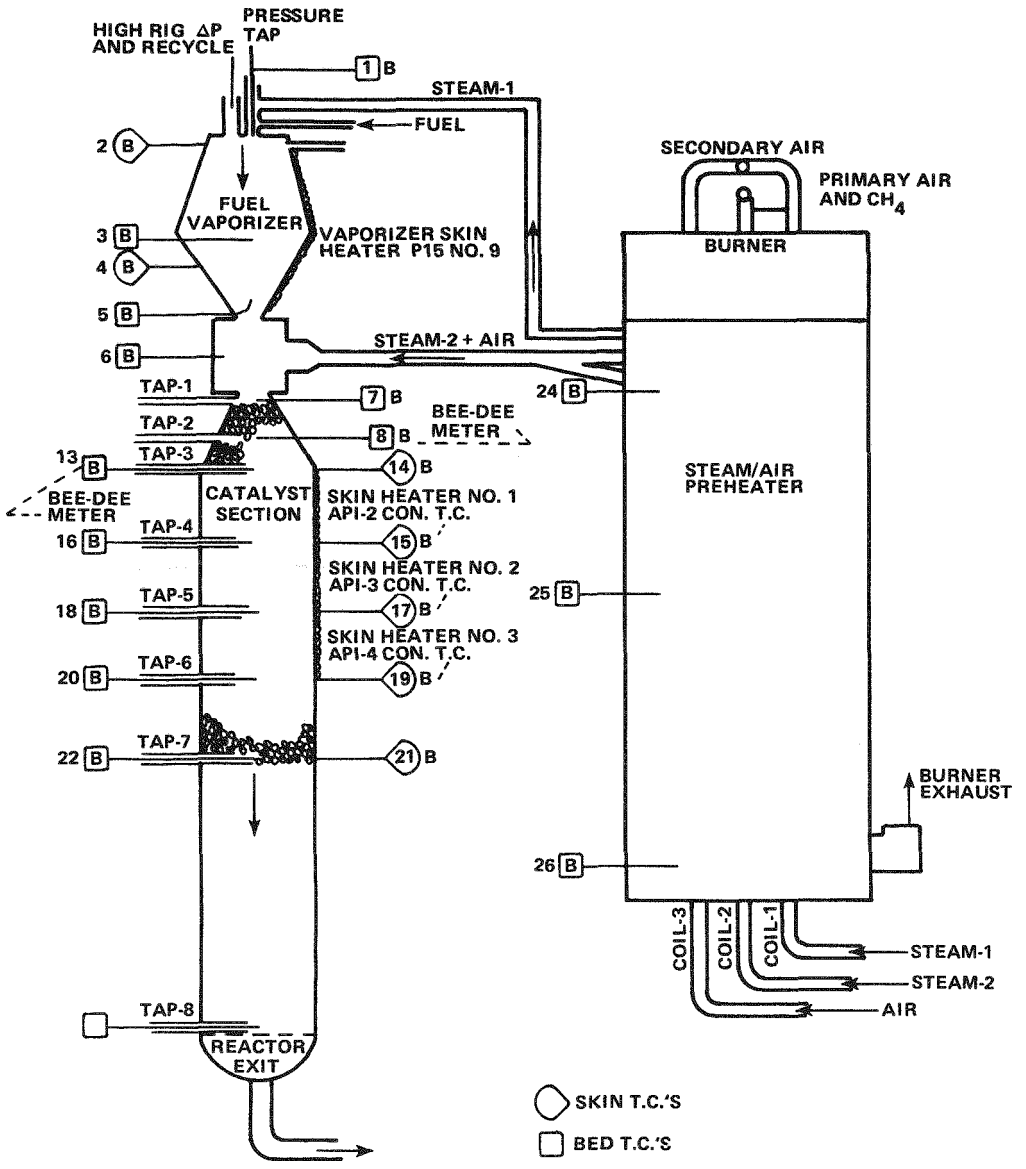

Figure 4-3. Schematic of 2-Inch Adiabatic Reformer and Reactor Preheater

Results of Configuration Tests in the 2 Inch Reactor

Three different mixer nozzle configurations were tested this year. The mixing characteristics of these nozzles have been described in a previous section. Configuration 8 was tested in both low residence time and high residence time modes by varying the quantity of catalyst. Configurations 1 through 8 used HGC-1026 catalyst. Configurations 9 and 10 used HGC-1030, a replacement catalyst having similar reforming and physical properties. These as well as other commercial catalysts will be discussed later. Configuration 1 had direct fuel injec-

tion with no fuel prevaporization. Configurations 8, 9 and 10 had a fuel vaporizer upstream of the mixer. Figure 4-4 shows the effect of mixer configuration on carbon boundary. Running at an oxygen to fuel carbon ratio equal to or above the line which is drawn to describe the carbon boundary would result in carbon-free operation of that system. Running at oxygen to fuel carbon ratios below that line would result in carbon formation which would plug the reactor. Configurations 8 and 9 result in the best carbon boundary, with configuration 10 being somewhat poorer. Configuration 8 with high reactant residence time gives the poorest carbon boundary of all of the configurations tested and is the only configuration having a poorer carbon boundary than configuration 1. This test indicated the importance of minimizing the fuel residence time at high temperatures to minimize cracking and carbon formation.

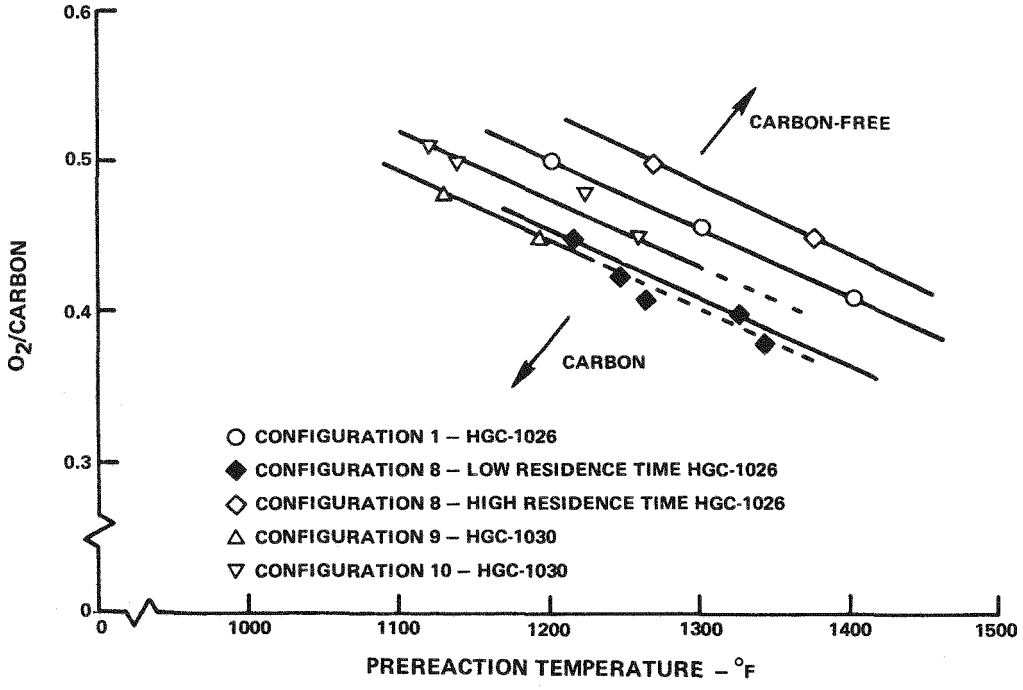

Figure 4-4. Effect of Configuration on Carbon Boundary

Some decay in the carbon boundary is observed with time, probably as a result of catalyst decay. This effect is shown in Figure 4-5 for configuration 10 with three different catalysts. To permit construction of Figure 4-5, in which data are compared at constant pre-reaction temperature, 1360°F, an extrapolation is made, from individual data points to the 1360°F condition assuming linear behavior of the carbon boundary. An example of the extrapolation is shown in

Figure 4-6. Thus displayed, the data of Figure 4-5 clearly shows that a period of 80 to 100 hours is required for the catalyst, and the reactor performance, to stabilize. In Figure 4-5, variation in the carbon boundary attained with configurations 8, 9 and 10 does not correlete with the efficiency of mixing as determined in the cold-flow measurements described earlier. Differences in performance between configurations later proved to lie within the band of reproducibility of a single configuration. Thus, despite large changes in configuration geometry, reflected in cold-flow-mixing measurements, no significant improvement in performance results. The decay in performance, evident in Figure 4-6, resulting from decay in catalyst activity, suggests that further improvement in the reactor performance must come from increased and stabilized catalyst activity.

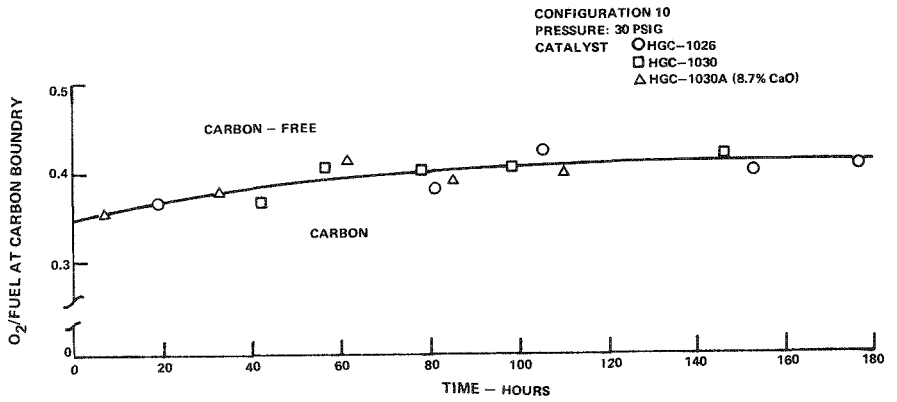

Figure 4-5. Effect of Time on Carbon Boundary

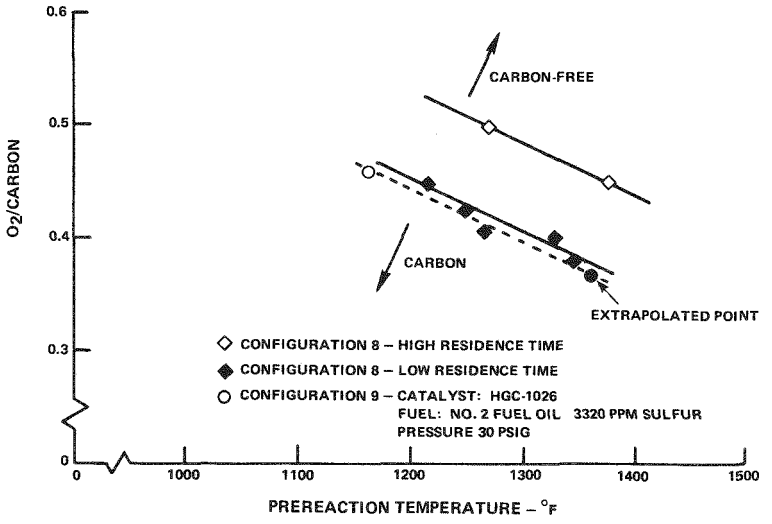

Figure 4-6. Extrapolation of Carbon Free Point to Construct the System Carbon Boundary

Carbon Formation and Catalyst Evaluation

In tests where the reactor was shut down and disassembled in a plugged condition, carbon was found between sample taps 3 and 4 of the reactor, (see Figure 4-3). The carbon produced in an adiabatic reformer is significantly different from that encountered in a conventional reformer. In a conventional reformer, carbon formation results in catalyst pulverization whereas carbon formation in an adiabatic reformer does not affect the catalyst integrity.

Figure 4-7a shows the carbon which was formed between the catalyst pellets, and Figure 4-7b shows some pellets which were broken to reveal the condition of the interior. The carbon is seen to be limited to the exterior of the pellet. This evidence which suggests that the carbon is formed in the gas phase and deposited on the pellet was reinforced by results obtained from scanning electron microscopy. The micrographs in Figures 4-8a and 4-8b show that the carbon plug contains spherical carbon particles with a range of diameters of up to a micron, frequently forming strings and chains. The higher magnification reveals the presence of some carbon filaments with ordered cylindrical structures of about 500 Å in diameter. These structures appear to be similar in form to those frequently associated with growth from nickel crystallites. The overall carbon structure was similar to that described by Lahaye et al (Ref.8) formed during steam cracking of hydrocarbons. They suggested that the globular carbon mass grew by deposition of spherules which formed in the gas phase and were trapped on the surface by the underlying microfilaments.

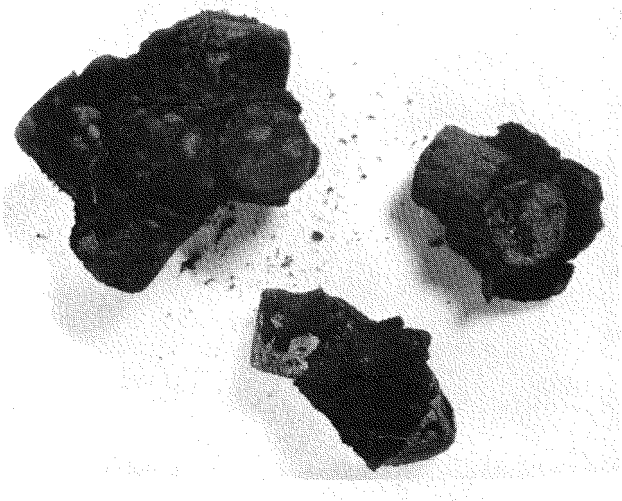

Figure 4-7a. Carbon Formation in Adiabatic Reactor - Inter-Pellet Space

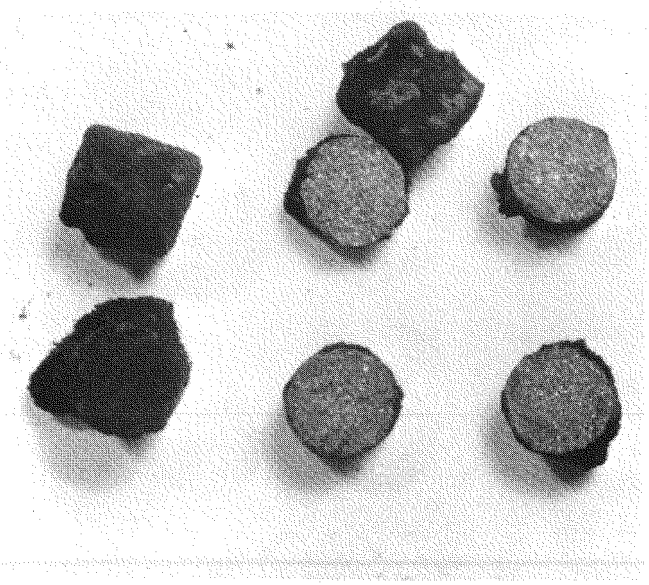

Figure 4-7b. Carbon Formation in Adiabatic Reactor - Pellet Interior

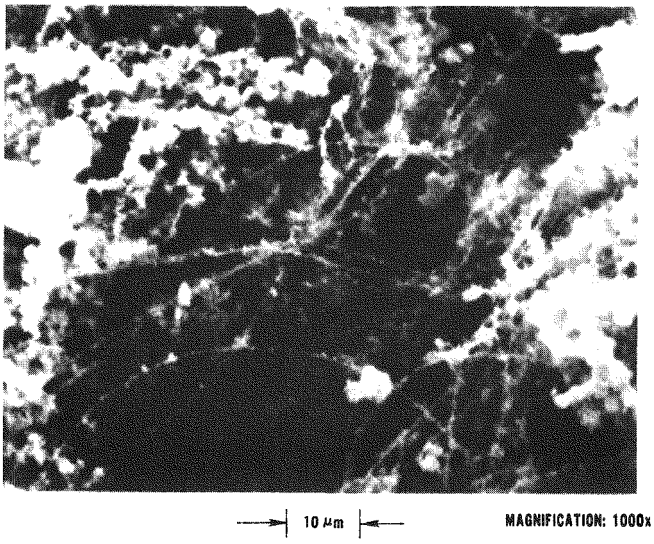

Figure 4-8a. Carbon Formation in Adiabatic Reactor - Spherical Particles

Figure 4-8b. Carbon Formation in Adiabatic Reactor - Carbon Filaments

Thermodynamic considerations of the overall process stream composition do not predict the formation of carbon. Solution of equilibria for all of the stable gaseous species present, (equations 1-4), does not predict the existence of solid carbon at any point in the reactor at the temperatures measured.

(1) $CH_4 + 2H_2O = CO_2 + 2H_2$

(2) $H_2O + CO = CO_2 + H_2$

(3) $2CO = C + CO_2$

(4) $CH_4 = C + 2H_2$

The entire adiabatic reformer is above 1200°F; and the overall oxygen to carbon ratio, including the oxygen from steam as well as air, is approximately 5. Figure 4-9, which describes the carbon formation boundaries for the hydrogen - carbon - oxygen system, shows that the adiabatic reformer does not operate in the carbon region. In addition, values for the experimentally determined reactant ratio for the Boudouard reaction (3), shown in Figure 4-10, lie far above the thermodynamic carbon regime. The formation of carbon in the reactor therefore appears to be kinetically controlled.

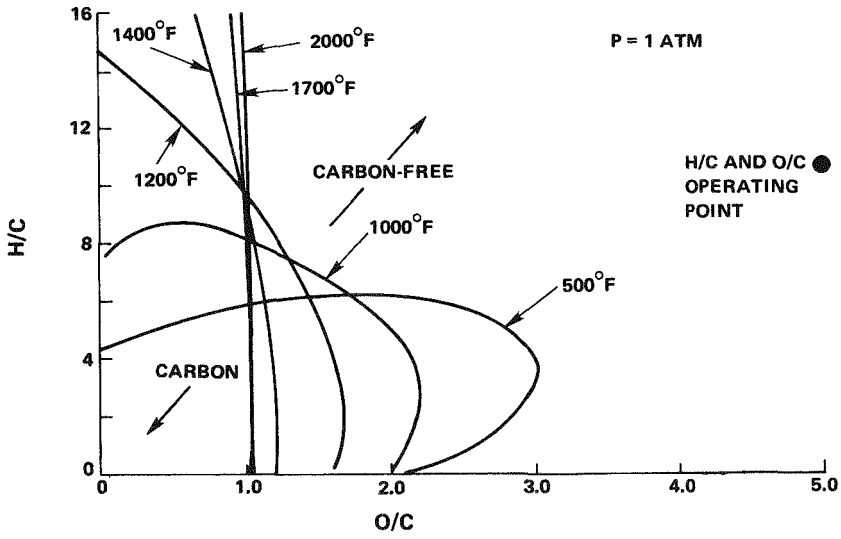

Figure 4-9. Carbon Formation Boundaries in the H-C-O System

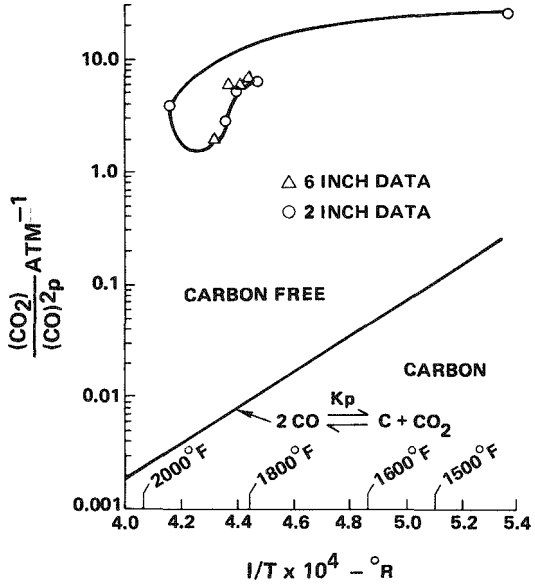

Figure 4-10. Boudouard Reaction Ratios in 2-Inch and 6-Inch Reactors

The carbon boundary defines a temperature at which the rates of carbon formation and removal are equal. With increases in reactor temperature beyond this point, by the addition of oxygen or increased reactant preheat, carbon removal exceeds formation and the reactor operates carbon free. This is represented as the intersection of the curves of rate versus temperature of the two processes in Figure 4-11.

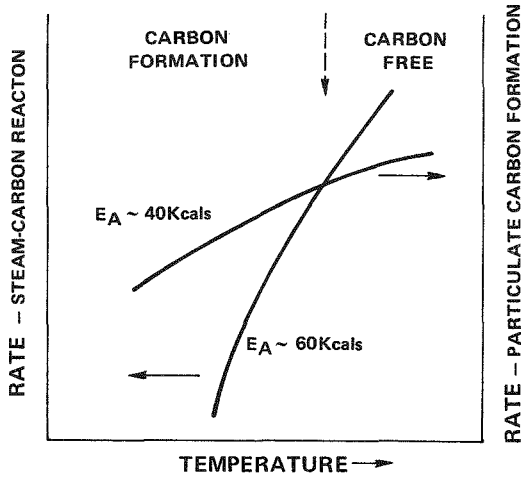

Figure 4-11. Steady-State Rates of Carbon Formation and Removal in the Adiabatic Reactor

The processes leading to carbon formation will be a complex function of the conditions in the reactor upstream of the point where carbon accummulates. Cracking of fuel, polymerization of the products, nucleation and growth of soot particles have each been proposed as critical steps. Rapid and efficient mixing as provided by the nozzles described previously will reduce the rates of the critical steps and minimize carbon formation. Catalyst formulations which change the relative rates of combustion and reforming reactions, and carbon gasification rates, will also effect carbon formation. Initial experiments in a program to investigate the effect of catalyst formulation on the performance of the adiabatic reformer are described below.

Three commercial reforming catalysts with different activities were run in configuration 9. These three tests resulted in a different carbon boundary for each catalyst, as shown in Figure 4-12. The HGC-2000 catalyst was found to be dimensionally unstable at adiabatic reformer temperatures and shrank more than 25%. Because of this shrinkage, the HGC-2000 data in Figure 4-12 has been extrapolated to zero time. Used samples of each of these catalysts taken from the 2 inch adiabatic reactor were tested for methane activity in a 3/8" microreactor. The Arrhenius plot of results of these tests, Figure 4-13, show that the catalyst with the highest reforming reaction rate was the one which operated carbon-free at the lowest oxygen to fuel carbon ratio. Figure 4-14 is a plot of the oxygen to fuel carbon ratio at the carbon formation boundary obtained by extrapolation

of the data to a common prereaction temperature of 1360°F versus the logarithm of the catalyst activity at 1800°F. This figure suggests that an activity of 0.31 hr^{-1} is required with nickel reforming catalyst to obtain an oxygen to fuel carbon ratio of 0.36. This effect of catalyst activity on the oxygen to fuel carbon ratio necessary to prevent carbon formation is consistent with the carbon boundary decay with time shown in Figure 4-5. As the catalyst is subjected to a high temperature steam environment it sinters badly, and as a result loses its reforming activity. It is known that sintering is most rapid during the initial contact period, and decreases markedly with time. This resultant loss in reforming activity, mainly from sintering, is reflected in the increased oxygen requirement to prevent carbon formation shown in Figure 4-5.

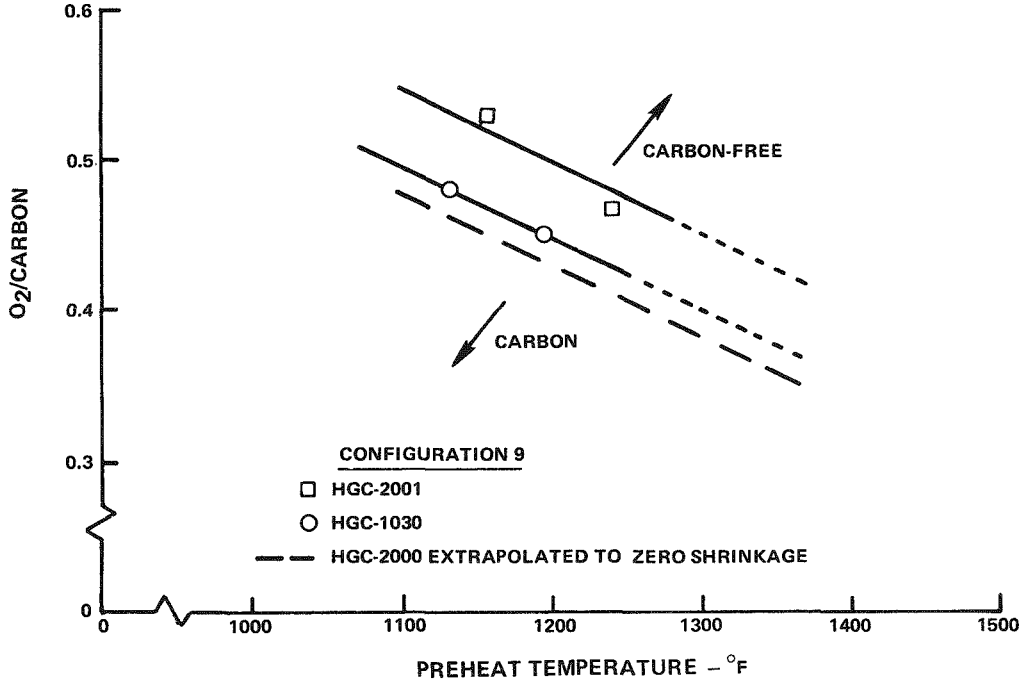

Figure 4-12. Effect of Catalyst on Carbon Boundary

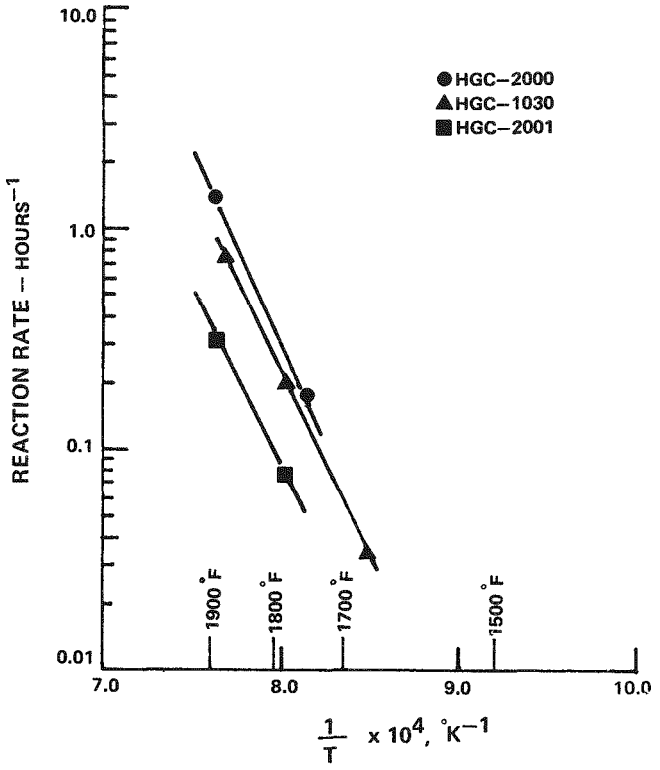

Figure 4-13. Activity of Used Catalyst Samples from Configuration 9 Tests

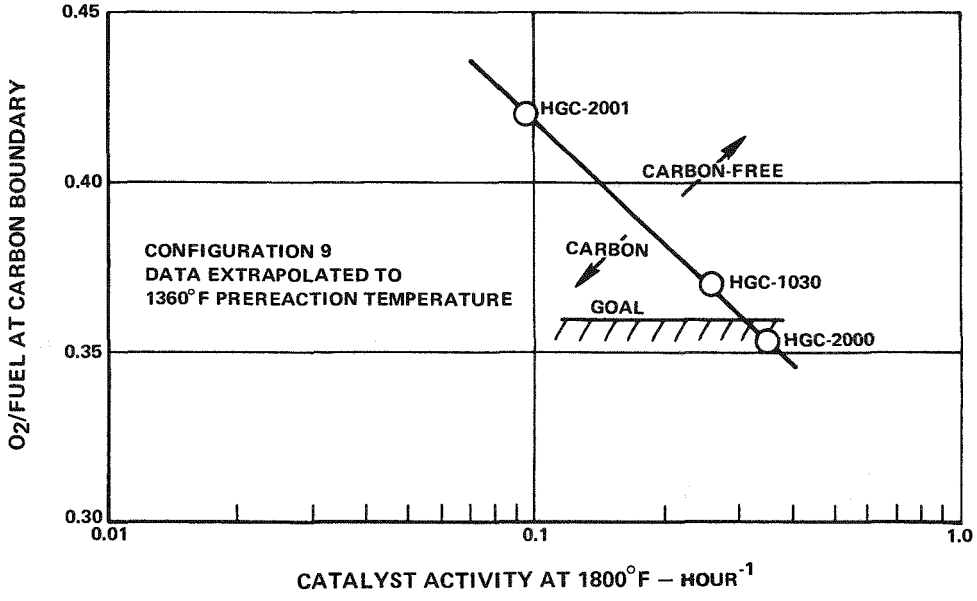

Figure 4-14. Effect of Nickel Catalyst Activity on Carbon Boundary

Two different catalyst approaches to lowering the carbon boundary were tested. One approach was to place an active steam reforming catalyst at the entrance of the reactor to reduce the concentration of hydrocarbon species in the high temperature combustion zone and thus the propensity for soot formation in that region. A second approach was to increase the rate of carbon removal by the steam-carbon reaction. Marson and Cobb (Ref.9) measured the rates of the steam-carbon reaction catalysed by sodium and calcium oxides. Sodium is the more effective, but at high temperature is lost from reforming catalysts by vaporization. Therefore calcium oxide was tested in an attempt to reduce the limiting O_2/fuel carbon ratios. This is the approach taken by Tomita et al (Ref.10).

Two catalysts with varying calcium content, HGC 1030 and HGC 1030A, were tested in the 2 inch reactor with header configuration 10. HGC 1030 is a commercial catalyst with no significant calcium content, while HGC 1030A is the same catalyst but with calcium oxide added. In the UTC funded parallel program these catalysts were found to be very similar in intrinsic reforming activity as shown in Figure 4-15. The catalysts behaved in a similar manner during testing. The initial carbon boundary was very low but increased with time to a steady performance level as shown in Figure 4-16. Within the experimental data scatter both catalysts demonstrated the same carbon boundary. The initial change in performance is consistent with catalyst deactivation and the effect of catalyst activity on the carbon boundary described above. The absence of any significant difference in the position of the carbon formation boundary associated with the two catalysts, however, does not agree with the reported activation of the steam carbon reaction by calcium oxide. Post test analysis of the catalyst showed that the calcium was present as calcium aluminate rather than calcium oxide. This result suggests that if calcium oxide is to be used to catalyze the carbon gasification reaction, then calcium will have to be added to the catalyst in excess of the stoichiometric amount required to form calcium aluminate.

In the second approach a short section of high activity HGC 2000 catalyst was loaded in the inlet section of the reactor upstream of HGC 1030A. Although the HGC-2000 catalyst constituted only 2.7% of the total catalyst weight, it was expected that it would catalyze the combustion and reforming reactions, increase the HGC 1030A catalyst temperature, and hence its activity for the carbon gasification reaction. Figure 4-17 shows that the temperature profile in the reactor did not change, indicating that the HGC-2000 did not accelerate the combustion process. Different catalyst formulations are being investigated in the UTC-funded parallel program and will be tested in the 2 inch adiabatic reactor at a later date.

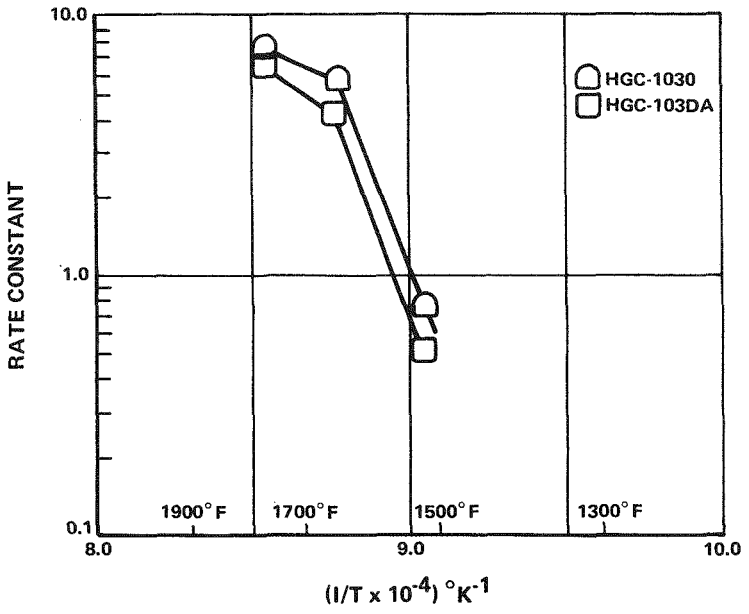

Figure 4-15. Rates for Reforming Ethane - 2500 PPMWS

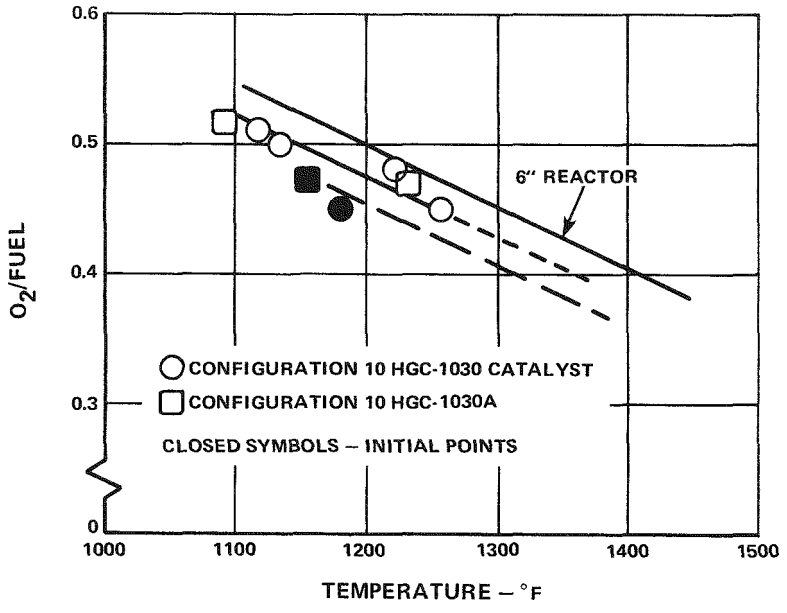

Figure 4-16. Effect of Catalyst Composition on Carbon Boundary

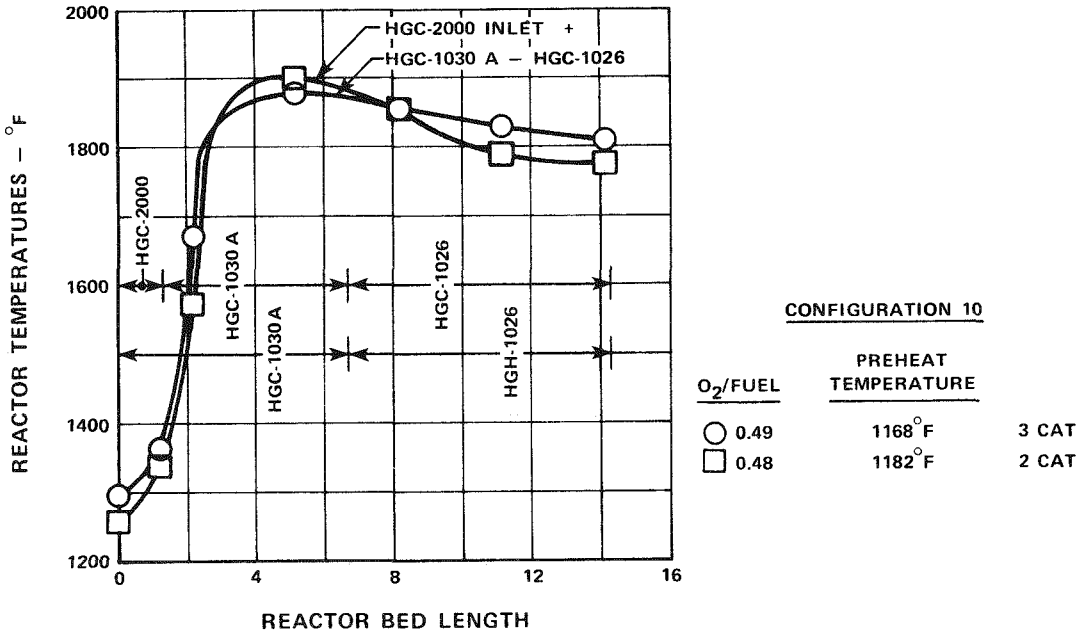

Figure 4-17. Effect of Inlet Catalyst on Reactor Temperature Profile

Effect of Operating Parameters

The effect of high reactant residence time on the carbon boundary in configuration 8 was discussed previously and shown in Figure 4-4. This poor carbon boundary was the result of fuel cracking and the formation of carbon upstream of the catalyst bed. Cracking of heavy hydrocarbons is indicated by the high methane concentration upstream of the catalyst. This methane, formed as a product of heavy hydrocarbon cracking, increases both with increased reactant preheat temperature and high reactant residence time upstream of the catalyst bed as shown in Figure 4-18.

Different catalysts and reactor configurations have resulted in somewhat different temperature profiles. In configuration 10, the effect of hydrogen addition was investigated since it was felt that increased hydrogen content would increase the combustion rate, increasing the temperature and thus the reforming rate. This would decrease the the fuel residence time at temperature. Figure 4-19 shows that the combustion rate was unaffected by a seven fold increase in hydrogen concentration. The carbon boundary also remained unaffected.

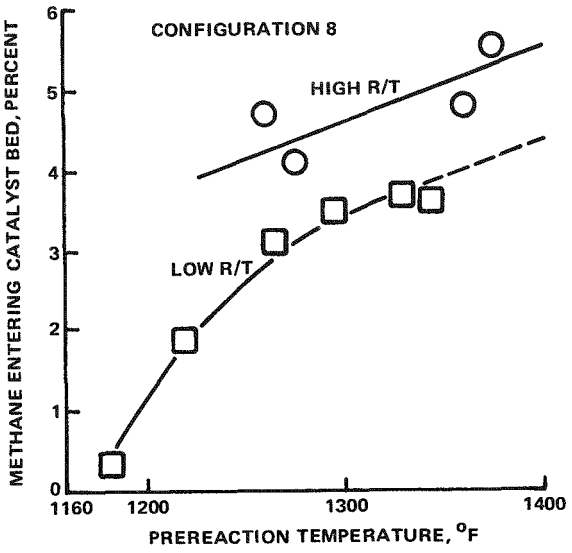

Figure 4-18. Effect of Pre-reaction Temperature and Residence Time on Methane Formation (Cracking) in Adiabatic Reforming

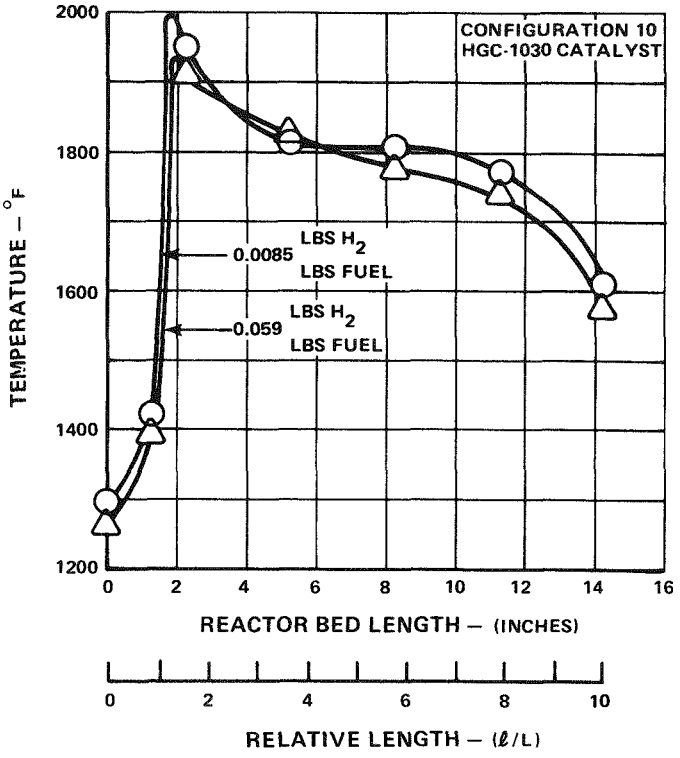

Figure 4-19. Effect of H_2 on Temperature Profile

Increased pressure was expected to increase the cracking rate and result in a less favorable carbon boundary. In the 2 inch reactor, there is no observable effect of pressure from 30 psig. to 50 psig. Similar results are observed in the six inch reactor.

Six Inch Diameter Adiabatic Reformer

The 6 inch adiabatic reformer test has the following objectives:

- Demonstrate process scaleup to 6 inch size (10 pph)
- Demonstrate endurance
- Demonstrate process improvements

During the past year, an improved mixer (Scheme A, Build 3) was built and tested for 280 hours, and an alternate fuel processing approach (Scheme B) was investigated. Contruction of a fourth Scheme A reactor to demonstrate direct scaleup from the 2 inch rig was also completed. The Build 4 test, which successfully demonstrated carbon boundary scaleup and endurance, was transferred to RP-1041, and these results are reported in references 11 and 12. A complete description of the six inch reactor test facility is given in Reference 4.

Scheme A, Build 3. The Build 3 mixer design was improved to correct catalyst fluidization problems exhibited in Build 1, and to correct mixer fouling problems observed in the Build 2 test. The Build 3 test also utilized HGC-2000, a higher activity catalyst identified in laboratory testing. This test operated for 280 hours on 10 pph of No. 2 fuel oil with 3200 PPM_w sulfur. During the Build 3 test, decay in the O_2/C ratio at the carbon boundary, and decay in fuel conversion were noted. This performance decay was attributed to problems with the new catalyst. At a prereaction temperature of 1400°F, the O_2/fuel carbon ratio required to avoid carbon laydown in the catalyst bed increased from 0.38 to 0.45, as shown in Figure 4-20. Decay was also observed in fuel conversion, which dropped from >99% to 98%, even though the catalyst bed exit temperature increased from 1650 to 1700°F (Figure 4-21). Inspection of the rig after disassembly showed that the catalyst pellets had shrunk and the bed catalyst level had dropped 3 to 4 inches below its initial level. Because of this shrinkage, residence time of the fuel, steam and air, upstream of the catalyst increased. This is believed to be the reason for the increasing O_2/C ratio requirements with time, since this phenomenon was also observed in the 2 inch rig.

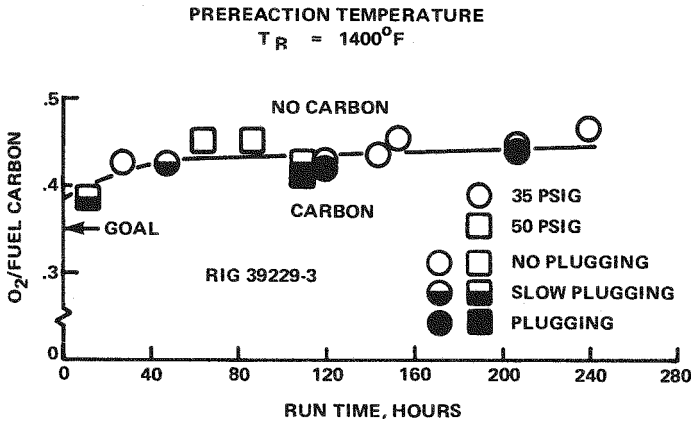

Figure 4-20. O_2/C vs. Run Time at Constant Prereaction Temperature

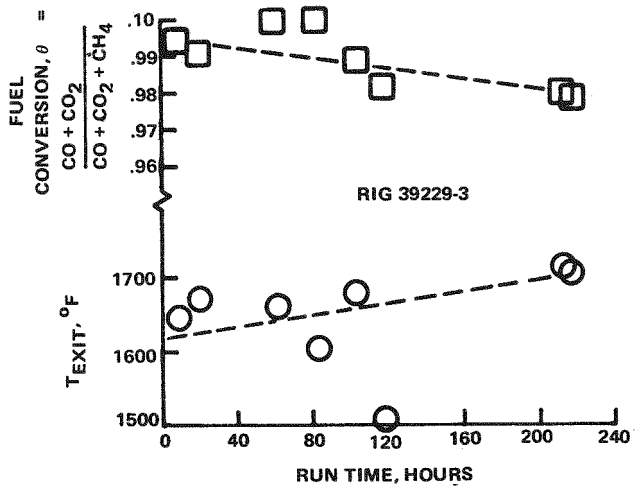

Figure 4-21. Fuel Conversion and Rig Exit Temperature vs. Run Time

Catalyst samples from the inlet and exit of the 6-inch pilot rig Build 3 were removed from the reactor at the end of the test. Post-test catalyst activity measurements were made on these samples in the 3/8" diameter isothermal microreactor. A comparison of the activity of these post-test samples with an asreceived catalyst sample indicates an activity loss for both the inlet and the exit catalyst (Figure 4-22). The inlet catalyst sample which is subjected to the maximum rig temperature shows a larger activity loss than the lower temperature exit catalyst sample.

During tests with the 6 inch pilot rig, Build 3, concentrations of reactants along the length of the reactor were determined from sample taps. Using this

data, the activity of the catalyst in the reactor could be calculated directly. This data is shown in Figure 4-22 superimposed on the microreactor data. The run duration at the time of the measurement is shown in parenthesis next to the data points. These measurements correlate well with the laboratory reactor results and indicate that most of the activity loss occurred during the first nine hours of operation on fuel.

Carbon boundary data was obtained at both 35 psig and 50 psig during the Build 3 test (Figure 4-21). Pressure does not affect the O_2/C ratio at the carbon boundary, as was the case with the 2 inch rig.

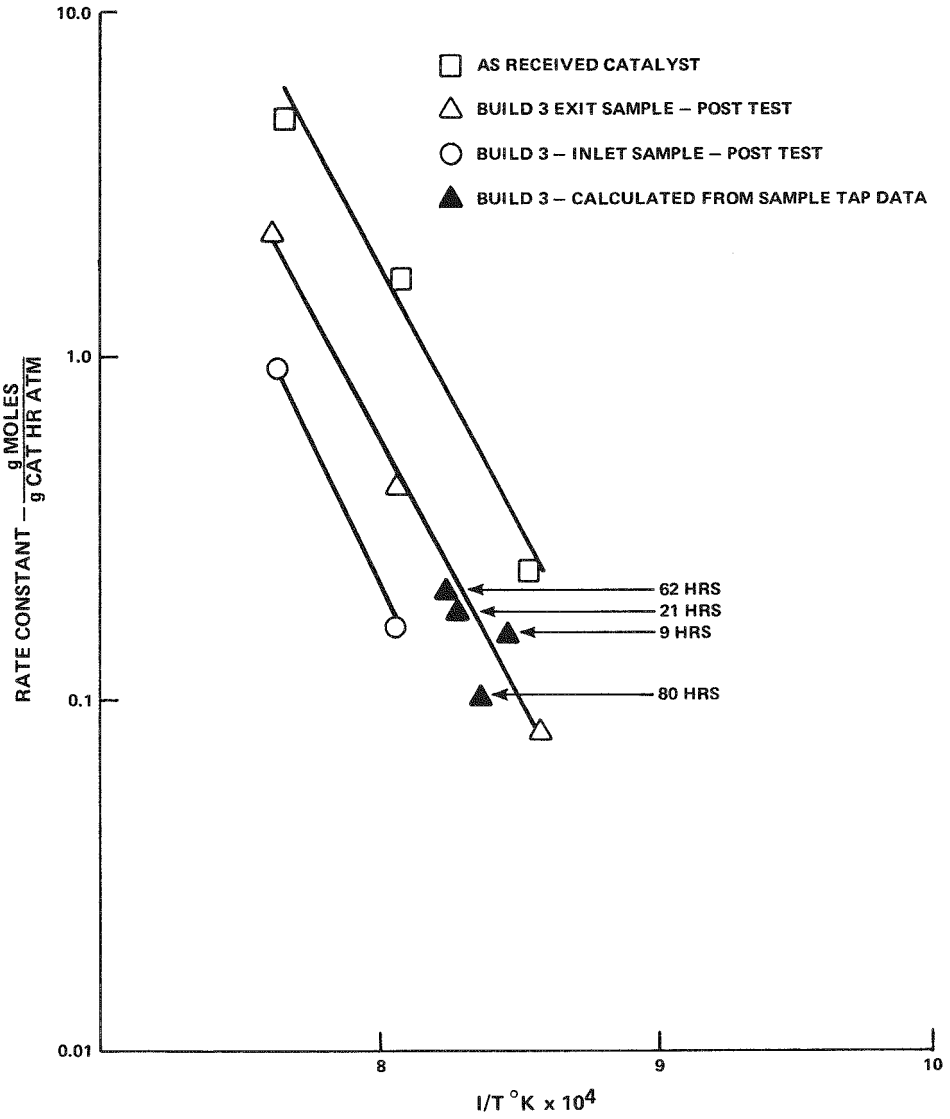

Figure 4-22. Activity of Catalyst Used in Adiabatic Reactor Build 3

Alternate Fuel Processing Approach - Scheme B. The objective of testing a second fuel processing approach (Scheme B) was to determine if the tendency to form carbon could be significantly reduced by preventing fuel/flame front contact. If this were the case, the requirement for strict control of fuel-oxidant mixing would be relaxed.

The Scheme B test was run for thirty three hours on No. 2 fuel oil. Results indicate this alternative approach is also sensitive to mixing requirements. As shown in Figure 4-23, the performance of Scheme B was poorer than the Scheme A 2 inch and 6 inch results. The deterioration in performance from the initial to the final point is probably due to catalyst shrinkage which increases fuel residence time upstream of the catalyst bed and decreases performance.

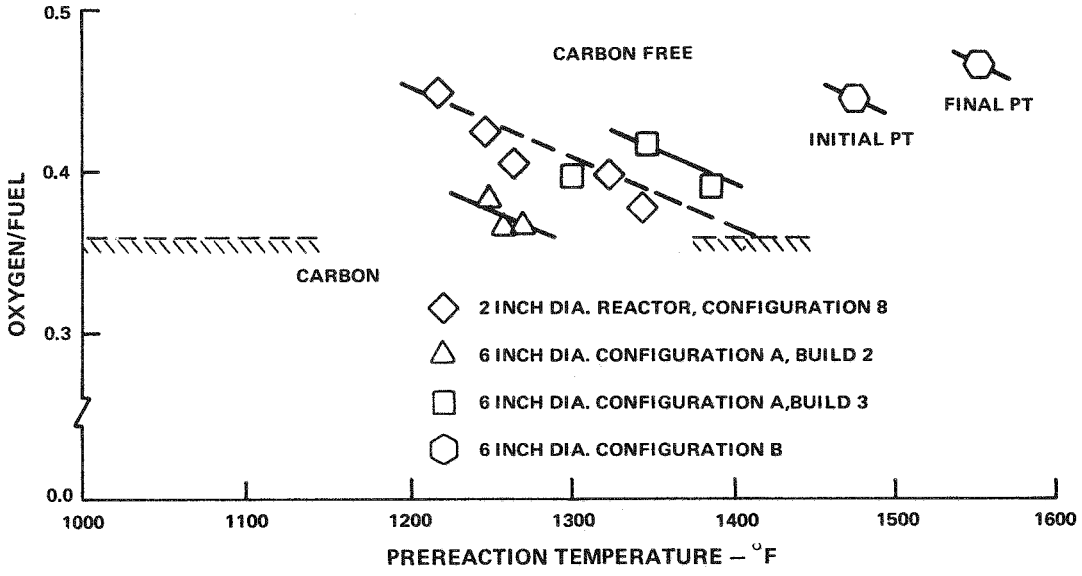

Figure 4-23. Effect of Carbon on Carbon Boundary

The rig was shut down in a plugged condition to determine the location of carbon. Inspection of the reactor internals revealed non-uniform carbon deposition in the catalyst bed and on the reactor walls; and catalyst shrinkage as shown in Figure 4-24. The original catalyst level was even with the top of the wall. The non-uniformities indicate inadequate mixing between the fuel and steam oxidant.

The results of this test indicated that the absence of a fuel/flame front contact did not qualitatively change the carbon formation characteristics of the reactor. It is necessary to assure adequate mixing of steam and fuel in both configuration

A and B. Since the configuration A mixer head has undergone an extensive optimization program, its development was continued.

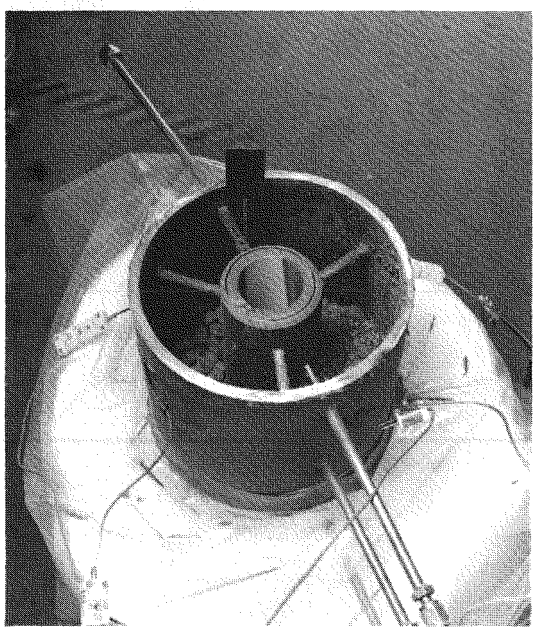

Figure 4-24. Reactor Internals Showing Location, and Catalyst Shrinkage

Scheme A, Build 4. The major objective of the Build 4 test was to demonstrate direct scaleup of carbon boundary performance from the 2 inch rig to the 6 inch rig. Configuration 10 mixer was selected for this test on the basis of cold flow mixing tests. The HGC-2000 catalyst was replaced by a more dimensionally stable type, to reduce the catalyst shrinkage problem experienced in the previous two tests. Secondary test objectives included an assessment of the effects of space velocity, exit temperature, and pressure on fuel conversion and the carbon boundary. The test demonstrates that varying the reactor pressure from 23 to 60 psig and fuel flow from 5 to 13 pph does not affect the O_2/C carbon boundary. Figure 4-25 shows the fuel conversion data at 23 psig, 35 psig, and 60 psig, versus exit temperature at 10 pph fuel flow. No effect of pressure on fuel conversion was observed over the range of 23 to 60 psig. Fuel flow rate does affect fuel conversion. Increasing fuel flow from 5 pph to 13 pph requires that the bed exit temperature be increased by 90°F to achieve the design goal fuel conversion. During the 342 hours of testing, no catalyst decay was evident (after an initial process lineout). On the 10 pph curve, data from 17.5 hours to 329 hours shows no change with time. Bed temperature profile data also confirms this observation.

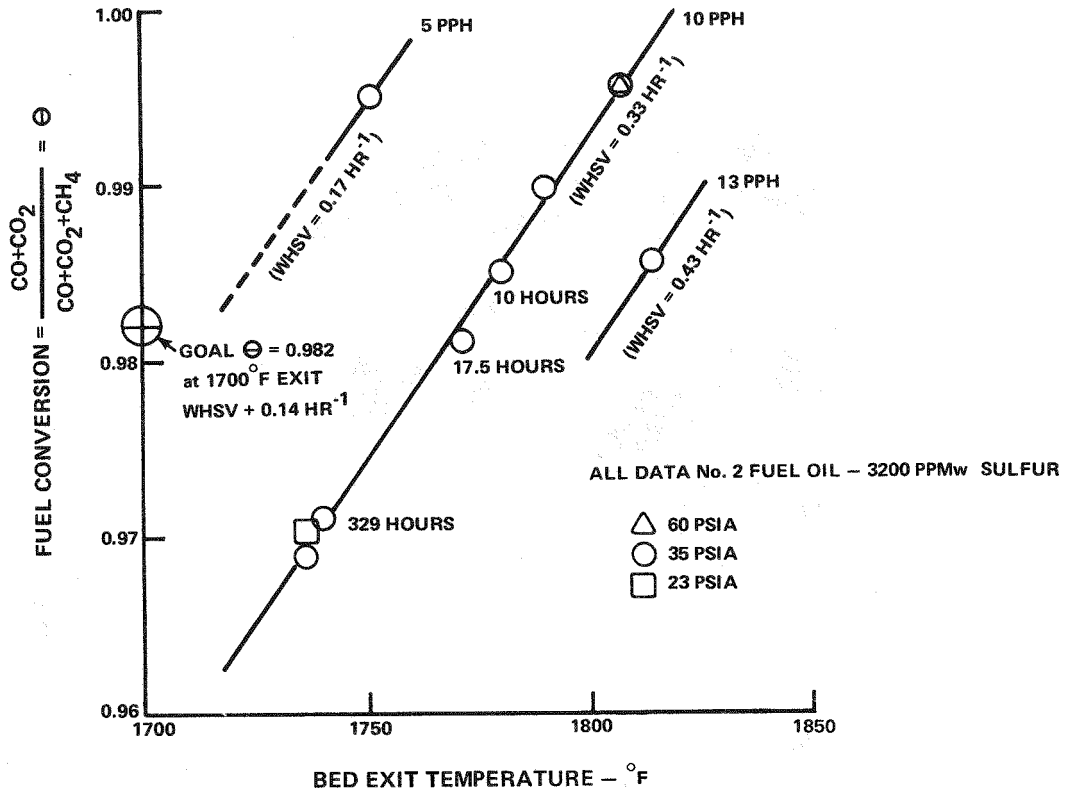

Figure 4-25. Adiabatic Reformer Fuel Conversion vs. Bed Exit Temperature

Summary of Adiabatic Reformer Testing.

Mixing criteria used in combustion designs have been successfully utilized to design and cold-flow test the effectiveness of adiabatic reformer mixing nozzles. Reformer tests have demonstrated that rapid reactant mixing, confirmed in inexpensive cold flow tests, results in a reasonably low oxygen to fuel carbon ratio for both the two inch and six inch reactors. These tests have demonstrated that similar mixing produces a similar carbon boundary regardless of reactor size. The present mixer design results in very thorough and rapid mixing of the reactants, so that further improvement in the degree of mixing is not a viable approach to an improved carbon boundary. Studies during RP-114-2 advanced the adiabatic reforming process from one which was mixer limited to one which is catalyst limited. However, it is expected that the design performance will be attained with a more active or sulfur tolerant catalyst. More active and sulfur tolerant catalysts will be required to attain design performance. Such catalysts are being pursued under RP1041-4.

REGENERABLE METAL OXIDE SULFUR SCRUBBER (RMOSS)

Current technology fuel cells require sulfur removal (scrubbing) from fuel gas feed to avoid performance deterioration due to sulfur poisoning. When relatively low sulfur naphtha fuels or natural gas are used to produce hydrogen, a once-through discardable zinc oxide scrubber is economically feasible. In advanced fuel processors utilizing heavy fuels for hydrogen generation, the sulfur level of the fuel is too high for removal with a once-through discardable sorbent. Regenerable sulfur scrubbers now available are either low-temperature liquid scrubbers or high-temperature fluidized-bed scrubbers. Neither type is easily adaptable to a compact, load-following fuel cell power plant. Present efforts are concentrated on the development of a fixed-bed regenerable sulfur scrubber operating over a temperature range consistent with an advanced fuel cell power plant. The system now being studied uses a metal oxide deposited on a high-surface-area support. The support is expected to stabilize the metal oxide against crystallite growth, loss in surface area, and loss of available metal oxide.

This scrubber will remove most of the sulfur in the gas stream, but it may not be capable of lowering the sulfur concentration to the required concentration level of less than one part per million. If it does not, it may be followed by a final discardable scrubber. In the proposed system, shown in Figure 4-26, two beds would continuously cycle between the scrubbing and regeneration modes. While one bed is scrubbing sulfur from the reformer product stream, the second bed would be regenerated by cathode exhaust passed through the bed. During regeneration, the air oxidizes the metal sulfide to sulfur dioxide. Two beds are shown, but it might be more efficient to use three beds and regenerate two while scrubbing with the third.

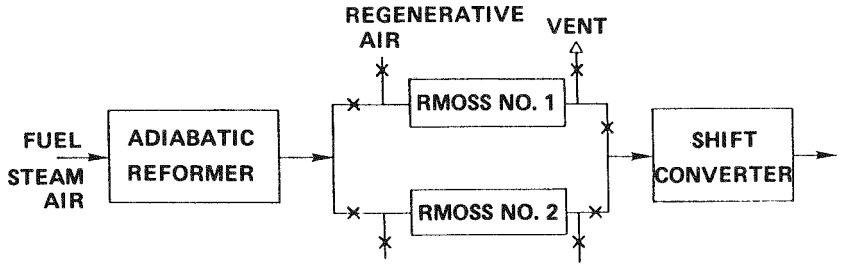

Figure 4-26. Regenerable Metal Oxide Sulfur Scrubber Process

During the previous reporting period, five different RMOSS formulations had been screened in the laboratory; but the results had not all been analyzed. One formulation demonstrated the potential for good sulfur capacity over repeated scrubbing and regeneration cycles. During the present reporting period, further tests were run in the laboratory and an automatic multi-cycle test facility was designed, constructed and used to test larger batches of the most promising RMOSS formulations. This test facility had high enough flows so that continuous sulfur analysis could be performed. The results of the tests in this facility suggest two candidate materials with multi-cycle sulfur removal capability. One material is strongly affected by the water content of the stream, and would require water removal from the sulfur containing stream. A second formulation shows a small but significant sulfur capacity without the need for water removal.

RMOSS Engineering Test Facility

An RMOSS engineering test facility was designed to operate unattended so that a large number of scrub and regeneration cycles could be performed without the need for excessive manpower coverage. A simplified diagram of this facility is shown in Figure 4-27. Reformer effluent is simulated with pure gases. Hydrogen sulfide is controlled with a fine metering valve, and originally a mass flowmeter having the capability of measuring 0-5 cc of hydrogen sulfide per minute was used to monitor the hydrogen sulfide flow. Unfortunately, the hydrogen sulfide, or impurities in the gas caused deposits to plug the Monel capillary tubes of the mass flowmeter sensing element. This occurred twice, in spite of a 2 micron filter placed upstream of the sensing element and the mass flowmeter had to be eliminated from the system. The hydrogen sulfide flow was finally set by sampling the reactor inlet gas with the sulfur detector and setting the the hydrogen sulfide concentration to 500 parts per million. Steam is controlled between 0.09 to 1.0 PPH with high temperature fine metering valves and a pressure transducer which measures the pressure drop across an orifice. An adjustable cycle timer is used to automatically actuate solenoid valves to switch from the scrub to regenerate part of the cycle. Temperature controlled resistance heaters, periodically monitored by computer are used to maintain the reactor temperatures.

Sulfur analysis is performed continuously on-line with a Meloy flame photometric sulfur analyzer. This instrument is capable of measuring sulfur concentrations to below one part per million, and because it measures on a continuous basis, is capable of detecting system transients as well as any erratic or anomalous behavior of the RMOSS system.

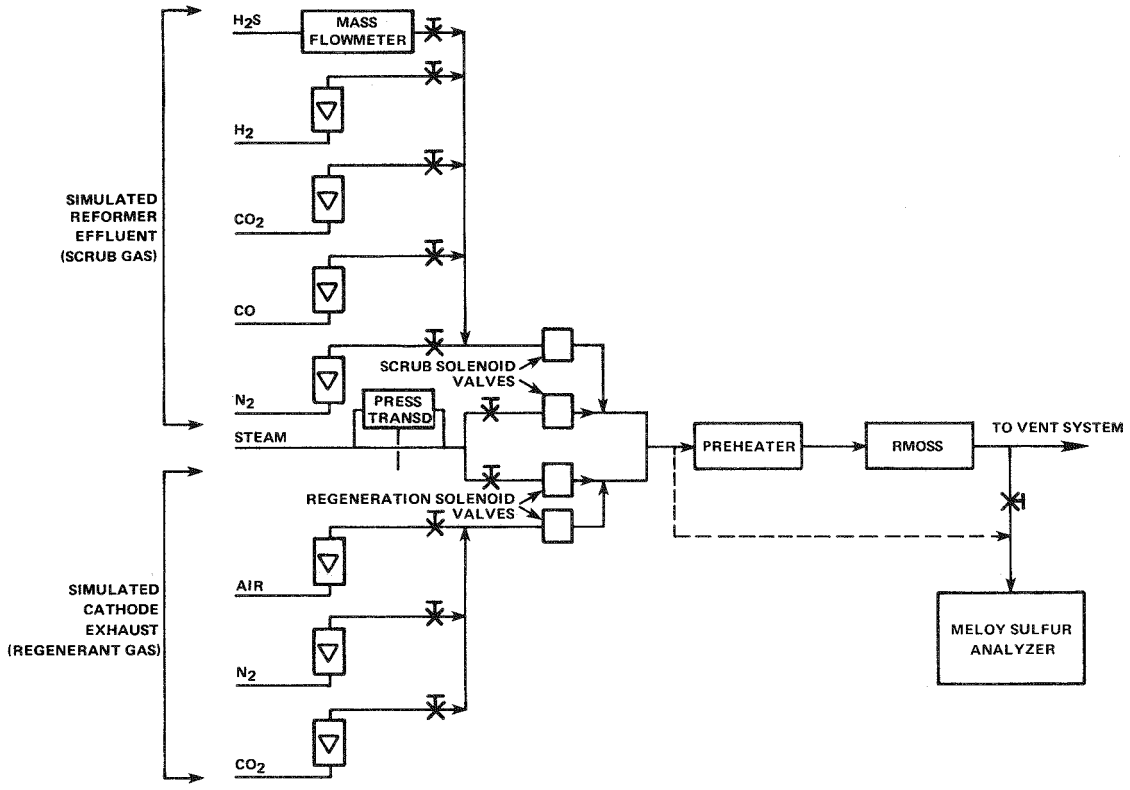

Figure 4-27. Simplified RMOSS Rig Schematic

Laboratory Results

Five different potential regenerable sulfur scrubber formulations were screened in the laboratory. One has demonstrated good performance and the potential for long life. The screening process consisted of five cycles of sulfur scrubbing from a simulated reformer gas and regeneration at the same temperature with simulated cathode exhaust gas. The sulfur effluent was measured only on the last cycle. Post-test analyses were run to determine any surface area losses and the degree of regenerability (amount of sulfur remaining on material after regeneration). The results of these tests, plotted in Figure 4-28, show a wide variation in performance. This figure compares the relative performance of the different scrubber formulations by showing the sulfur content of the processed gas as a function of the quantity of gas processed. It can be seen that formulations A, C, and D can process a reasonable amount of gas before regeneration would be required while formulation E has a significantly lower capacity. Formulation C does not lower the sulfur level as low as formulations A and D and would require the use of a fairly large nonregenerable zinc oxide bed downstream of the regenerable scrubber.

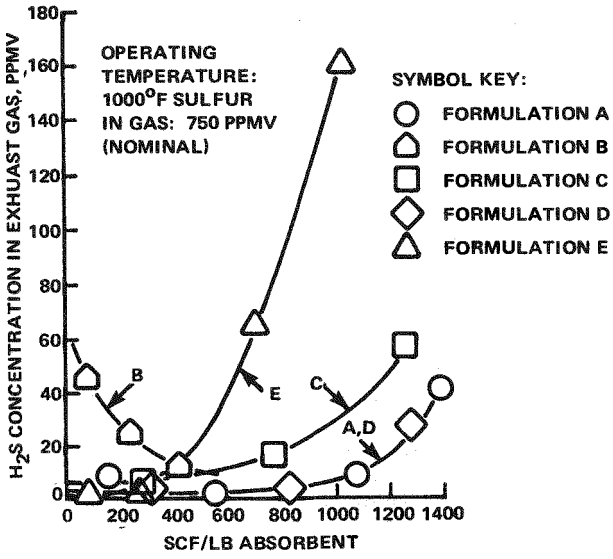

Figure 4-28. Regenerable Sulfur Scrubber Results After Five Cycles

Post-test analysis showed a large decrease in surface area in formulation A and a high residual sulfur content in formulation C. This indicates that the structure of formulation A is deteriorating and that formulation C is not regenerating fully. Because of this, neither of these formulations appears to have a good potential for long life. Table 4-2 shows formulation D to be the best of the five formulations tested in the laboratory. Formulation D demonstrates high scrubbing capacity, low sulfur in the effluent gas, and has good potential life because of little surface area loss and the high sulfur removal during regeneration.

Table 4-2
POTENTIAL OF REGENERABLE SULFUR FORMULATIONS
SCREENED IN THE LABORATORY

FORMULATION	CAPACITY TO 20 PPM BREAKTHROUGH (SCF/LB) ABSORBENT)	INITIAL SULFUR LEVEL IN EFFLUENT (PPM)	POTENTIAL LIFE
A	1230	Low 0-5	Poor
B	--	Very High 40-60	----
C	840	High 5-10	Poor
D	1230	Low 0-5	Good
E	480	Low 0-5	Good

Formulation D was tested at 900°F and 1000°F to investigate the effect of temperature on sulfur capacity and regenerability. It appears that initial sulfur capacity is somewhat higher at 900°F than at 1000°F; however regeneration is incomplete at 900°F so subsequent scrubbing cycles showed poor capacity at 900°F. Returning to 1000°F brought the capacity back to normal.

These results are shown in Figure 4-29. It can be seen that the first and seventh cycles, which were run at 900°F, demonstrated excellent capacity, but the second to fourth cycles had poor sulfur capacity because of poor regeneration. The fifth and sixth cycles, regenerated and run at 1000°F, demonstrated high capacities.

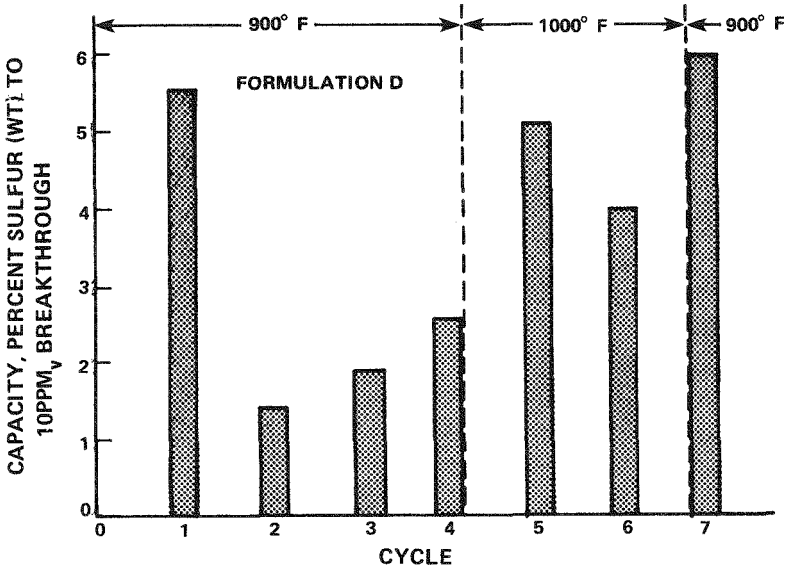

Figure 4-29. Effects of Temperature on Sulfur Capacity and Regenerability

Regeneration at 1000°F results in a high initial sulfur dioxide concentration in the exhaust gas, as shown in Figure 4-30. It is obvious from Figure 4-29, that simply dropping the temperature to 900°F is not a suitable solution as regeneration is incomplete. This problem was left for further study in the engineering test facility. A final laboratory test was run to determine the effect of particle size before starting a test in the engineering facility. All laboratory tests were run with 20-40 mesh scrubbing materials. This would create an excessive pressure drop in a powerplant, so a test was run with a more typical extrusion, manufactured in 3/16" size. This test shows that the process is definitely

diffusion limited and the capacity strongly affected by particle size. Figure 4-31 shows that this increase in particle size decreased the time to reach 20 PPM sulfur in the effluent, or scrubbing capacity, by about a factor of seven. The capacity of the pellets is still reasonable, but because it is significantly less than expected, a more careful study is required in the engineering rig to insure that the scrubbing and regeneration cycle times will be adequate to insure a sulfur-free hydrogen stream for the cell.

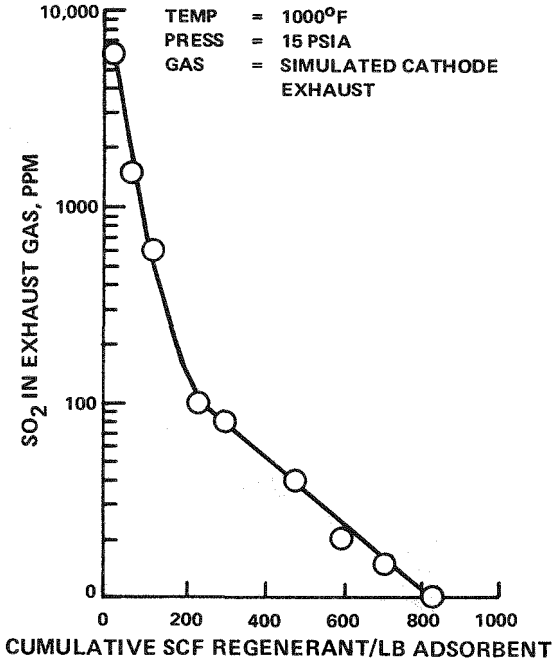

Figure 4-30.
Regeneration of Formulation D

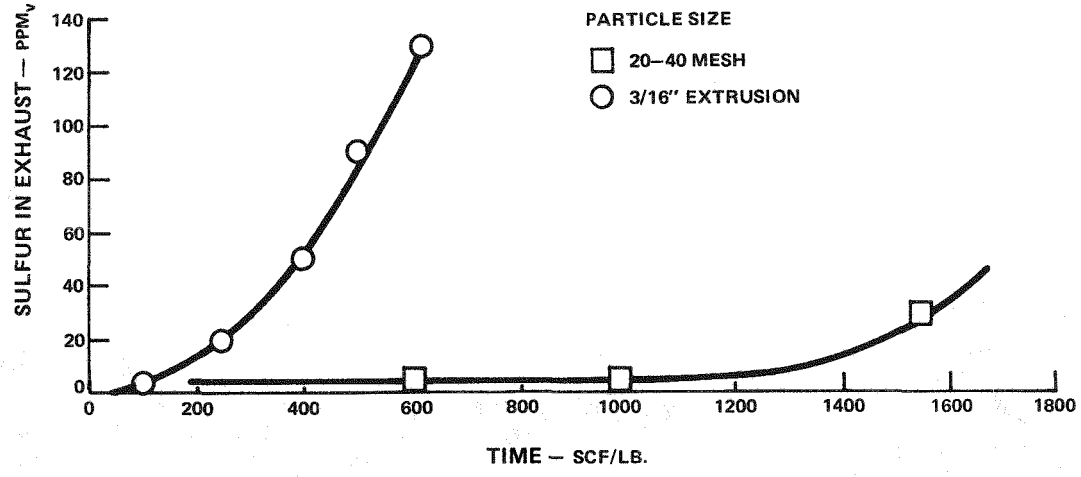

Figure 4-31. Sulfur Removal on Formulation D - Effects of Particle Size

Results from Engineering Test Rig

The engineering test reactor was constructed from a 1.0 inch stainless steel tube, and was loaded with 40-100 grams of absorbent instead of the 4.0 grams used in the 3/8" laboratory reactor. This reactor is large enough in diameter to minimize channeling with full size pellets and only full sized pellets were tested. Studies in the laboratory reactor were conducted with 17% water, which simulated one case for shift converter effluent from a conventional reformer. The unshifted adiabatic reformer effluent contains 30% - 40% water. Initial tests in the engineering reactor were made to study the effect of water concentration on the scrubbing capacity of Formulation D to evaluate the RMOSS system as it would be incorporated into an adiabatic reformer system. Figure 4-32 shows the effect of water on the sulfur removal with formulation D; the sulfur breakthrough time decreases with increased water in the reactant gas, and the absolute sulfur level prior to breakthrough also increases.

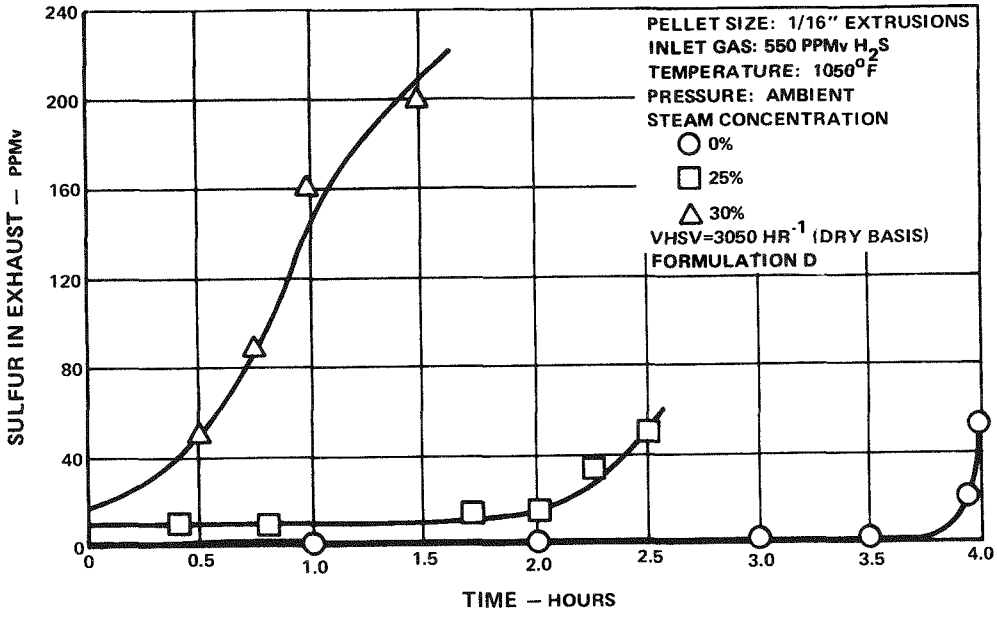

Figure 4-32. Effect of Steam Concentration on RMOSS Performance

Figure 4-33 is a replot of the data in Figure 4-32, and shows that for the 1/16 inch extrusions, water must be reduced below 25% in order to achieve significant scrubbing times with this formulation. As the water content of the stream is increased beyond 25%, the scrubbing time to 20 parts per million sulfur in the processed gas decreased significantly. This condition can be helped somewhat by

an increase in bed size; however doubling the length of the bed only doubled the breakthrough time. This indicates that the reaction front is very sharp, utilizing a very small part of the bed, and the usable bed capacity is a very small fraction of its maximum stoichiometric capacity.

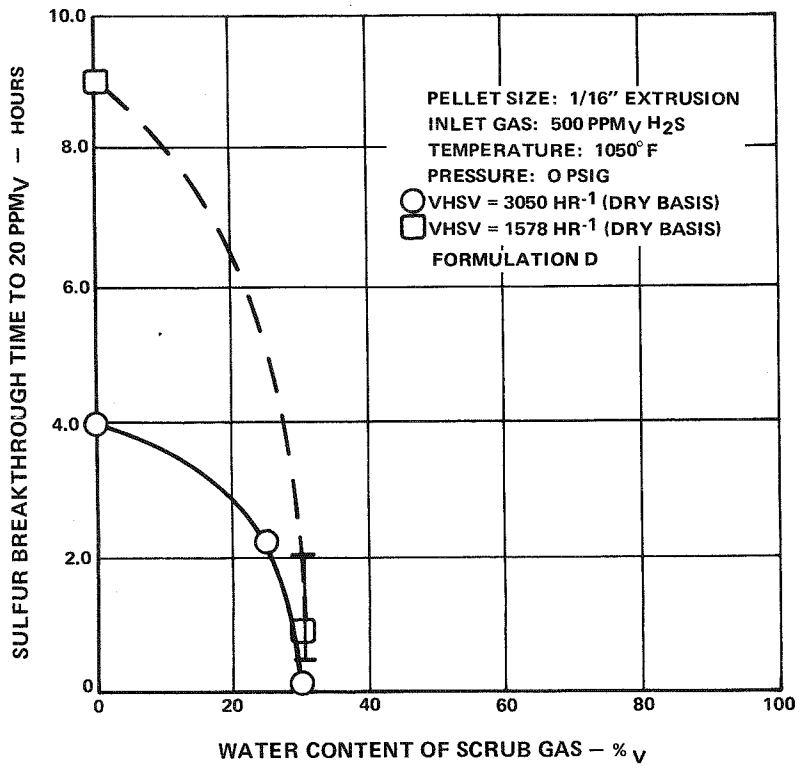

Figure 4-33. Effect of Space Velocity and Water in Scrub Gas on Sulfur Breakthrough Time

Formulation D requires a more complicated sulfur removal system than originally envisioned. Since the water content of the gas to be scrubbed is greater than 30%, water removal is required in order for this formulation to be workable in a fuel cell powerplant. The added heat exchangers and condensers required to remove the water from the process stream for formulation D would add between $5 - $10 per kilowatt to the cost of the powerplant.

In order to eliminate the need for added condensers to the powerplant, another material, Formulation E, with somewhat different chemical and physical properties was tested. Formulation E has larger pores and is less polar than Formulation D, so would be expected to be less affected by water. A temperature map was run with this formulation with a dry gas stream and with 40% water in the gas. The

effect of temperature on the capacity of formulation E is shown in Figure 4-34. This figure shows the time to 20 PPM sulfur breakthrough in the RMOSS exit gas as a function of temperature, and indicates that although there is some loss in capacity with 40% water in the gas, a significant capacity still exists with this formulation.

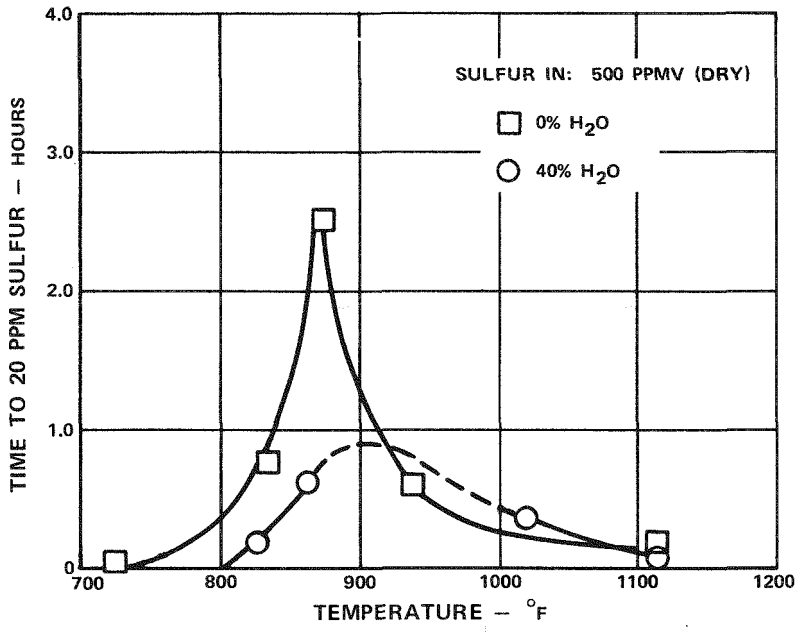

Figure 4-34. Effect of Temperature on Sulfur Breakthrough Time for Formulation E

A typical breakthrough and regeneration curve for formulation E is shown in Figure 4-35. This curve describes the sulfur content of the gas exiting the RMOSS as a function of time. There are two significant features of the data; the initial high sulfur level at the beginning of the scrub cycle which was also seen with Formulation D, and the initial high sulfur content of the gas during regeneration. These occur at every temperature tested. The initial peak during the scrub part of the cycle is thought to be caused by the reduction of metal sulfate to hydrogen sulfide and metal oxide by hydrogen. If this is the case, sulfate is formed during the regeneration part of the cycle and indicates that the metal oxide is being inadequately regenerated. Thermodynamic data indicates that sulfate formation could occur during the early stages of regeneration where SO_2 concentration is high. Sulfate formation and its subsequent reduction can be investigated by control of the regenerant gas composition, and by post-test analy-

sis of absorbent. The initial sulfur peak during regeneration reflects the initial rapid rate of sulfide oxidation and can be controlled with the proper system design.

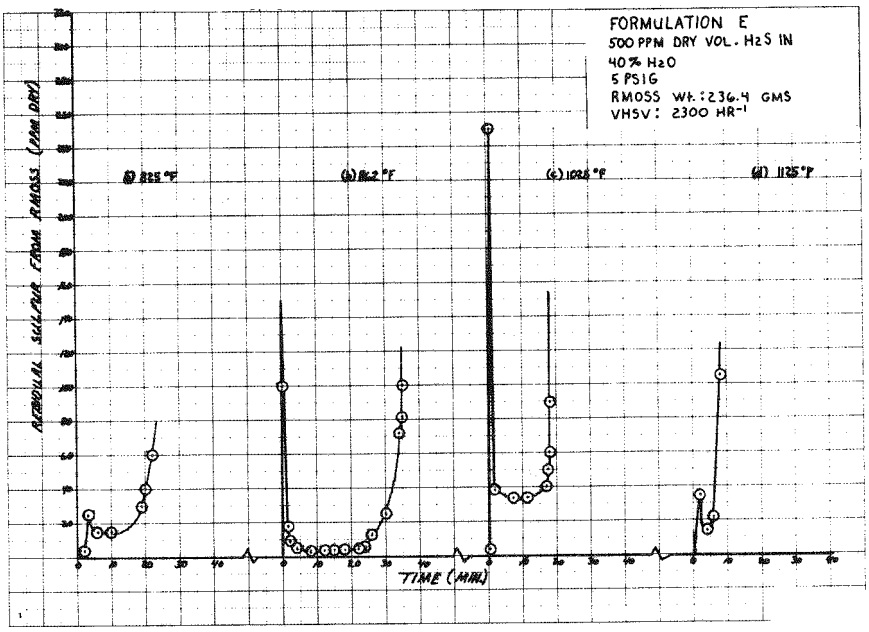

Figure 4-35. Effect of Temperature on RMOSS Performance

The present RMOSS Formulation E capacity ranges between 2% and 5% of the theoretical capacity based on 100% of the metal oxide reacting with hydrogen sulfide to form metal sulfide. In the presence of dry gas, the maximum capacity is 5% of the theoretical, and in the more realistic case where the gas contains 40% water, the capacity is 2% of theoretical. With this 2% capacity, a typical RMOSS system for a 4.8-MW powerplant would require two 42-ft^3 RMOSS beds cycling every 30 minutes. These beds would be operating between 850°F and 1000°F, and would have a sulfur breakthrough curve similar to that shown in Figure 4-36. A downstream bed of zinc oxide would be used to scrub the residual sulfur exiting the RMOSS. This residual sulfur is made up of three parts:

a. The sulfur spike at the beginning of the scrub cycle,
b. The sulfur slip during the main part of the scrub cycle, and
c. The sulfur increase as breakthrough commences.

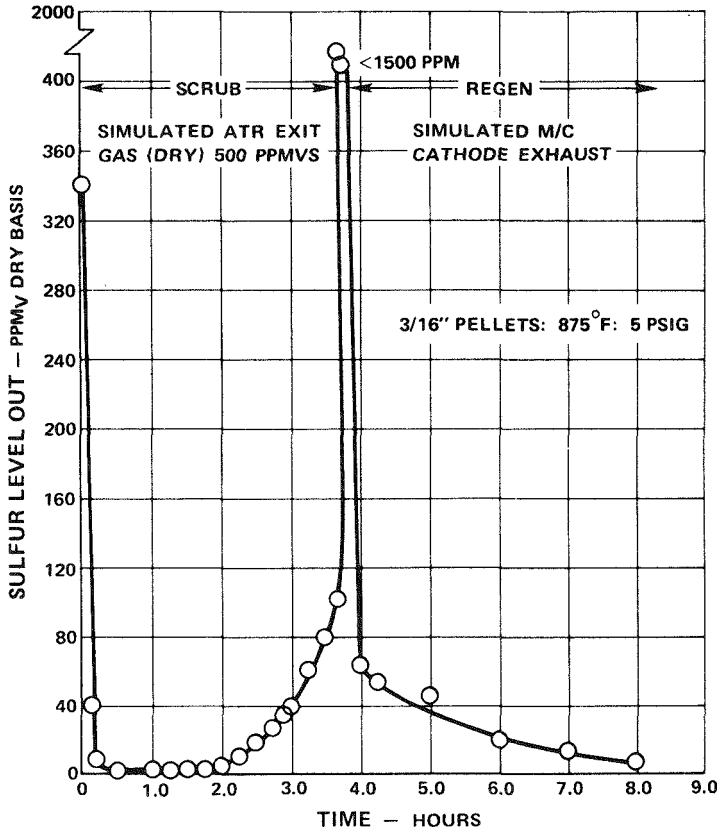

Figure 4-36. Typical Sulfur Breakthrough Curve for Formulation E

The sulfur from (c) can be reduced by shortening the cycle time. The sulfur from (a) can be eliminated by preventing sulfate formation during regeneration or minimized by increasing the capacity of the RMOSS material relative to the spike.

As the RMOSS cycle time is increased, the sulfur spike produced from the reduction of metal sulfate becomes insignificant. It is advantageous to minimize this sulfur spike relative to the sulfur absorption on the RMOSS material in order to decrease the cost of the "throw away" zinc oxide bed being used to scrub the residual sulfur. Table 4-3 shows how this sulfur spike influences the total sulfur burden of the zinc oxide bed. At 825°F, this spike is insignificant, but at 862°F, where the best performance was obtained, the sulfur spike accounted for almost three times the normal sulfur level leaving the reactor. In order to make this sulfur spike account for only 20% of the total residual sulfur, the breakthrough time must be increased to 113 minutes.

Table 4-3
INFLUENCE OF RMOSS PERFORMANCE ON
ZINC OXIDE RESIDUAL SULFUR SCRUBBER

Curve from Figure 4-34	TEMP (°F)	Sulfur Level from RMOSS (ppm)	Equivalent Sulfur Level with Spike Included (ppm)	Breakthrough Time to 35 ppmS [equiv. to 20 ppmS Wet Basis] (min)
(a)	825	15	13	20
(b)	862	4	11	31
(c)	1025	34	45	16
(d)	1125	20	24	6
*	862	4	5	113

* Scrub time required for the sulfur spike in (b) to be equivalent to only 20% of the total residual sulfur.

Significant conclusions to date from these studies are: absorbents similar to formulation E offer low but significant breakthrough capacities; and there is a high sulfur spike produced at the beginning of the scrub cycle which must be minimized. Thermodynamic analysis indicates that the initial high sulfur spike can be controlled, and the sulfur capacity increased by varying the system variables.

Increased capacity of the RMOSS is expected to be achieved through three different routes:

1. Control of the gaseous composition and temperature variables.
2. Reactor design changes.
3. Optimization of formulations similar to E.

Since only about 2% of the theoretical sulfur capacity is presently being utilized it is not unreasonable to expect a possible increase in sulfur capacity through the use of the above mentioned routes.

SYSTEMS ANALYSIS OF ADVANCED FUEL PROCESSORS

Advanced fuel processing systems are being developed to extend operation of dispersed fuel cell power plants to both petroleum and coal derived liquid distillate fuels. The sulfur and aromatic content of these fuels demand high process temperatures to achieve the required fuel conversion. Three possible candidate processes are being evaluated: an adiabatic reformer, a hybrid reformer

and a cyclic reformer. The adiabatic (Figure 4-37A) consists of a simple catalyst bed with sufficient air added to the process fuel and steam to provide the endothermic heat of reforming within the reactor. The hybrid reformer (Figure 4-37B) consists of a primary and secondary reformer, similar to conventional reforming for ammonia synthesis. The cyclic reformer (Figure 4-37C) is a dual bed reformer in which heat generated in one reactor by combustion of the fuel cell anode exhaust is stored in the heat capacity of the bed to supply the endothermic heat for reforming in the subsequent reform cycle.

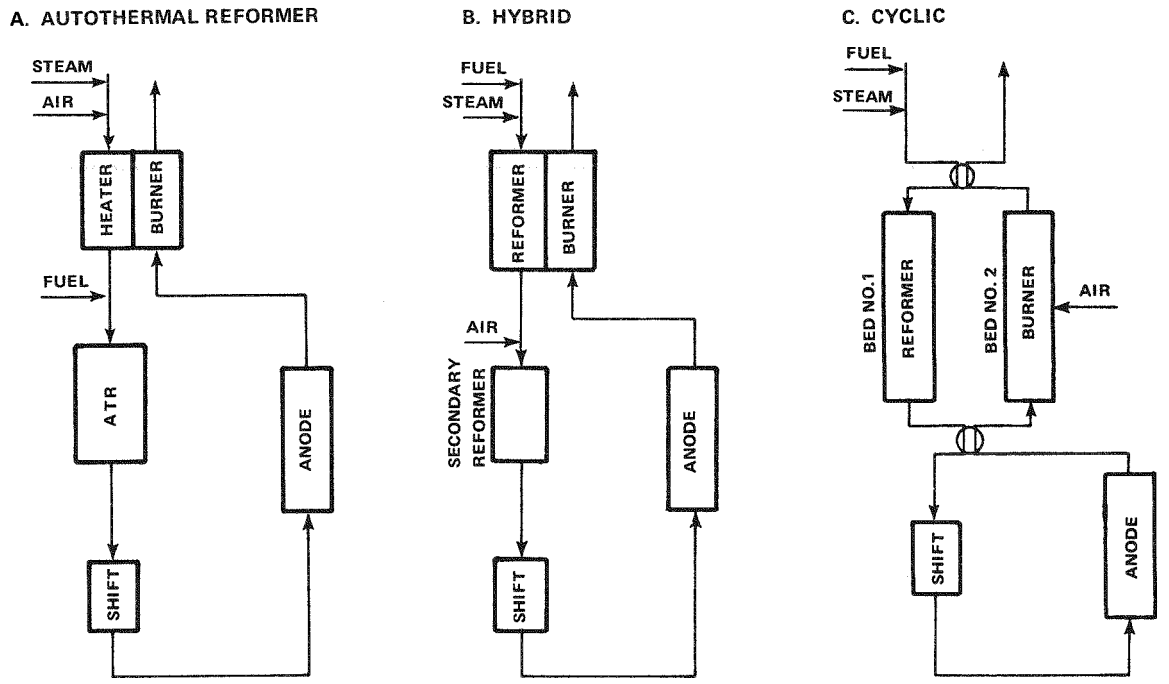

Figure 4-37. Fuel Processing Systems Studied

System studies were conducted to evaluate the cost and efficiency potential of the three fuel processing systems. Each fuel processor was sized to provide sufficient H_2 for a 4.8 MW phosphoric acid power plant. The fuel cell and fuel processing conditions were adjusted so that each system operates at a design heat rate of 9300 BTU/kWh.

The adiabatic reformer, which has been the subject of extensive experimental and system studies, is the baseline for the comparision. The adiabatic reactor size, fuel conversion and O_2/C ratio were optimized to minimize system cost using a reactor model and catalyst activity measured in the presence of sulfur. (Figure 4-38) The fuel conversion has been verified in subscale reactor tests. The carbon formation limit must be improved for operation at the design O_2/C ratio.

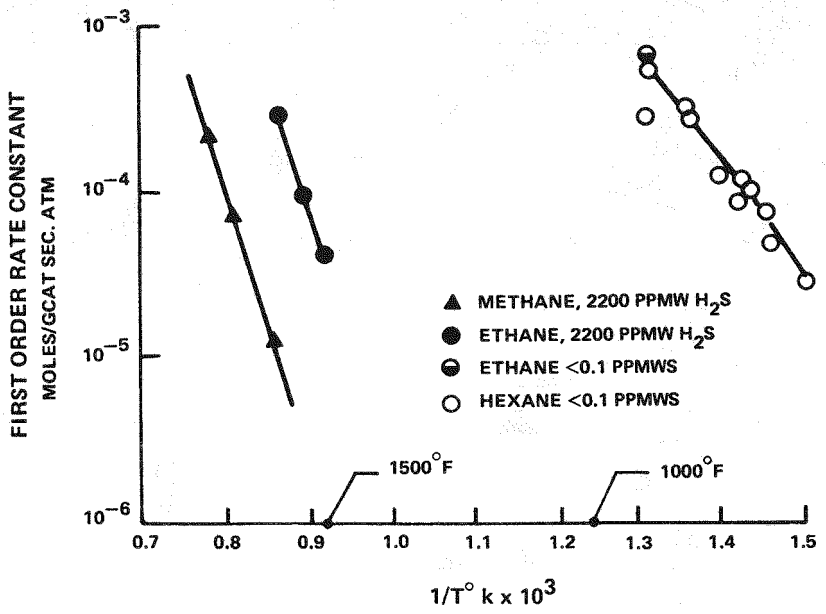

Figure 4-38. Effect of Sulfur on Steam Reforming Activity of Supported Nickel Catalyst

The primary reformer of the hybrid fuel processor was sized using a catalytic tubular reformer model and the catalyst activity from the adiabatic reformer tests. The secondary reformer was sized using the adiabatic reformer model and catalyst activity. System studies were conducted to determine the optimum primary reformer fuel conversion and the secondary reformer O_2/C ratio to minimize the system cost. The two key issues with the hybrid system are the ability of the primary reformer to run without carbon formation or decay at the bed temperature profile required for high burner thermal efficiency and the ability of the secondary reformer to operate on the incomplete fuel conversion products of the primary reformer without carbon formation at the required O_2/C ratio. The process conditions required for the fuel cell application are only now being experimentally verified.

The cyclic reformer was sized based on preliminary cycling tests of a small single bed reactor. Additional test data and models are required before the system can be optimized. The effect of the interaction of bed switchover with the fuel cell remains to be determined. Long-term operation of mechanical components and catalysts must be demonstrated.

A summary of the results of the studies evaluating the three fuel processing systems is shown in Table 4-4.

Table 4-4
COMPARISON OF FUEL PROCESSORS

Processor	ATR	Hybrid	Cyclic
O_2/C	0.36	0.19	0.0
Processor Thermal Efficiency (%)	83.0	85.0	87.3
Fuel Conversion (%)	98.2	95.0	93.8
Fuel Gas Quality			
H_2 (Vol %)	19.2	57.3	72.4
CO (Vol %)	1.5	1.0	1.0
Acid Cell Performance			
(Heat Rate = 9300 Btu/kWh)			
Cell Voltage (V/c)	0.628	0.612	0.595
Current Density (ASF)	208.0	293.0	340.0

The thermal efficiency and quality of the fuel gas produced decrease as the O_2/C ratio of the fuel processor increases. The cyclic reformer does not require the addition of oxygen (air) to the fuel process stream and it has the highest thermal efficiency and produces the highest quality H_2. The performance of the hybrid system, which requires about half of the O_2 of the ATR, is between that of the cyclic and autothermal reformers. The O_2/C ratio has a similar impact on the fuel conversion. Increasing the O_2/C ratio reduces the amount of H_2 produced and a higher fuel conversion is required to maintain a reasonable H_2 utilization in the fuel cell.

As the fuel processor thermal efficiency increased, the power section efficiency was reduced to maintain the design heat rate at 9300 BTU/kWh. The lower cell voltage required plus the higher quality fuel gas results in a large increase in the current density as the O_2/C ratio is reduced. The cyclic reformer reduces the total cell area 40% compared to that required with a ATR.

The relative power plant costs for the three fuel processing systems are shown in Figure 4-39. The baseline system is the autothermal reformer which has been studied in greatest detail. The hybrid reformer reduces the power plant cost 15%, and there is an additional 9% reduction with the cyclic reformer. The cost decrease is primarily due to reduced cell area and smaller, less expensive heat exchangers as the O_2/C ratio is decreased.

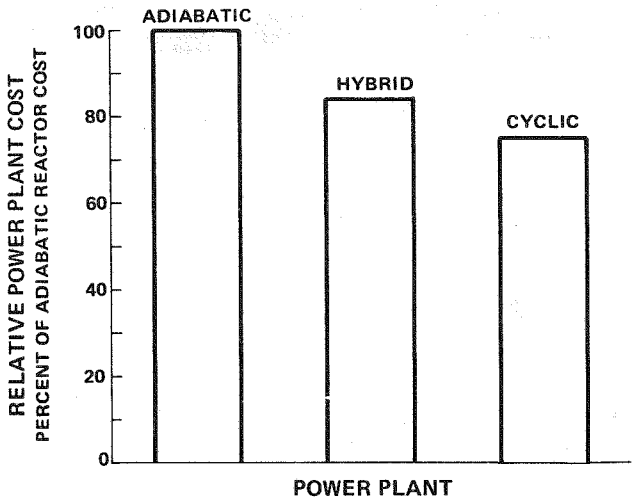

Figure 4-39. System Cost Comparison for 4.8 MW Phosphoric Acid Power Plant at 9300 Btu/kWh

These processes are in a early stage of development. The power plant costs depend upon the ability of the fuel processors to perform as estimated during the power plant life. The ATR has been demonstrated in a subscale (10 pph) reactor as reported in Task 3. Some improvement in the carbon limit is required to meet the design O_2/C ratio objective. The hybrid system has not yet been demonstrated. To achieve the high thermal efficiency required of the primary reformer dictates a nearly linear temperature profile from the reactor inlet to exit. Catalyst tests are being conducted in a laboratory reactor by another EPRI contractor to demonstrate that the primary reformer will operate without carbon formation with the required temperature profile and fuel conversion. Secondary reformer tests will be required; a) to demonstrate that the secondary reformer can operate in the presence of sulfur on the products of incomplete fuel conversion from the primary reformer, without decay or carbon deposition, and b) to verify that the required fuel conversion can be achieved with the design O_2/C ratio and inlet temperatures. The cyclic reformer has been demonstrated in principle by several tests with a subscale reactor. Additional studies are required to show that two beds can be switched without interrupting the H_2 flow to the fuel cell, or causing large pressure pulses, or large purge losses. Additional tests of a cyclic reformer reactor are required to demonstrate the endurance of the reactor, catalysts, and mechanical components with operation at the design fuel conversion.

Section 5

TASK 4 - USE OF COAL AND COAL PRODUCTS IN FUEL CELL POWER PLANTS

No work was done on this task during the reporting period. Studies of alternative fuel processors for coal liquids are reported in Task 3.

Section 6

REFERENCES

(1) "Status of 40-kW and 4.8 MW Fuel Cell Programs," L. M. Handley, National Fuel Cell Seminar Abstracts, June 26-28, 1979.

(2) "4.8-MW Fuel Cell Demonstration site preparation, K. Glasser, ibid.

(3) "Advanced Technology Fuel Cell Program," EPRI Project 114-1 Final Report No. EM-335, October 1976, Power Systems Division of United Technologies Corporation.

(4) "Advanced Technology Fuel Cell Program," EPRI Project 114-2 Interim Report No. EM-956, December 1978, Power Systems Division of United Technologies Corporation.

(5) The RM Process - A Methanation System, G. A. White, pg 129 Pipeline Gas Symposium, October, 1977.

(6) Effect of Reaction Parameters on Methanation of Coal Gas to SNG, K. H. Eisenlohr, F. W. Moeeler, pg 113 Advances in Chemistry Series 146, 1979.

(7) Methanation in Substitute Natural Gas Production, C. Woodward, Energiespectrum pg 342, December 1977.

(8) J. Lahaye, P. Badie & J. Ducret, Carbon 5, 87, 1977

(9) C. B. Marson and J. W. Cobb, Gas J. 175, 882 (1926)

(10) T. Tomita, K. Kikuelic and Sukamoto, U. S. Pat 4,025,487 May 24, 1977.